Stellingen behorende bij het proefschrift

# New Concepts for EMC Standards Applicable to Multimedia Products

door

Nico van Dijk

Eindhoven, 27 juni 2007

1. De snelle ontwikkelingen in elektronische producten vragen om een geheel andere aanpak van de gangbare EMC metingen, testen en normalisatie.

   *N. van Dijk, P. F. Stenumgaard, P. A. Beeckman, K. C. Wiklundh, and M. Stecher, "Challenging research domains in future EMC basic standards for different applications," IEEE EMC Society Newsletter, pp. 80-86, Spring 2006.*

2. De vorm van het antennediagram van een ontvangstantenne zegt veel over de uiteindelijke afwijking die verwacht moet worden in emissieresultaten. Een grotere bundelbreedte zorgt voor een kleinere afwijking.

   *Zie hoofdstuk 3 van dit proefschrift*

3. De directivity (richtwerking) van het Equipment Under Test (EUT) is minder belangrijk in conversie van emissieresultaten dan vaak gesuggereerd wordt.

   *Zie hoofdstuk 4 van dit proefschrift*

4. Ondanks het sterk variërende elektromagnetische veld in de Reverberation Chamber (RC) kan deze toch gebruikt worden voor compliance metingen.

   *Zie hoofdstuk 4 van dit proefschrift*

5. De huidige immuniteitstestsignalen zijn niet meer representatief voor signalen die toegepast worden in draadloze multimedia producten.

   *Zie hoofdstuk 5 van dit proefschrift*

6. In de wereld van de EMC normen wordt teveel gedacht in termen van 'worst case' en te weinig in termen van 'representative case'.

7. Elektromagnetische Compatibiliteit (EMC) van een product wordt vaak behandeld vanuit een juridisch oogpunt, maar hoort beschouwd te worden vanuit een verantwoordelijkheidsethiek.

8. Het niet-lineaire effect van faseruis in oscillatoren ten gevolge van stoorsignalen kan lineair geanalyseerd worden doormiddel van een lineair tijdsvariante aanpak.

   *S. B. Worm and N. van Dijk, "Susceptibility analysis of oscillators by means of ISF-method," 4th International Workshop on EMC of Integrated Circuits, EMC Compo 2004, Angers, 2004.*

9. Het geloof gaat de rede te boven, maar sluit haar niet uit.

10. Ofschoon Ultra Wide Band (UWB) communicatiesignalen een laag spectraal niveau hebben kunnen deze toch draadloze LAN verbindingen die tussen 5 GHz en 6 GHz werken bijna geheel verstoren.

    *G. Manzi, M. Feliziani, P. Beeckman, and N. van Dijk, "Experimental EMC assessment of different ultra wide band technologies," Workshop Int. Symp. on EMC, Barcelona, Sep. 2006.*

11. In vergelijking met directe communicatie van mens tot mens, verdwijnt bij telecommunicatie vaak de interactie en wordt de communicatie sterk gereduceerd.

12. Als het elektrische veld van een dipoolantenne gemeten wordt in drie half-echovrije meetfaciliteiten kan dit een substantiële deviatie van ±4 dB opleveren.

    *N. van Dijk, "Development and validation of tools for simulation of radiated emission testing," M.S. thesis, Eindhoven University of Technology, Eindhoven, The Netherlands, January 2001.*

13. Leidinggeven betekent niet alleen een medewerker helpen zijn taak succesvol uit te voeren, maar ook de bereidheid om de ander te begeleiden in het streven naar verandering en groei.

14. De ervaring dat in de praktijk de hoevraag als vanzelf de waaromvraag oproept wijst erop dat wetenschap op zich onvoldoende overtuigend is voor het verstand.

15. Als op een indicator van een bepaald gedrag of resultaat gestuurd wordt is het geen goede indicator meer.

# New Concepts for EMC Standards Applicable to Multimedia Products

# New Concepts for EMC Standards Applicable to Multimedia Products

PROEFSCHRIFT

ter verkrijging van de graad van doctor aan de
Technische Universiteit Eindhoven, op gezag van de
Rector Magnificus, prof.dr.ir. C.J. van Duijn, voor een
commissie aangewezen door het College voor
Promoties in het openbaar te verdedigen
op woensdag 27 juni 2007 om 16.00 uur

door

**Nico van Dijk**

geboren te Hengelo

Dit proefschrift is goedgekeurd door de promotoren:

prof.dr. A.G. Tijhuis
en
prof.dr.ir. F.B.J. Leferink

Copromotor:
dr.ir. P.A. Beeckman

ISBN 978-90-74445-78-8
NUR 959


Cover design by Oranje vormgevers
Printed by Universiteitsdrukkerij TU Eindhoven

*Als Gods Woord bij mij is,*
*vind ik in den vreemde mijn weg,*
*in onrecht mijn recht,*
*in de onzekerheid mijn zekerheid,*
*in de arbeid mijn kracht,*
*in het lijden geduld.*

- Dietrich Bonhoeffer -

# Contents

# List of abbreviations

| | |
|---|---|
| AF | Antenna Factor |
| AM | Amplitude Modulation |
| ANOVA | Analysis of Variances |
| APD | Amplitude Probability Distribution |
| ANSI | American National Standards Institute |
| AV | Audio and Video |
| BEP | Bit Error Probability |
| CALTS | Calibration Test Site |
| CD | Committee Draft |
| CDF | Cumulative Distribution Function |
| CDMA | Code Division Multiple Access |
| CE | Consumer Electronics |
| CISPR | International Special Committee on Radio Interference |
| CSMA | Carrier Sense Multiple Access |
| DAB | Digital Audio Broadcasting |
| DC | Document for Comment |
| DCS | Digital Communication System |
| DECT | Digital Enhanced Cordless Telephone |
| DoE | Design of Experiments |
| DSSS | Direct Sequence Spread Spectrum |
| DVB | Digital Video Broadcasting |
| DVB-T | Digital Video Broadcasting – Terrestrial |
| DVB-H | Digital Video Broadcasting – Handheld |
| xDSL | x-type Digital Subscriber Line |
| EMC | Electromagnetic Compatibility |
| EMI | Electromagnetic Interference |
| EUT | Equipment Under Test |
| FAR | Fully Anechoic Room |
| FCC | Federal Communications Commission |
| FDM | Frequency Division Multiplexing |
| FM | Frequency Modulation |
| FSK | Frequency Shift Keying |
| GFSK | Gaussian filtered Frequency Shift Keying |
| GMSK | Gaussian filtered Minimum Shift Keying |
| GSM | Global System for Mobile communication |
| HDMI | High-Definition Multimedia Interface |
| IEC | International Electrotechnical Commission |
| IEEE | Institute of Electrical and Electronics Engineers |
| iFFT | Inverse Fast Fourier Transformation |
| ILC | Inter Laboratory Comparison |
| IT | Information Technology |
| ITE | Information Technology Equipment |

| | |
|---|---|
| JTF | Joint Task Force |
| LAN | Local Area Network |
| LF | Low-Frequency |
| MAC | Medium Access Control |
| MER | Message Error Rate |
| MIMO | Multiple Input Multiple Output |
| MoM | Method of Moments |
| MRI | Magnetic Resonance Imaging |
| MSK | Minimum Shift Keying |
| NC | National Committee |
| NSA | Normalized Site Attenuation |
| OATS | Open Area Test Site |
| OFDM | Orthogonal Frequency Division Multiplexing |
| OSI | Open Systems Interconnection |
| PC | Personal Computer |
| PDF | Probability Density Function |
| PRF | Pulse Repetition Frequency |
| RADAR | Radio Detection and Ranging |
| RC | Reverberation Chamber |
| RF | Radio-Frequency |
| RMS-AV | Root Mean Square - Average |
| RBW | Resolution Bandwidth |
| RRT | Round Robin Test |
| SAR | Semi Anechoic Room |
| SC | Sub Committee |
| SCART | Syndicat des Constructeurs d'Appareils Radiorécepteurs et Téléviseurs |
| SVSWR | Site Voltage Standing Wave Ratio |
| TC | Technical Committee |
| TDM | Time Division Multiplexing |
| TEM | Transversal Electro Magnetic |
| TETRA | Terrestrial Trunked Radio |
| TR | Technical Report |
| TV | Television |
| USB | Universal Serial Bus |
| UWB | Ultra Wide Band |
| WiMax | Worldwide Interoperability for Microwave Access |
| WG | Working Group |

# 1 Introduction

## 1.1 EMC of evolving electronic products

*Electromagnetic compatibility*

Electromagnetic Compatibility (EMC) of a product is the ability of the product to function satisfactorily in its electromagnetic environment without introducing intolerable electromagnetic disturbances to anything in that environment [52]. EMC of a product includes two phenomena: emission and immunity. Emission is the phenomenon considering the electromagnetic energy emanating from a product. Vice versa, immunity to a disturbance is the ability of a product to perform without degradation in the presence of an electromagnetic disturbance. Emission measurements and immunity tests are performed to determine the EMC behavior of products. From the definition of EMC we see that EMC of a product depends on its electromagnetic environment. In other words, products within a specific environment can be called electromagnetic compatible if they work together in harmony. Accordingly, EMC tests should emulate the electromagnetic aspects of the environment appropriately. An impression of a typical home environment is shown in Figure 1.1.
The definition of EMC states that a product should function satisfactorily in its environment. In the European Union (EU), the EMC requirement of a product is regulated in the EMC Directive 2004/108/EC [32]. Harmonized EMC standards may be used to demonstrate compliance of a product. In this way, the interpretation of satisfactorily functioning of a product is implemented in immunity requirements and emission limits as defined in the applicable harmonized standards.

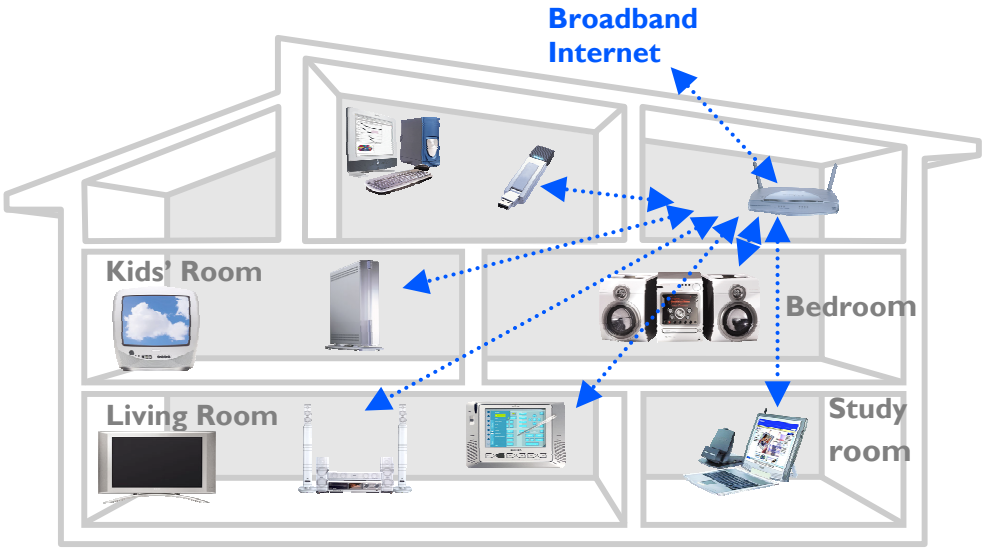


Figure 1.1 An example of a typical home environment.

*EMC standardization*

EMC standards are developed in various committees within the International Electrotechnical Commission (IEC). In Technical Committee (TC) 77 of the IEC, basic standards for low-frequency (≤9 kHz) applications (77A) and basic standards for immunity tests (77B) are developed and maintained. Another important IEC committee that develops and maintains EMC standards is the International Special Committee on Radio Interference (CISPR). CISPR subcommittee A (CISPR/A) develops and maintains basic standards for emission measurements. CISPR includes subcommittees for the development and maintenance of EMC product standards. For example, CISPR/I is responsible for the development of new standards for multimedia products and the maintenance of the current Audio and Video (AV) standards and the Information Technology Equipment (ITE) standards. In the EU, the EMC standards are developed and maintained in TC 210 of the European Committee for Electrotechnical Standardization (CENELEC). In general, the IEC and CISPR standards are adopted by CENELEC with minor modifications resulting in an equivalent European Norm (EN). Further details about the organization of EMC standardization will be explained in Chapter 2.
EMC test methods as described in the standards are based on simplifications of real-life situations. For the purpose of emission measurements, the Electromagnetic Interference (EMI) receiver was standardized within CISPR/A. The standardized EMI receiver (CISPR receiver) emulates an Amplitude Modulation (AM) radio receiver and the annoyance perception of disturbance. The EMI receiver used for emission measurements was standardized to protect the analog AM radios. However, radio broadcasting also uses Frequency Modulation (FM) already over many decades. During the last decade, Digital Audio Broadcasting (DAB) was introduced equipped with digital radio receivers.
The standardization of the EMI receiver to protect AM broadcasting is an example how simplifications made in history need to be reconsidered when new technologies are applied in electronic products. The standardization bodies are coping with the continuous development of new technologies.

*Trends in electronic products*

Over the last decades, a considerable evolution in electronic products can be observed. A convergence is recognized of consumer electronics products, telecommunication systems, personal computers (PC), and gaming products. This convergence means that many applications of the classical separate products are nowadays combined into single products. This convergence is explicit for so-called multimedia products, where Audio and Video (AV) and Information Technology (IT) functions are integrated into a single product. The convergence is also driven by the trend that electronic products become increasingly digital products.
In addition, we can observe a growing number of interfaces between electronic products, i.e., products work together as a system or network instead of stand-alone. This trend is accelerated by the application of wireless communication systems, which typically use digital modulation schemes and apply frequencies above 1 GHz.

Figure 1.1 gives an impression of the trend of wireless interacting multimedia products. As an example, Figure 1.2, shows a home control panel, which is a typical 'converged' multimedia product including AV functions, IT functions and a wireless LAN connection. Nowadays, classical analog broadcast systems are rapidly replaced by digital broadcasting, i.e., Digital Audio Broadcasting (DAB) and Digital Video Broadcasting (DVB). Moreover, many new digital broadcast systems are combined with mobile communication, e.g., DVB-H (DVB-Handheld) television reception in a GSM mobile phone. The main trends in electronic products can be summarized as follows:

- convergence of conventionally different products,
- different products work as a system,
- products become digital,
- products operate at frequencies above 1 GHz,
- products become part of distributed wireless networks,
- digital broadcasting replaces analog broadcasting,
- increasing density of electronic products.

These trends are also of significant importance for the EMC aspects of the products in its environment. Digital radio-communication signals will be present in the electromagnetic environment of modern homes due to the increasing application of wireless communication systems and consequently new potential disturbance sources will be present. Vice versa, the wireless communication systems can be disturbed by emissions of other products in the environment. This means that new potential interference threats are present. We can conclude that both the products and their electromagnetic environment are drastically changing [37]. The above-listed trends in electronic products were also recognized by the former CISPR president P. J. Kerry [63] and in the strategic research agenda on EMC in the 7$^{th}$ research framework program [67].


Figure 1.2 Multimedia home control panel with wireless LAN connection.

*Trends in EMC measurement methods and standardization*

The above-mentioned trends also have consequences for the way in which products are tested for EMC. An important change within CISPR was the creation of a new subcommittee, subcommittee I, in order to cover the trends that multimedia products work as a system and are 'converged' applications (e.g., television and PC). CISPR/I has replaced the former subcommittees E and G [63]. Within CISPR/I new EMC product standards for multimedia products are under development, i.e., CISPR 32 for emission measurements and CISPR 35 for immunity tests. A few years ago, CISPR/H was initiated for dealing with new interference scenarios and corresponding limits.
The replacement of analog broadcasting by digital broadcasting as well as the trend of the increasing application of wireless communication systems make clear that the conventional interference scenario for radio protection, based on analog broadcasting, is getting outdated. Actually, two interference scenarios for radio protection exist: the first is based on the protection of digital broadcast services; the second is based on the wireless communication systems in the home. The specification of the standardized CISPR receiver and its weighting detector should be reconsidered critically. New concepts for weighting detectors equivalent to the interference behavior of digital receivers have been developed, which will be reviewed in Chapter 2.
For immunity tests, a similar conclusion can be drawn, that the conventional immunity test signal for emulation of analog broadcast signals should be reconsidered. DVB systems and wireless communication systems use digital modulation schemes. Digitally modulated signals are in general broadband whereas analog modulated signals are typically narrow-band. This relates also to the development of High-Definition (HD) TV that also requires larger bandwidths. New types of immunity test-signals equivalent to the modern digitally modulated communication signals need to be developed.
Concurrent to the trends in electronic products, new EMC test facilities were developed [95], which can be useful for testing above 1 GHz. The performance of emission measurements and immunity tests above 1 GHz is a logical consequence of the trend that products increasingly utilize frequencies above 1 GHz, and the enormous growth of all types of wireless communication systems that operate at frequencies above 1 GHz. The Fully Anechoic Room (FAR) and the Reverberation Chamber (RC) are two examples of such new facilities. A picture of the RC as EMC test facility is shown in Figure 1.3. However, when different facilities are used for compliance demonstration, the topic of limit conversion arises. Conversion between alternative methods and established methods is recognized as an important topic in getting the alternative methods ready for introduction in EMC product standards. Conversion studies yield emission limits or immunity requirements for specific EMC facilities in order to achieve the same degree of protection or immunity.
Besides the new topics discussed above, also the electromagnetic understanding of current measurement methods is important. This is also related to the subject of uncertainty studies, which aim to discover and quantify possible uncertainty effects. The influence of the properties of receive antennas during radiated emission measurements within Semi Anechoic Rooms (SAR) and the way they are calibrated is subject of maintenance within CISPR/A.

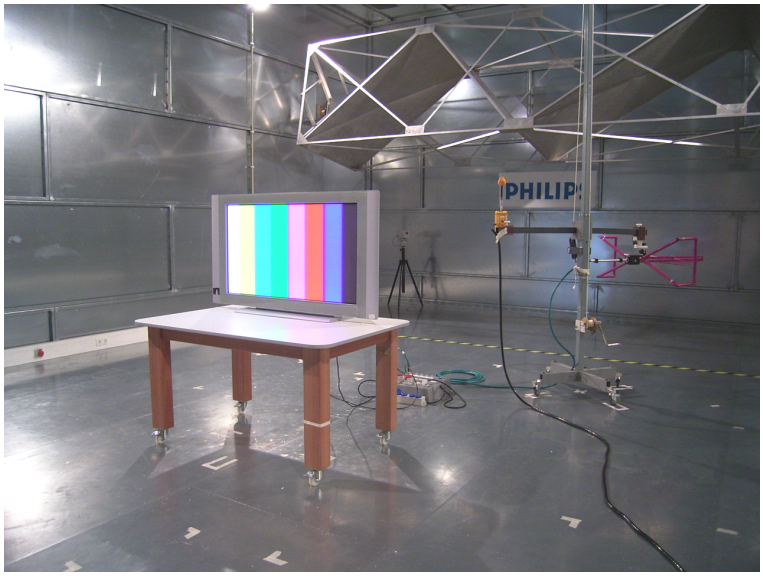


Figure 1.3 Test configuration in the reverberation chamber at the Philips EMC center.

## 1.2 Objectives

In this section, the goals of the thesis are stated. The thesis describes various new concepts for EMC standards applicable to multimedia products. The content of the thesis is focused on the results of three studies. These studies have relevance in covering the trends mentioned in the previous section.

First, a review of both the current status of EMC standardization and the underlying technical issues will be presented in Chapter 2. Chapter 2 is divided into two parts. The first part continues with some trends in EMC standardization. The organization of EMC standardization is explained. One of the topics relevant for the trend of increasing application of digital receivers is the assessment of emission results. For that purpose, the topics of weighting detectors and statistical evaluation of emission results are explored. The current status of the new EMC product standards for multimedia products, CISPR 32 and 35, is reviewed. The first part is finished by a review about the topic of uncertainty.
The second part of Chapter 2 aims to prepare the three main studies of the thesis by exploring the background of the standardization along with technology developments relevant for these studies. The contributions of these studies are defined in this second part of Chapter 2.
The review in Chapter 2 is summarized by presenting a list of priorities of technical topics necessary to adapt the standards in accordance with the trends in electronic products that need to be resolved as explained in Section 1.1.

Subsequently, a study is presented about the uncertainties caused by using different types of receive antennas in Chapter 3. Different types of typical receive antennas are investigated that are commonly used in the field of EMC. Two types of references are used in this uncertainty study, i.e., a tuned-dipole reference and an E-field reference. The E-field reference means that the electric field-strength in absence of the receive antenna is used as reference. The method of antenna calibration is taken into account as well. The study contains many aspects of the modeling of radiated emission measurements. The antenna-type uncertainty is investigated and quantified in the frequency range 30-1000 MHz as well as in the range 1-18 GHz for the 3 m SAR method.

The second study concerns the conversion between radiated emission results obtained in a SAR and a RC. This study is presented in Chapter 4. The SAR and RC are different methods to measure the radiated emission of a product. Insight into the correlation of the emission results obtained by the two methods is important for the determination of emission requirements for the RC method. Therefore, this study is relevant in order to get the RC facility ready as test and measurement method suitable for EMC product standards. The conversion of emission results is investigated with respect to its possible uncertainty parameters. Special attention is paid on the role of the directivity property of the EUT and its significance in the topic of conversion. The conversion factors will be analyzed by using both numerical simulations and experiments.

Chapter 5 presents the third study, in which new concepts of immunity test-signals representative for digitally modulated communication signals are investigated. The following communication signals are considered in this study: GSM, DECT, Bluetooth, wireless LAN, and Ultra Wide Band (UWB) signals. It is preferable that new immunity test-signals can be generated by applying commonly available EMC test equipment. The new concepts for immunity test-signals will be derived by considering different interference scenarios.

Finally, the thesis will be completed by a summary of the conclusions and an outlook to future research topics.

# 2 Review of developments in EMC standardization

This chapter contains two parts. The first part is an extension of the topics mentioned in Chapter 1 and are presented in Sections 2.1-2.5. The organization of EMC standardization is overviewed in more detail. Furthermore, the standardization along with the technology developments are reviewed related to the trends in electronic products. For that purpose, the subjects of weighting detectors and statistical evaluation of emission are reviewed. The new EMC product standards for multimedia products are reviewed. Some words are spent to review the subject of uncertainties.
The second part of this chapter includes reviews of technology and standardization developments. These reviews can be seen as preparations on the three main studies of the thesis and are presented in Sections 2.6-2.8. For that purpose, the standardization developments concerning receive antennas are reviewed. The trend of increasing use of alternative measurement methods was introduced in Chapter 1. Therefore, the developments of the Fully Anechoic Room (FAR) and the Reverberation Chamber (RC) methods are explored. It is explained that the increasing application of alternative measurement methods raised the question how different emission results obtained from different methods correlate. This question introduces the subject of conversion of emission results and conversion of limits. The developments concerning immunity test-signals are reviewed. This chapter is completed with a summary of the review by presenting a list of seven topics necessary for an appropriate adaptation of the standards.

## 2.1 Organization of the EMC standardization process

In the introduction of the thesis already some aspects of the standardization process were explained briefly. More details are presented in this section. EMC standards are developed within the International Electrotechnical Commission (IEC) framework. Two IEC committees, TC 77 and CISPR, are responsible for development of basic EMC standards. In addition, IEC product committees develop product specific EMC standards that use these basic standards. An overview of the organization of IEC work on EMC is shown in Figure 2.1.

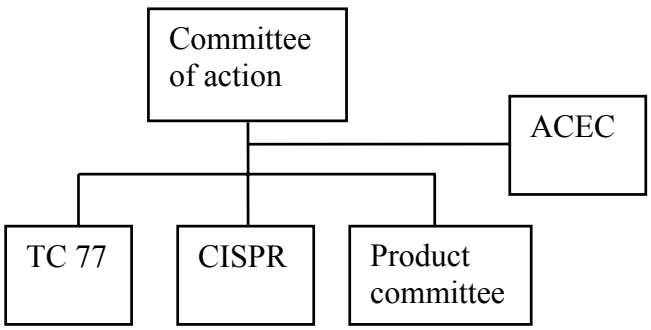


Figure 2.1 Organization of EMC standardization in IEC (source: IEC Guide 107 [52]).

The Advisory Committee on Electromagnetic Compatibility (ACEC) is a committee in the field of EMC and its responsibility can be summarized as follows:

- coordinating the EMC work of various IEC technical committees,
- avoiding duplication of efforts by advising on allocation of tasks,
- preventing conflicting standards,
- coordinating the EMC work of the IEC and other organizations,
- identifying market needs.

Technical Committee (TC) 77 is a technical committee with a horizontal function primarily responsible for basic standards for immunity in the whole frequency range and for emission in the low frequency range (≤9 kHz). Definition of standards for the low frequency phenomena is the responsibility of Sub Committee (SC) 77A. For the topics discussed in this thesis, especially the immunity standards developed and maintained by SC 77B are relevant. These standards have typically a reference number IEC 61000-4-#, where # is a specific number covering a specific immunity aspect. For example, the radiated immunity test method is described in IEC 61000-4-3 [53].
Both subcommittees can handle emission as well as immunity standards, but for SC 77B, the RF-emission (>9 kHz) is handled by CISPR. CISPR is an IEC technical committee with a horizontal function. Originally, CISPR was a separate committee for radio protection. CISPR is primarily responsible for developing the following types of standards in the Radio-Frequency (RF) range above 9 kHz:

- basic EMC standards for unwanted RF emissions (CISPR/A),
- generic EMC standards with regard to unwanted RF emissions (CISPR/H),
- product and product family emission standards for radio protection,
- immunity standards for sound and television broadcasting receiving installations,
- product and product family immunity standards.

CISPR consists of different subcommittees, CISPR/A through CISPR/I. In CISPR/A the standards for the emission measurement methods are developed and maintained as well as the requirements for measurement equipment, e.g., the facility, receive antenna, EMI receiver. CISPR/H develops and maintains generic standards related to the definition of new limits. CISPR/I is the merger of the former subcommittees E and G and is the product committee responsible for the definition of standards for multimedia products. Other examples of product committees are CISPR/B for Industrial Scientific and Medical (ISM) equipment, CISPR/D for products applied in vehicles, and CISPR/F for domestic appliances. CISPR/S is the CISPR steering committee responsible for coordination and communication between the various CISPR subcommittees.
Specific EMC standards for a particular product or environment may be developed by an IEC product committee when the TC 77 and CISPR standards are not considered suitable. For example, the IEC 61326 standard for measurement and laboratory equipment or the IEC 60601 standard for medical equipment.

## 2.2 The assessment of emission results

One of the trends in electronic products is the application of an increasing number of radio-communication systems equipped with digital receivers. In addition, the replacement of analog TV broadcasting by digital TV broadcasting was identified in Chapter 1. This means that the conventional assessment of emission for protection of analog receivers should be reconsidered. In this section, the developments concerning weighting detectors and statistical evaluation of emission are considered.

### 2.2.1 Weighting detectors

Radiated and conducted emission measurements are performed to prevent radio interference. This is performed by using a transducer (coupling network or antenna) and a receiver. The human perception of interference is taken into account in conventional radiated emission measurements by applying the quasi-peak weighting detector in the CISPR measurement receiver. A weighting detector can be seen as a 'translation' of the measured emission by taking its annoyance effect into account. The quasi-peak detector was optimized for protection of analog (AM) radio receivers. The perception of the received interference in digital radio receivers can be expressed objectively by using the Bit Error Probability (BEP). When the traditional CISPR (analog) receiver is to be used for testing the radiated emission impact on digital radio receivers, we need different weighting detectors. Such a weighting detector can be seen as the perception by digital receivers of the received interference expressed into the associated BEP.
CISPR/A has anticipated on the increasing application of digital receivers by developing a new weighting detector, i.e., the Root Mean Square-Average (RMS-AV) weighting detector. This detector was developed by investigation of various types of digital radio-communication systems [82]. Further technical background about the development of the RMS-AV detector can be found in [85][86].
In Figure 2.2, an overview is presented of the conventional weighting detector curves (Quasi-peak, Peak, and Average) and the RMS-AV weighting detector curve. A weighting curve defines the permitted interference level for a fixed BEP as a function of the Pulse Repetition Frequency (PRF) of the interference signal. The RMS-AV weighting curve of Figure 2.2 is proposed for publication in CISPR 16-1-1 for band C and D (30-1000 MHz).

### 2.2.2 Statistical evaluation

Statistical methods are useful because they provide insight into the probability of some important parameters of the radiated emission signal. Mostly, we are interested in the probability density or distribution of the amplitude level of the signal or its envelope in the time domain. In [27], already the Amplitude Probability Distribution (APD) was introduced as useful statistical function in the characterization of signals.

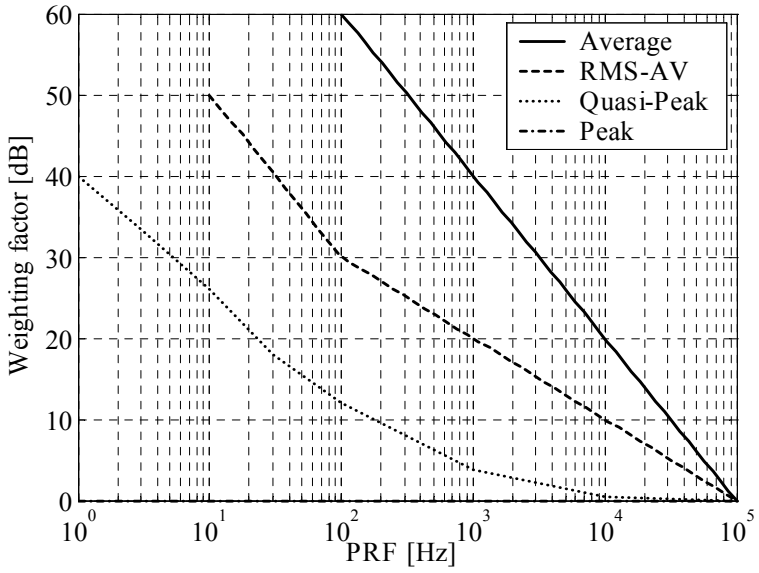


Figure 2.2 Weighting curves applicable for Average, RMS-AV, Quasi-Peak, and Peak detector.

Detailed information about the use of the APD in relation to radiated emission measurements can be found in [90][91]. The APD function expresses the probability *cc*(*a*) that a random variable "*A*" will have a realization larger than "*a*":

$$APD(a) = cc(a) = P(A > a) \qquad \Rightarrow \qquad cc(a) = 1 - c(a) \tag{2.1}$$

where *c* stands for the Cumulative Distribution Function (CDF) and *cc* stands for the Complementary CDF that is equal to the APD. The APD can be measured by using a spectrum analyzer at the Intermediate Frequency (IF) output at a fixed frequency and certain resolution bandwidth (RBW). In Chapter 5, we will use MatLab software to simulate the spectrum analyzer including its APD capability in order to investigate the relevant parameters of new immunity test-signals. The APD can also be measured in the time domain, e.g., by using an oscilloscope.

Recently, the APD is also subject of investigation in CISPR/A as a new method to assess radiated emission in CISPR 16-2-3. Using the APD for that purpose, a 'two-dimensional' limit will be applied, i.e., the emission level along with the probability of exceeding that emission level. In conventional radiated emission measurements, the assessment is performed by comparing the radiated emission to a fixed limit line.

In [41], the correlation between APD and BEP is demonstrated as well as the correlation between the APD and the RMS-AV weighting detector. The use of a weighting detector is more suitable from a practical point of view, because it can be applied in the same way as the conventional weighting detectors. The APD method, however, gives the opportunity to quantify protection levels for specific communication systems. Therefore, the APD emission method can be seen as a new way in the field of radio protection with potential opportunities for spectrum management.

## 2.3 The new emission product standard CISPR 32

The new CISPR 32 emission standard is currently under development within WG 2 of CISPR/I. The emission standard CISPR 32 contains conducted and radiated emission measurements for multimedia products. Multimedia products are defined as products that have any kind of audio, video, or IT function. Examples of IT functions are: data processing, data storage, measurement, and computation. In March 2006, the first Committee Draft (CD) was circulated to the National Committees (NC). The purpose of the new emission standard CISPR 32 is to replace the current Audio and Video (AV) emission standard CISPR 13 as well as the Information Technology Equipment (ITE) emission standard CISPR 22 in the future. This means that the scope of products that are covered by this standard is expected to be enormous. It will be the main standard for emission measurements for the typical multimedia products present in the home environment discussed in Section 1.1 (Figure 1.1).

*Radiated emission measurement*

The radiated emission measurement in accordance with the CISPR 32 standard can be performed by applying various measurement methods. By using one of these measurement methods, compliance of an EUT may be demonstrated. This will give test houses with several facilities considerable flexibility. However, the possibility of using completely different methods for compliance demonstration of the same EUT is also an enormous challenge for the conversion of emission results necessary for proper limit setting as will be discussed in Section 2.7. CISPR 32 prescribes a system-test like CISPR 22. A system-test means that the EUT is measured in a way representative for the customer application including its associated equipment. For example, a combination of PC, PC loudspeakers, and printer or a combination of TV and home cinema set. The system-test satisfies the trend that products increasingly become part of a system or network as discussed in Section 1.1. The new emission standard CISPR 32 includes also emission requirements for the range 1-6 GHz. At frequencies above 1 GHz, the RC measurement method, the FAR measurement method, and the OATS/SAR measurement method may be used. In the lower frequency range (30-1000 MHz), both the SAR and FAR measurement methods may be used for radiated emission measurements.

*Conducted emission measurement*

In CISPR 13, conducted emission measurements are only prescribed for the mains connection. Within WG 2 of CISPR/I, the question arises whether conducted emission measurements on the antenna port are necessary. To address that issue, a questionnaire was sent to the NCs. The main questions were: are there any interference issues noticed or can we expect interference issues in the future when the conducted emission measurements on the antenna ports are omitted? Some interference issues were noted. Experiments with a TV and DVD player have shown that for some ‘simple’ equipment conducted measurements on the antenna port deemed not to be necessary [31]. Simple in this sense

means equipment including only a mains and antenna connection. However, exceptions were found as well. In other words, a general conclusion about omitting conducted emission measurements on antenna ports could not be drawn. It was therefore decided to manage the antenna port similarly as the telecom port as currently in the CISPR 22 standard.

*Screening effectiveness of tuners*

The screening effectiveness measurement for tuners in the current CISPR 20 standard (immunity) will be replaced to the CISPR 32 standard (emission) because the underlying interference scenario is actually an emission issue. The cable network in combination with the EUT should comply with the maximum radiated power requirements addressed in the EN 50083-2 standard [35]. These requirements are needed, because central antenna installations share frequency ranges with aviation and emergency services. An insufficiently screened tuner or a bad connector may cause emission in these bands via the antenna cable. To cover this interference scenario adequately in the CISPR 32 standard, a system-test in a radiated emission configuration is proposed instead of the absorbing clamp method described in CISPR 20. In this way, the screening effectiveness measurement can be performed faster (in combination with the radiated emission measurement) and is more relevant from a practical point of view.

## 2.4 The new immunity product standard CISPR 35

*Radiated immunity*

The first phase in the development of a multimedia EMC product immunity standard was started in the Spring of 2006. The aim of this work is to merge the immunity standards CISPR 20 and CISPR 24. The general concept of the new CISPR 35 immunity standard is based on the use of basic standards (IEC 61000-4-series). The performance criteria for specific product functions (e.g., video, audio, copy, data storage) will be placed in annexes. In this way, a logically structured document can be obtained. An important issue is the conversion from TEM waveguide (Jacky) immunity requirements defined in CISPR 20 towards FAR requirements in accordance with IEC 61000-4-3 and used in CISPR 24. The conversion is needed because of the limited operational range (up to 150 MHz) of the TEM waveguide. A Document for Comment (DC) of the CISPR 35 standard was circulated to the NCs in March 2006. The first CD is expected in March 2007.

*Conducted immunity*

Within CISPR/I WG 4 (CISPR 35), a proposal of British Telecom (BT) [74] was discussed about an additional conducted immunity test by applying broadband noise in order to test x-type Digital Subscriber Lines (xDSL), which are very often applied for broadband internet connection. The motivation for such a test is the occurrence of field problems of

many xDSL applications when they are subject to broadband emission in the range 150 kHz-80 MHz. It was decided to include this proposal in the CISPR 35 DC. From this development, it is observed that new kinds of disturbance signals enter into the standardization process. In Chapter 5, a study about new concepts for immunity test-signals equivalent to typical digital communication signals is presented. Furthermore, the conducted immunity test of CISPR 24 is adopted, which is described in basic standard IEC 61000-4-6.

## 2.5 Uncertainties

The topic of uncertainty is introduced and reviewed here because it plays an important role in Chapters 3 and 4 of this thesis. Therefore, some background concerning standardization activities and technical developments is presented.
These days, accredited test houses are obliged to derive the uncertainty budgets of their radiated emission compliance measurements in accordance with the ISO/IEC 17 025 standard [57], which is one justification to quantify possible uncertainty sources. Uncertainty of radiated emission measurements is an important topic within CISPR, especially within WG 2 of CISPR/A. The uncertainty expresses the lack of reproducibility when an emission measurement is reproduced in accordance with the same emission standard and by using a test configuration validated in the same way. In order to obtain a qualitative insight into the uncertainties, CISPR/A started the compliance uncertainty project [39]. In this context, an extensive Round-Robin Test (RRT) was performed in the frequency range 30-300 MHz [40]. This RRT demonstrates that the EUT configuration including its corresponding cable routing already causes substantial uncertainty. This RRT was supported by numerical simulations as described in [23][24]. These simulations were based on Pocklington's thin-wire approximation and a conjugate-gradient iterative solver [88][96]. From these numerical simulations, it was demonstrated that numerical tools are very useful in uncertainty and parameter studies. Efficient numerical computations for parameter studies can be achieved by using marching-on-in-anything (time, location, frequency) algorithms [10].
Uncertainty tables are included in CISPR 16-4-2 [17] for various radiated emission measurement configurations. It should be stated that these CISPR tables only include instrumentation uncertainty and omit uncertainties caused by the EUT configuration itself. In practice, the latter uncertainty is in general larger than the instrumentation uncertainty. Examples of instrumentation uncertainties are: uncertainty of the measurement facilities themselves, the measurement equipment, cable losses and mismatch uncertainties, geometrical uncertainties (turntable step size, height-scan step size, measurement distance), and uncertainties related to the receive antenna. The combination of separate instrumentation uncertainties results in so-called $U_{\mathrm{CISPR}}$ uncertainty values for 3 m and 10 m SAR measurement configurations. The results of an Inter Laboratory Comparison (ILC) [9] confirm the $U_{\mathrm{CISPR}}$ uncertainty values for practical circumstances.

## 2.6 Receive antenna characterization

For the measurement of the radiated emission emanating from an EUT, receive antennas are used. A radiated emission measurement configuration by using a bilog antenna is shown in Figure 2.3. A bilog antenna consists of a biconical/bow-tie part and a log-periodical part [77]. Conventionally, an Open Area Test Site (OATS) or Semi Anechoic Room (SAR) was used for the radiated emission measurement. The measurand of this OATS/SAR method is defined as the maximum emission found after height scanning of the receive antenna, after rotating the EUT in 360°, and after measuring the horizontal and vertical polarization. The height-scan range of the receive antenna depends on the measurement distance and is 1 - 4 m for 3 m and 10 m distance and 1 - 6 m for 30 m distance.
Conventionally, the measurand of the OATS/SAR method was defined by using tuned dipoles as receive antennas. These antennas are known as CISPR reference dipoles. Recently, it was decided in CISPR to adopt the electric field-strength in absence of the receive antenna as the maximum emission measurand. This is called the E-field reference. The E-field reference makes sense for two main reasons. Firstly, the corresponding limits are also defined in electric field-strengths. Secondly, it makes sense that the measurand of a radiated emission method is independent of the applied receive antenna because many types of receive antennas may be used in practice. However, the E-field reference is a theoretical quantity because a receive antenna is always needed to measure electric field-strengths in practice.
A proper definition of the measurand is important because it is used as reference for the quantification of uncertainties. Subsequently, specifications for instrumentation are needed to achieve certain levels of uncertainties. This makes clear that the measurand of a radiated emission method is important for the complete definition and specification of the measurement and applied instrumentation. It is useful to remark that within CISPR also the measurement sites themselves are defined as instrumentation. For conversion of emission results a proper measurand is also important as is explained in Subsection 2.7.3.

The receive antenna is characterized by its frequency dependent Antenna Factor (AF). This means that the receive antenna properties are represented by using a single number and applied in a measurement facility including an electrically conducting ground-plane. This means that a direct wave and a reflected wave are incident on the receive antenna. Years ago it was already suggested that the use of AFs might cause deviations [34][40] even if the calibration is performed accurately.
The maximum measured voltage is converted to electric field-strength by using the AF. The AF of a receive antenna can be determined in various ways. The American National Standards Institute (ANSI) standard C63.5 defines the standard-site method for determination of the AF [3]. Another way of AF definition is the free-space method. The project team for antenna calibration within CISPR/A WG 1 is currently working on calibration methods for defining AFs for both radiated emission measurements and site validation. This work is intended as a future amendment to CISPR 16-1-5.

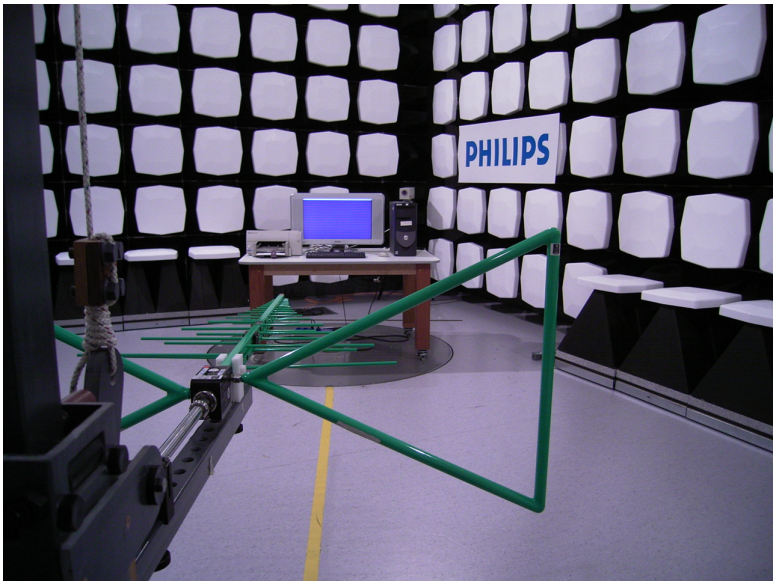


Figure 2.3 Radiated emission configuration within a SAR by using a bilog antenna.

The current CISPR 16-1-5 standard includes only information about the specifications for antenna calibration sites. A site for antenna calibration is called a Calibration Test Site (CALTS) within CISPR. A CALTS is an OATS or SAR with a measured SA deviating not more than 1 dB compared to the calculable Site Attenuation (SA). The SA for CALTS specification is determined by applying tuned dipoles. Currently, it is discussed in CISPR/A how useful receive antenna specifications can be set. The current specifications are only defined for 10 m sites and are not related to deviations in radiated emission results, i.e., they are not related to a properly defined measurand. A new maintenance cycle for specifications of receive antennas has started in 2007.

In Chapter 3, a study is presented of the deviations in radiated emission results caused by the use of different types of receive antennas characterized by their AF. The deviations in radiated emission results are investigated for receive antennas calibrated by using both the free-space method and the standard-site method. As mentioned above, the conventional measurand is defined by using tuned dipoles as receive antennas. Therefore, the deviations due to the use of different receive antennas are investigated by using the tuned-dipole reference. It was explained above that a new measurand was introduced in the standard, i.e., the E-field reference. It was noted that this is an interesting measurand because it is independent of the receive antenna. Therefore, the deviation is also investigated by using the E-field reference. This gives the opportunity to compare the two measurands with respect to the associated antenna-type uncertainty. The investigations are combined with considerations of the antenna-pattern specifications of the receive antennas, like directivity and beamwidth specifications. The study presented in Chapter 3 contributes to the insight into possible deviations caused by using different types of receive antennas. This insight may be used for defining reasonable approximations for the expected uncertainty and it can support the definition of relevant specifications for receive antennas.

## 2.7 Development of alternative measurement methods

Emission methods described in basic standards for which limits are defined are called established methods. These methods have proven to be able to protect the radio systems adequately for many years. The OATS/SAR method is the best-known example of an established method. The method is described in CISPR 16-2-3 and the associated radiated emission limits are defined in, e.g., the CISPR 22 standard for Information Technology Equipment (ITE). Alternative measurement methods are defined as methods that are described in basic standards, but limits are not yet available in IEC/CISPR standards. The Fully Anechoic Room (FAR) and Reverberation Chamber (RC) are examples of test facilities that can be used as alternative for radiated emission measurements. When various methods are used to measure the radiated emission of an EUT, then the question raises how the obtained results correlate.

### 2.7.1 Fully Anechoic Room

The FAR method for radiated emission measurements has started as a European standard. Nowadays this method has also been included into CISPR 16-2-3. The FAR has also absorbing material at the bottom. Therefore, the ground reflection as present within the SAR does not exist in the FAR. The main benefit of a radiated emission measurement using the FAR is that no height scan of the receive antenna is required. This benefit results in less measurement time and smaller chambers. The validation method of the FAR in the range 30-1000 MHz is based on the Normalized Site Attenuation (NSA), which is also used in the validation method for the OATS and the SAR in the same frequency range. The requirement is that the NSA deviation is less than ±4 dB.
A few years ago, a new radiated emission measurement method for the frequency range 1-18 GHz was published in CISPR 16-2-3 Amendment 1. This new method is based on a FAR. The measurement distance may be chosen in the range 1-10 m. The method does not prescribe a height scan of the receive antenna. This aspect of the method was investigated and significant deviations in radiated emission results were found [38][68]. The deviations were determined by comparing the results obtained with and without performing a height scan. The deviations are caused by omitting the height scan of the receive antenna. These results have caused the maintenance of the current standard. The proposal is now to perform a height scan over a limited range. At small measurement distances (<2 m), it was found that near-field contributions can deteriorate the radiated emission results [7], i.e., the straightforward far-field transformation is not suitable for small measurement distances.
A Joint Task Force (JTF) was initiated in order to develop a general FAR standard for both radiated emission and radiated immunity. The reference number of that new standard is IEC 61000-4-22. The JTF is a cooperation between CISPR/A and SC 77B.

### 2.7.2 Reverberation chamber

The RC provides application of a measurement method based on an overmoded cavity. This is a reflective chamber that physically operates as a resonant cavity from which the modes (standing wave patterns) are continuously varied by rotating one or more stirrer(s). A stirrer is an electrically conducting paddle wheel that varies the electromagnetic boundary conditions. Conventional measurement methods like the OATS/SAR or FAR are deterministic methods and based on straigthforward wave propagation. These methods aim to measure the maximum electric field of an EUT at a certain measurement distance in a free-space or semi-free space environment. The RC method is a statistical method and utilizes multiple reflections in a shielded enclosure. This method aims to find the total radiated power of an EUT by taking samples at various stirrer positions. In the RC method, the total radiated power of the EUT is measured, which can be converted to electric field-strength if a reasonable directivity approximation of the EUT can be made. By using the OATS/SAR or the FAR method, the emission is measured by converting the measured voltage to electric field-strength by using the Antenna Factor (AF) of the receive antenna. In conclusion, the radiated emission of an EUT is measured within the RC in a quite different way than within anechoic types of chambers.
The standard for the RC method is IEC 61000-4-21 [54]. This standard includes a site validation method, a radiated emission method, and a radiated immunity test method. Technical aspects of this standard and the theoretical background of the RC emission method are discussed in Chapter 4. A maintenance cycle of the IEC 61000-4-21 has started in 2006. The IEC 61000-4-21 is also the responsibility of a JTF.

### 2.7.3 Conversion

In Section 2.3, it was introduced that the current CISPR 32 draft standard allows several radiated emission methods to demonstrate compliance. This is one of the indications of the increasing application of alternative measurement methods. It was explained in the previous subsection that the RC method, the OATS/SAR method, and the FAR method are all different methods that capture a maximum emission of an EUT in a quite different way. Because of the increasing availability and application of alternative measurement methods, the following question raised: how can we correlate the emission results of an EUT obtained from different measurement methods? This is important when product committees are interested in introducing alternative measurement methods in EMC product standards. Introduction of alternative measurement methods can only be performed if a corresponding limit can be given.
For that purpose, a project team for alternative measurement methods was initiated within WG 2 of CISPR/A a few years ago. The result is a Technical Report (TR) published in CISPR 16-4-5 [18]. The TR contains a conversion method and examples for conversion of OATS and FAR results based on numerical simulations.
The advantage of this conversion method is that it starts with the definition of the reference quantity. This reference quantity is the ‘target’ quantity useful for radio protection, e.g., the maximum radiated electric field-strength at a certain distance of the EUT. The use of the

reference quantity is useful because both the established method and the alternative method may deviate from this reference quantity. In this way, the same degree of protection is expected. The same degree of protection means that the conversion should result in a limit for the alternative method that yields the same pass and fail probability as the established method.

The conversion method is applied to radiated emission results obtained from the RC in Chapter 4. This study contributes by presenting the application of the conversion method when RC results are involved. It contributes by an extensive discussion concerning the uncertainties of the RC method compared to the uncertainties of the SAR and the FAR methods. The instrumentation uncertainty (e.g., site and test equipment) is considered as well as the so-called 'measurement method uncertainty' or 'inherent uncertainty'. This uncertainty is caused by the method itself. For example, horizontally polarized emission cannot be found in the SAR measurement at low frequencies (30-100 MHz) due to the limited height scan (1 - 4 m). Also the directivity of the EUT may cause inherent uncertainty. The uncertainty comparison is an important step in the conversion method because it has influence on the pass and fail probability. The study contributes by the determination of the conversion factors for calculable EUTs, e.g., isotropic point sources, tuned dipoles, and a fixed dipole. Furthermore, the study contributes by analyzing the influence of the directivity of EUTs on the inherent uncertainty and deviation. This is done by evaluating a statistical EUT model and by applying this model to the conversion method, by performing simulations of a fixed-length dipole, and by measurements of an artificial EUT (coplanar strips). Finally, the study contributes to the determination of conversion factors based on measurement results of realistic CISPR 22 system-test EUT configurations. The study demonstrates the suitability of compliance measurements for CISPR 22 system-test EUT configurations performed within the RC.

## 2.8 Immunity test-signals

From the increasing application of radio-communication systems integrated into multimedia products, it was concluded that new potential disturbance sources are present. These new potential disturbance sources are originating from the radio-communication systems. Typically, the signals of these systems are digitally modulated and the systems typically operate at frequencies above 1 GHz. Conventionally, the 1 kHz 80% Amplitude Modulated (AM) immunity test-signal is applied in conducted and radiated immunity tests. The case given in Section 2.4 about conducted immunity tests (CISPR 35) for xDSL types of lines by using impulsive noise immunity test-signals may also be seen as an example of changing specifications for immunity test-signals. New radio-communication signals, evolving victim products, and changing applications cause the need for other and more representative immunity test-signals. For example, a change in application is that conventional immunity tests were performed for protecting products against broadcast signals relatively far away, but nowadays the radio-communication signals are integrated into multimedia products and are in the vicinity of other products in the home. Moreover,

the conventional interference mechanism was very often the nonlinear detection of products while sensitive receivers integrated into multimedia products are potential new victims nowadays. This means that the interference scenario is substantially changed.
Within CISPR/I WG 4, discussions about immunity tests above 1 GHz are going on, but currently not included in the CISPR 35 draft standard. The basic immunity-test standard IEC 61000-4-3 [53] includes already immunity specifications above 1 GHz. As an example, the product standard IEC 61326 for electrical equipment for measurement, control, and laboratory use refer to the above 1 GHz specifications of IEC 61000-4-3 by specifying immunity requirements up to 2.7 GHz.
In Annex A of the immunity-test standard IEC 61000-4-3 [53], results are presented about interference levels of various products when subjected to Time Division Multiplexing (TDM) radio-communication signals, like GSM and DECT. It was concluded that the 1 kHz 80% AM test-signal is always the worst case. This conclusion, however, is not in compliance with the presented results. In addition, the investigations presented in Annex A of IEC 61000-4-3 do not anticipate on the changing application of radio-communication systems in multimedia products and the corresponding interference scenario. This means that the term 'worst case' test-signal is not relevant because it only defines something about the interference level and nothing about the interference scenario. The relevant question is: what is the representative case?

New concepts of immunity test-signals are developed in Chapter 5. This is performed by considering two interference scenarios, i.e., the conventional interference scenario and the coexistence interference scenario. These interference scenarios are defined and used to develop relevant immunity test-signals that should be simple from a practical point of view. Simple means that preferably existing and commonly available test equipment should be used for the generation of the new test-signals. The following communication signals are considered in this study: GSM, DECT, Bluetooth, wireless LAN (OFDM), and Ultra Wide Band (UWB) signals. The study in Chapter 5 contributes by the specification of immunity test-signals representative for modern digitally modulated radio-communication signals. Using a relatively common set of EMC test equipment can generate these new test-signals. MatLab simulations are used to support the specifications of the new test-signals. In this way, conventional and relevant coexistence immunity tests can be performed with minor additional investments. These concepts may be used for future specifications of new test-signals in EMC standards.

## 2.9 Summary

Various developments in the area of EMC standardization and measurement techniques were reviewed in this chapter. In [27], the results of an evaluation study were presented concerning the research agenda to develop appropriate EMC standards to cope with the trends in electronic products. This evaluation resulted in a list of seven topics where new developments of the standards are necessary:

1. extension of radiated emission measurements above 1 GHz,
2. development of a new weighting detector for digital receivers,
3. development of new statistical techniques (e.g., Amplitude Probability Distribution (APD)) for processing of radiated emission measurement results,
4. extension of radiated immunity tests above 1 GHz,
5. extension of radiated immunity tests by using digitally modulated signals,
6. development of alternative measurement methods,
7. development of multimedia EMC product standards.

The first six topics are necessary to make topic 7 possible, i.e., the development of adequate EMC product standards for multimedia products.
The review in this chapter was partially obtained from the mentioned evaluation study [27]. The Chapters 3-5 contain the main contributions of the thesis about the following subjects:

- receive antenna related deviations in radiated emission results,
- conversion of emission results obtained from the Reverberation Chamber (RC) method,
- new concepts for immunity test-signals.

These studies may contribute to future standardization concerning the topics 1, 4, 5, and 6 of the list of seven topics listed above and may therefore contribute to the development of relevant EMC basic and product standards.

# 3 The receive antenna in radiated emission measurements

In this chapter, the uncertainty related to the receive antenna will be subject of investigation. Various parts of this chapter were published earlier [25][26]. A few years ago, CISPR subcommittee A has started to improve the radiated emission standard by quantifying most of the uncertainty sources as already introduced in Section 2.6. In that section, the uncertainty was defined as the lack of reproducibility when an emission measurement is reproduced in accordance with the same emission standard and by using a test configuration validated in the same way. In radiated emission measurements, the receive antenna radiation properties are expressed by a single figure of merit, namely, the Antenna Factor (AF). This simplified characterization may result in different measurement results when different types of receive antennas are used. These differences are investigated by performing numerical analyses for a 3 m SAR measurement configuration. The analyses are performed in the frequency range from 30 MHz to 1000 MHz as well as in the range from 1 GHz to 18 GHz.

## 3.1 Formulation of problem

Radiated emission measurements are performed at a site with an electrically conducting ground plane, e.g., an OATS or a SAR. An overview of the measurement configuration is shown in Figure 3.1. The goal of the radiated emission measurement is to find the maximum emission of an EUT. The conducting ground plane causes a reflection. This means that two waves are incident on the receive antenna, a direct wave and a reflected wave. The two waves interfere, constructively or destructively at the point of the receive antenna. In order to measure the maximum emission, the receive antenna is scanned in height and is rotated to measure in horizontal and vertical polarization. The EUT is rotated 360° by using a turntable. The antenna signal is measured by using an EMI receiver. Subsequently, the measured voltage is converted to electric field-strength by multiplying with the AF of the receive antenna. So, the measurand of a radiated emission measurement performed at an OATS is: the maximum emission after the height scan (1 - 4 m) of the receive antenna, after measuring the horizontal and vertical polarization, and after rotating the EUT over 360°. In the definition of the measurand the maximum emission can be related to two references: the tuned-dipole reference and the E-field reference. A review of these references has been given in Section 2.6. Two calibration methods are mainly used for determining the AFs of receive antennas. A free-space determined AF is often used, while the antennas are used within chambers which have highly conducting ground planes. The ANSI C63.5 standard-site method is another calibration method that can be used to determine AFs including a ground-plane effect [3][59][81]. These two methods are explained in the next section.

Several types of receive antennas are used for radiated emission measurements. In the past, the application of different receive antennas was justified under the following assumption: if the AFs of different antennas are known accurately, then the different receive antennas should give the same result in a radiated emission measurement. However, various investigations [34][40][60] suggest that the AF is not always an adequate figure of merit to describe the overall antenna performance in the case of a non-uniform incident plane-wave configuration, which is always the case in measurement chambers containing a ground plane.

For that reason, this uncertainty source is investigated in this chapter. The deviations caused by using different types of receive antennas are considered for the two references (tuned dipole and E-field). Moreover, the influence of the two types of AF calibrations (free-space and standard site) on the deviations is considered. The deviations are investigated for 3 m sites. Details about the AF calibration method are given in the next section. The Sections 3.3-3.5 discuss the analysis of the deviation in the frequency range 30-1000 MHz. The deviation $\Delta E_{rad}$ is defined as the measured radiated emission $E_{rad}$ by using the receive antenna minus the reference radiated emission $E_{ref}$:

$$\Delta E_{rad} = E_{rad} - E_{ref}, \tag{3.1}$$

where $E_{ref}$ is the reference obtained by using either the tuned-dipole reference antenna or the E-field reference (Section 2.6). The $E_{rad}$ is obtained by a receive antenna that is calibrated by using either the free-space method or the standard-site method.

The deviation in the frequency range 1-18 GHz is discussed in Section 3.6. In the analysis above 1 GHz, the radiated emission method of the Federal Communications Commission (FCC) part 15 standard [36] is used, i.e., an OATS/SAR method applied to frequencies above 1 GHz as well. The motivation for this choice is explained in Section 3.6.

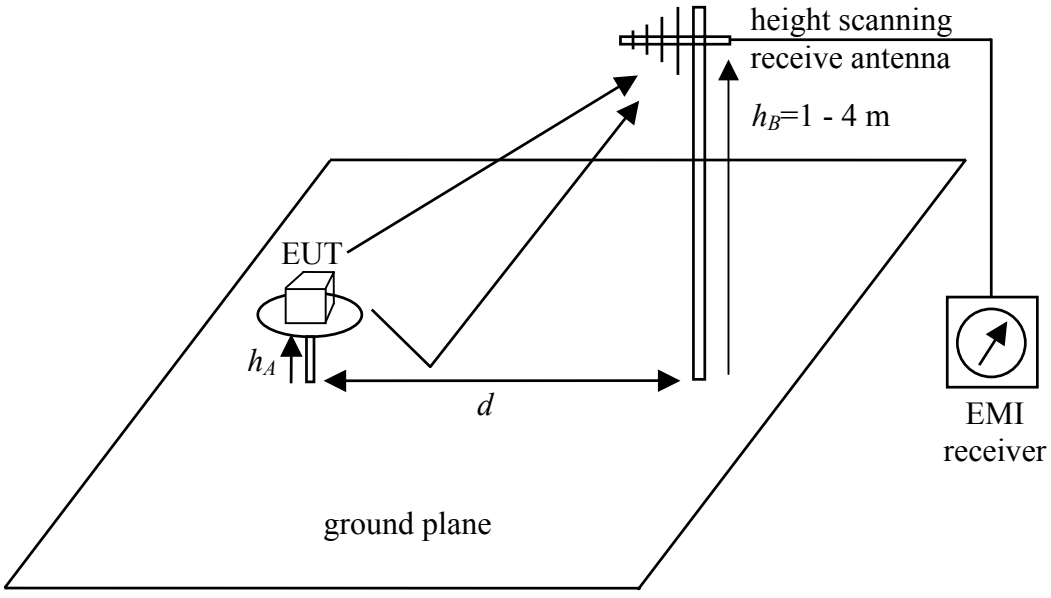


Figure 3.1 Radiated emission measurement configuration.

## 3.2 Receive antenna calibration

In this section, a brief overview of the two main calibration methods is presented. After this section, the uncertainty due to the use of different types of receive antennas will be investigated using the free-space method as well as the standard-site method. For a useful and practical introduction to antenna calibration focusing on EMC applications, we refer to a guide of the National Physical Laboratory in the UK [2].

### 3.2.1 Free-space method

The free-space antenna factor of a receive antenna can be determined by using the configuration depicted in Figure 3.2. The shown dipole antenna is only meant as example. The antenna is illuminated by a uniform plane wave denoted by $E_r^i$, which is the incident electric field. This illumination of the antenna will generate a received voltage $V_r$ over the termination impedance $Z_L$ of the antenna. By using the incident electric field and the corresponding received voltage, the free-space AF of the receive antenna can be defined as follows:

$$AF = \frac{\left|E_r^i\right|}{\left|V_r\right|}. \tag{3.2}$$

The unit of AF is $m^{-1}$. After the radiated emission measurement, the received maximum voltage, $V_r^{\max}$, is multiplied with the AF in order to obtain the maximum radiated emission expressed in terms of electric field:

$$E_{rad}^{\max} = V_r^{\max} \cdot AF. \tag{3.3}$$

The uniform plane wave necessary for free-space AF calibration can be generated in various ways. A proper and frequently used way of generating a uniform plane-wave for AF calibration purposes is the use of a far-field site.

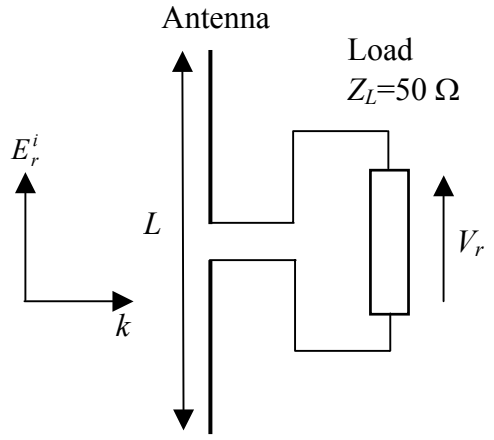


Figure 3.2 Configuration for determining the free-space AF.

The AF and the directive gain, $G$, of the antenna are related by the following equation [87]:

$$AF = \sqrt{\frac{4\pi \cdot \eta_0}{Z_L \cdot G \cdot \left(1-\rho^2\right) \cdot \lambda^2}}, \tag{3.4}$$

where $\eta_0$=377 Ω is the free-space wave impedance, ρ is the coefficient of reflection due to mismatch at the antenna input terminal, $Z_L$ is the impedance of the load at the antenna terminal, and λ is the wavelength.

### 3.2.2 Standard-site method

Besides the free-space AF calibration, the standard-site method as described in ANSI C63.5 can be used as well [3]. In the standard-site method, the calibration is performed at an OATS and the configuration is similar to the radiated emission test configuration where the receive antenna will actually be used. A height scan of the receive antenna (to be calibrated) is performed along with an identical antenna as transmit antenna at a fixed height of 1 m and at a horizontal distance of 3 m or 10 m. So, the test distance applied during the standard-site calibration method and the measurement distance applied in the radiated emission measurement are the same. Both antennas are horizontally polarized for the calibration. Figure 3.3 shows an overview of the standard-site method.

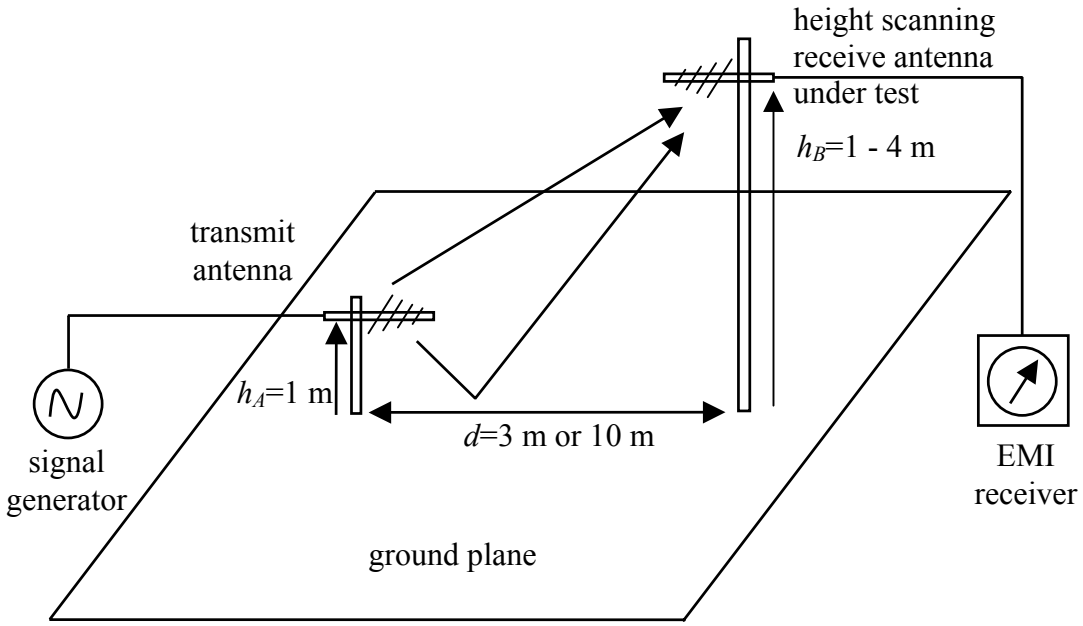


Figure 3.3 Overview of the standard-site method for AF calibration.

The first step in this method is to determine the Site Attenuation (SA) which is defined as:

$$SA = \frac{\left|V_r^{\max}\right|}{\left|V_{through}\right|}, \tag{3.5}$$

where $V_{through}$ is the 'through' voltage measured when the cable connectors at the antenna terminals are connected directly (without antennas) with each other, while $V_r^{\max}$ is the maximum received voltage measured by the antenna under calibration after height scanning (1 - 4 m) [24]. For the standard-site method only horizontal polarization is measured. By using the measured SA determined by two identical antennas, the AF of these antennas can be determined from the following equation:

$$AF = \sqrt{\frac{SA \cdot f_M \cdot E_D^{\max}}{279.1}}, \tag{3.6}$$

In ANSI C63.5, this equation is defined in dBs:

$$AF_{dB} = \frac{1}{2}\left(SA_{dB} + 20 \cdot \log_{10} f_M - 48.92 + E_D^{\max}\right), \tag{3.7}$$

where $f_M$ is the frequency expressed in MHz and $E_D^{\max}$ is the maximum electric field in dB μV/m generated by a tuned dipole, excited with 1 pW input power, on an OATS in the height range 1 - 4 m. The quantity $E_D^{\max}$ is a calculable parameter and is tabulated in ANSI C63.5 and in [81]. In [81], the rationale of the standard-site method is explained. It is emphasized that the standard-site method yields an AF that is specific for the measurement distance, whereas the free-space method yields an AF independent of the measurement distance. The SA and the $E_D^{\max}$ are specific for the measurement distance in Eq. (3.7).

## 3.3 Radiated emission simulation model and approach

To simplify the test setup for simulation purposes, a fixed-length dipole can be used to simulate an EUT, as shown in Figure 3.4. In this way, the actual radiated emission measurement is modeled as a coupling measurement between a transmit and a receive antenna. The analysis of the deviation due to the use of different receive antennas is performed using two types of EUTs (i.e., a large EUT simulated by a 100 MHz resonant dipole ($L_A$=1.5 m), referred to as 'Dip100 EUT', and a small EUT simulated by a 250 MHz resonant dipole ($L_A$=0.6 m), referred to as 'Dip250 EUT'). Both are simulated with a radius of $a$=9 mm. The two EUTs (transmit antennas) are used to investigate the possible influence of EUT size and the corresponding directional behavior on the deviation. The test configuration is simulated by a semi free-space environment and an infinite and perfectly electrical conducting ground plane.

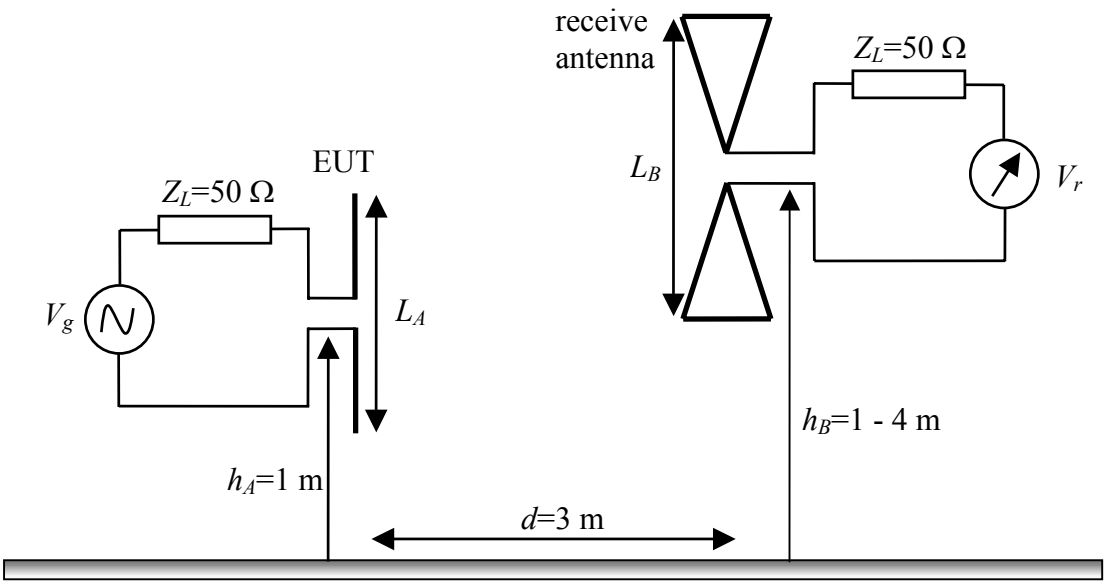


Figure 3.4 Simulation configuration of a radiated emission measurement.

Figure 3.4 depicts a schematic overview of the simulated emission measurement configuration. This configuration is based on the coupling of two antennas at a horizontal distance of $d$=3 m as the equivalence of a radiated emission measurement. In all configurations, the transmit antenna and the receive antenna have 50 Ω terminations. The transmit antenna, used for simulation of the EUT, is placed at a fixed height of $h_A$=1 m and the receive antenna is scanned in height $h_B$=1 - 4 m.
The FEKO software suite by EM Software & Systems was used to perform both the AF and the radiated emission simulations. FEKO is based on the method of moments (MoM). Details about the numerical techniques implemented in FEKO can be found in [22][59].

The following four-step procedure is used to obtain the radiated emission results:

1. determine the free-space AF (Eq. (3.2)) and the ANSI C63.5 AF (Eq. (3.7)) of the various types of receive antennas,
2. determine the maximum received voltage over the height $h_B$ (1 to 4 m, 10 cm step size),
3. convert the maximum voltage into a maximum electric field (Eq. (3.3)) by using the AF (free-space or ANSI C63.5) obtained in step 1,
4. compare the radiated emission results obtained using the various types of receive antennas.

The radiated emission results are compared in step 4 with both reference results obtained by using the tuned-dipole reference (i.e., CISPR reference dipoles) and the E-field reference results. This comparison is discussed in Section 3.5.

The following types of receive antennas are considered in the analysis of the deviation: tuned dipole, biconical antenna, log-periodical antenna, and bow-tie antenna. The simulated log-periodical receive antenna is based on the log-periodical part of the Chase bilog antenna (CBL6141), shown in Figure 3.5. The tip of the log-periodical antenna is depicted in Figure 3.6, where we can see the MoM elements (wire segments and triangular surface elements). Thin wires between the rods and the surface elements are used to create a connection between the rods and the surface elements suitable for the numerical solver, i.e., to prevent numerical problems. The reason is that FEKO needs the nodes for defining the segments on the wire and the triangular segments on the surface to coincide [22, Sec. 5.5].
Two models of biconical antennas are simulated, i.e., a closed-surface model and a wire model shown in Figure 3.7 and Figure 3.8, respectively. The simulated wire-model is based on the Eaton 2198 biconical antenna. The closed-surface model of the biconical antenna will only be used in the AF evaluation (Section 3.4) and not in the simulations of the radiated emission. In addition, also two types of bow-tie antennas are investigated, which are depicted in Figure 3.9. The bow-tie antennas are based on the 'bicon' parts of so-called bilog antennas that consist of a log-periodical part and a bow-tie part [77].

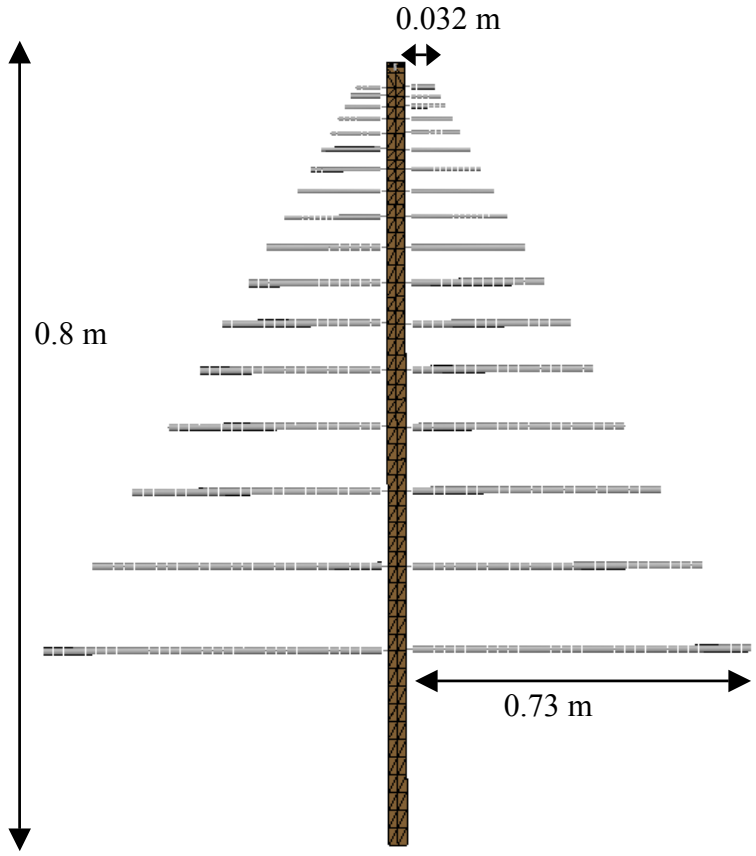


Figure 3.5 Simulated log-periodical antenna discretized in wire segments and triangular surfaces.

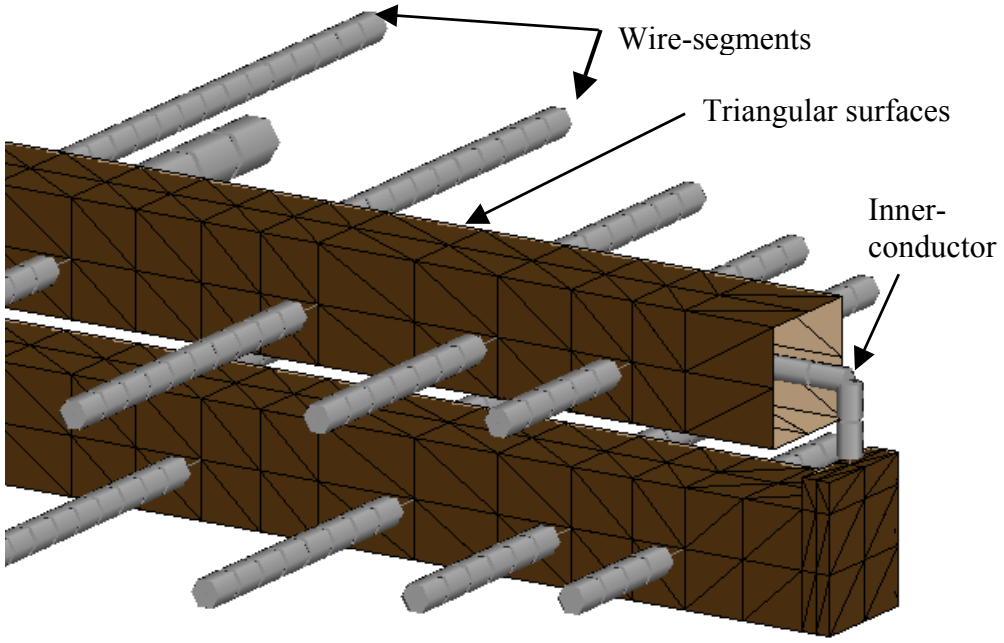


Figure 3.6 Tip of the log-periodical antenna discretized in wire segments and triangular surfaces.

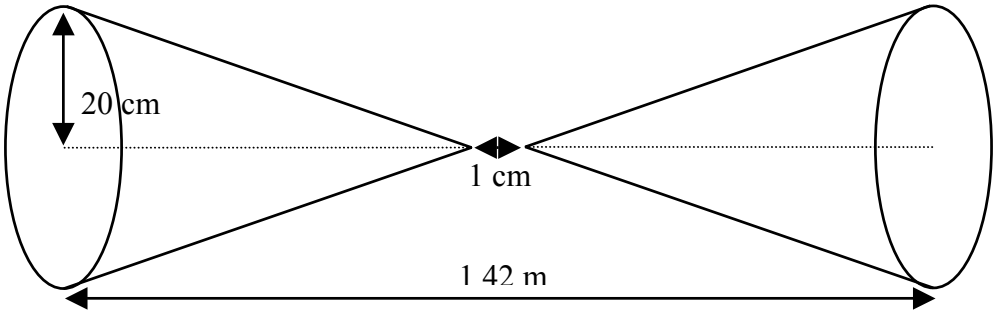


Figure 3.7 Closed surface model of biconical antenna.

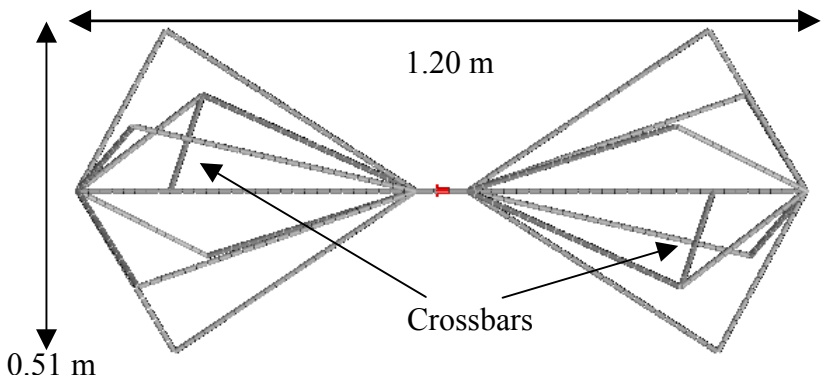


Figure 3.8 Simulated biconical antenna discretized in wire segments.

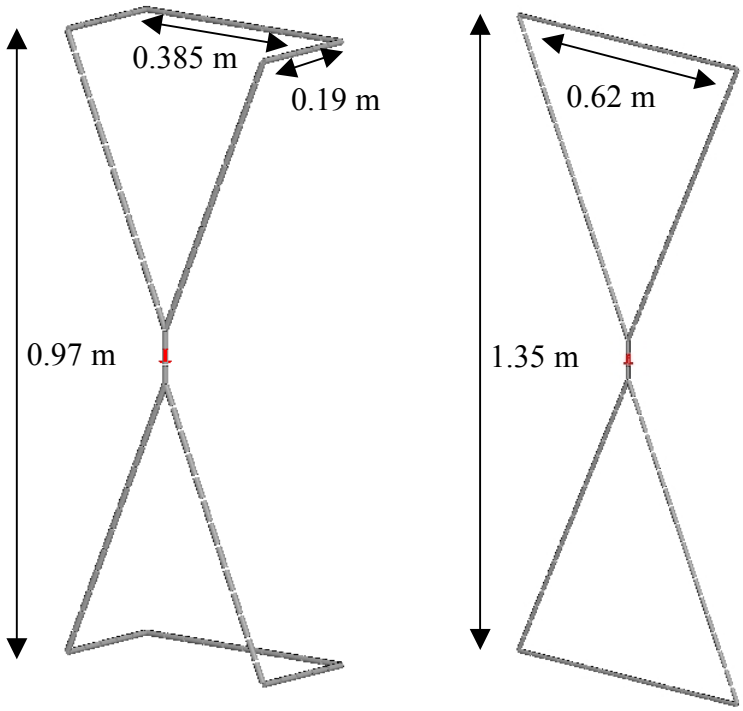


Figure 3.9 Simulated bow-tie antennas A and B discretized in wire segments.

## 3.4 Antenna factor results

### 3.4.1 Frequency range 20-300 MHz

In the frequency range from 20 to 300 MHz, the AF simulations of the biconical and the bow-tie receive antennas will be considered. The simulated AFs of the investigated receive antennas are depicted in Figure 3.10 A and B and have been obtained by using the ANSI C63.5 method and the free-space method, respectively. The free-space AFs of the bow-tie antennas show peaks between 200-300 MHz. Further investigation using the antenna patterns showed that the antenna patterns of the bow-tie antennas deteriorate rapidly above 200 MHz, showing lobes and zeros; while below 200 MHz the bow-tie antenna patterns follow the well-known doughnut shape as shown in Figure 3.12 A. This deterioration of the antenna pattern is called multilobing. In the ANSI C63.5 calibrated AFs (Figure 3.10 A), it can be observed that the peak values of the bow-tie antennas between 250-300 MHz are much smaller. This is caused by the fact that in accordance with the ANSI C63.5 method a ground plane is present and a height scan ($h$=1 - 4 m 10 cm step) is performed. Then the impact of the mentioned zeros in the antenna pattern is not so extreme, because also a reflected component of the electric field will be received.
Furthermore, additional AF investigations are carried out using biconical receive antennas, where two biconical antenna models are compared: a closed-surface model and a wire model. The results are presented in Figure 3.11 A. The simulated wire model is based on an existing biconical antenna (Eaton 2198), which does not include crossbars. In addition, the same wire model is also simulated including the crossbars to find out what effect they

would have, but in this frequency range we could not discover any differences. However, narrow-band cage resonances could appear at these frequencies [1][70]. Alexander et al. [1] state that a dipole antenna will exhibit multilobing if the antenna length is above 1.4 λ; this multilobing was not apparent when using a biconical antenna of the same length. However, we found that the biconical antenna pattern started to deteriorate at an antenna length above 1.6 λ (350 MHz), i.e., where multilobing occurs. The term multilobing is used for the effect of the presence of side lobes with approximately the same level as the main lobe. Multilobing of antennas induces large uncertainties in the radiated emission results. This will be considered in detail in Section 3.5.

### 3.4.2 Frequency range 300-1000 MHz

In the frequency range from 300 to 1000 MHz, the AFs of the log-periodical receive antenna were simulated. The measured and simulated AFs of the log-periodical antenna at higher frequencies (300-1000 MHz) are depicted in Figure 3.11 B. It is observed that the differences between the simulated and the measured AF for the log-periodical antenna are less than 2 dB. The simulation model includes only the log-periodical part of the bilog antenna. It must be noted that the measured AF results of the log-periodical antenna, shown in Figure 3.11 B, are achieved including the bow-tie part. The interaction between the log-periodical part and the bow-tie (bicon) part, concerning the AF, is negligible in this frequency range [77]. The slight peak differences between the simulated and the measured AF for the log-periodical antenna are possibly caused by impedance mismatches and directive gain variations (Eq. (3.4)). Figure 3.12 B shows antenna patterns of the log-periodical antenna. This figure shows that multilobing starts above 800 MHz. Larger deviations can accordingly be expected above 800 MHz.

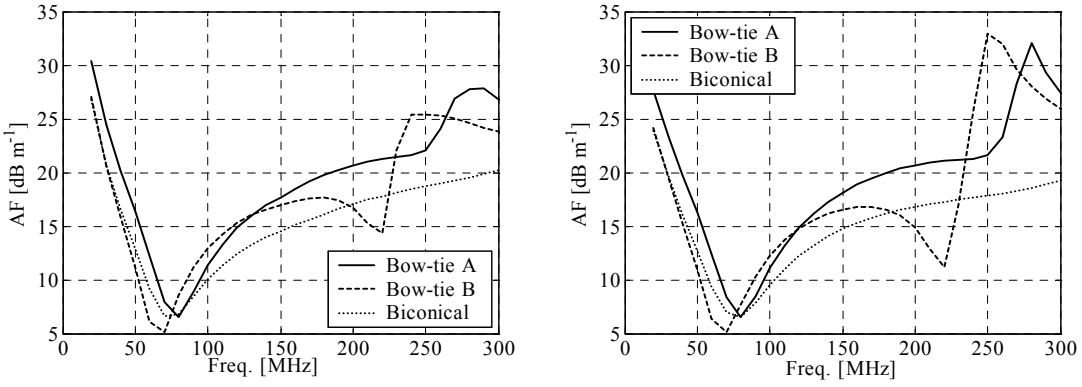


A. ANSI C63.5 AF B. Free-space AF

Figure 3.10 Simulated antenna factors obtained by using the ANSI C63.5 method (A) and the free-space method (B).

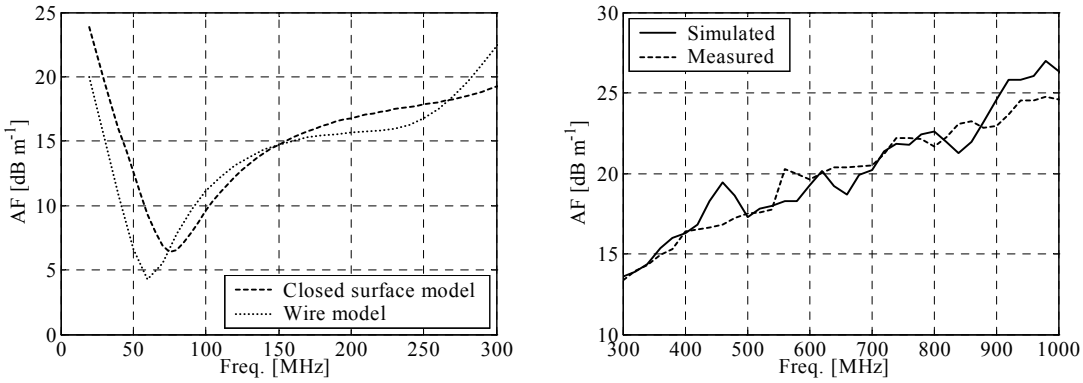


A. Biconical antennas B. Log-periodical antenna

Figure 3.11 Simulated antenna factors for two types of biconical antennas (A) and antenna factor results (simulated and measured) for the log-periodical antenna (B).

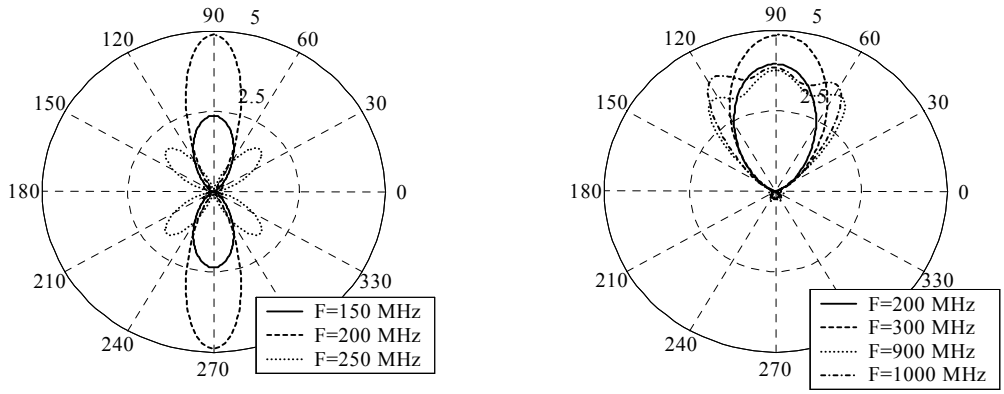


A. Bow-tie B antenna B. Log-periodical antenna

Figure 3.12 Antenna diagrams (linear directivity) of bow-tie B antenna (A) and log-periodical antenna (B).

## 3.5 Radiated emission results

In the previous section, the behavior of the AF of various receive antennas was analyzed (see step 1 in Section 3.3). In this section, the consequences of the different behavior of the receive antennas in simulated radiated emission results will be considered (step 2 and 3). The radiated emission results are obtained by simulating a 3 m SAR measurement configuration including a height scan for two polarizations. In Subsection 3.5.1, we will discuss the lower frequency range (20-300 MHz), and in Subsection 3.5.2 we will treat the higher frequency range (300-1000 MHz). Radiated emission standards generally start at a frequency of 30 MHz. In these experiments, a start frequency of 20 MHz is used to facilitate the interpretation of the effects around 30 MHz. The radiated emission results will be compared with measurement results in Subsection 3.5.3. In Subsection 3.5.4, the attention is focused on the differences in uncertainty when either the tuned dipole or the E-field is used as reference. This section is completed by a discussion and conclusions in Subsection 3.5.5.

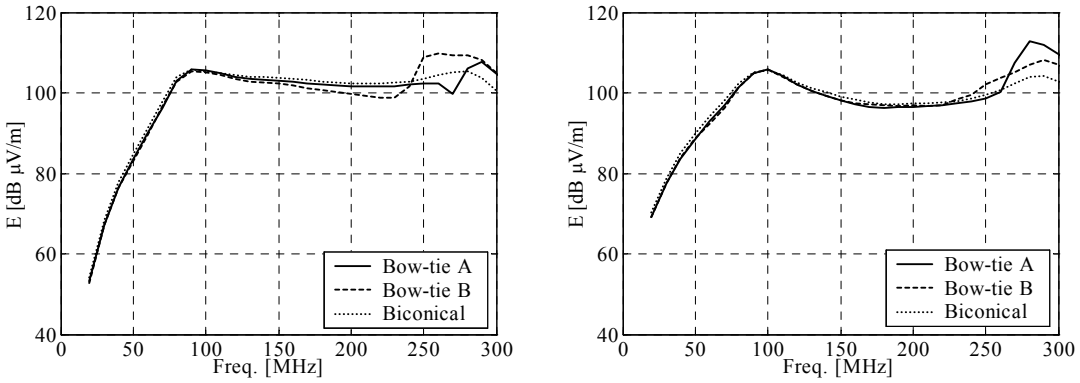


A. Horizontal polarization B. Vertical polarization

Figure 3.13 Simulated radiated emission results of the Dip100 EUT obtained by using receive antennas with free-space AFs.

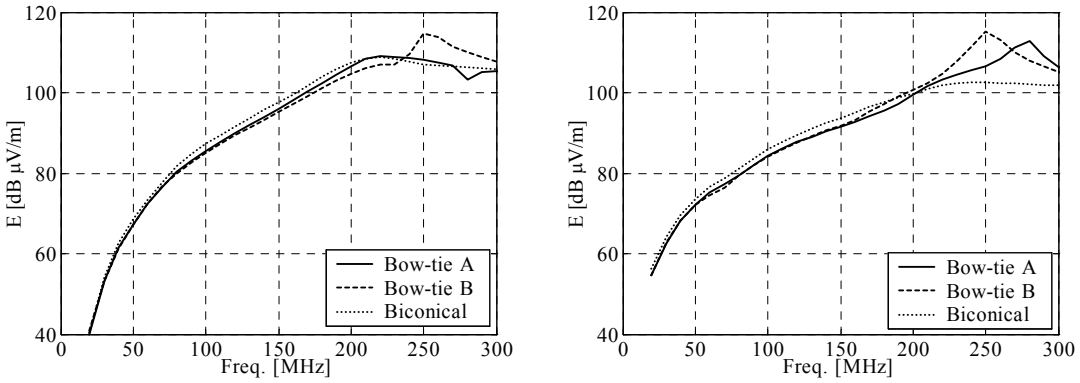


A. Horizontal polarization B. Vertical polarization

Figure 3.14 Simulated radiated emission results of the Dip250 EUT obtained by using receive antennas with free-space AFs.

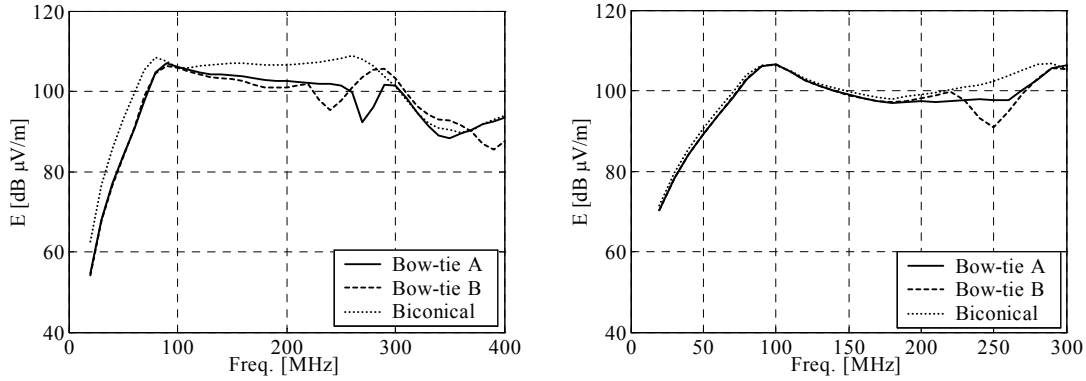


A. Horizontal polarization B. Vertical polarization

Figure 3.15 Simulated radiated emission results of the Dip100 EUT obtained by using receive antennas with ANSI C63.5 AFs.

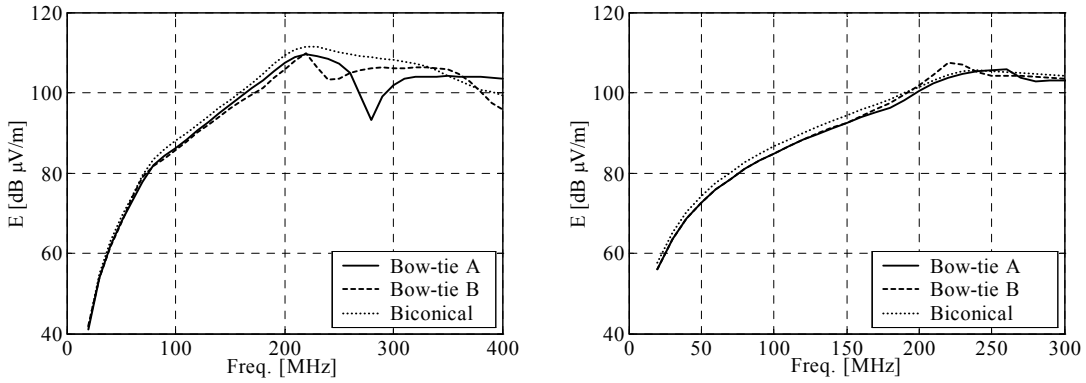


A. Horizontal polarization B. Vertical polarization

Figure 3.16 Simulated radiated emission results of the Dip250 EUT obtained by using receive antennas with ANSI C63.5 AFs.

### 3.5.1 Frequency range 20-300 MHz

The simulation results of the radiated emission of the Dip100 EUT and the Dip250 EUT by using free-space AFs are depicted in Figure 3.13 and Figure 3.14, respectively. In these figures, we can see large deviations in the results obtained using the bow-tie antennas compared to the radiated emission result obtained with the biconical antenna. These deviations correspond to the peaks in AFs of the bow-tie antennas between 200-300 MHz that were observed in Figure 3.10 B. These observations lead to the following general guideline concerning the operating bandwidth of receive antennas characterized by their free-space AF and usage in chambers containing a ground plane (e.g., a SAR): a receive antenna must have its maximum gain in the direction for which the AF was determined. Based on the antenna patterns (Figure 3.12), we can conclude that the bow-tie antennas do not perform properly above 200 MHz. However, these antennas are always used as a part of a bilog antenna, which can operate above 200 MHz. Furthermore, a biconical antenna should not be applied above 300 MHz. The design bandwidths of practical antennas used for EMC applications generally already comply with this guideline.

The deviations in radiated emission of the horizontal polarization of a Dip100 EUT and Dip250 EUT relative to the radiated emission obtained by using a tuned-dipole reference are listed in Tables 3.1 and 3.2, respectively. The biconical antenna shows a maximum deviation of 1.2 dB in its operating bandwidth of 20-300 MHz. When the operating bandwidth of the bow-tie antennas is defined from 20 to 200 MHz, a maximum deviation is observed of 2.5 dB. However, it should be emphasized that the bow-tie antennas are always implemented in bilog antennas in practice, i.e., in combination with log-periodical antennas, see Subsection 3.5.2.

The simulation results of the radiated emission of the Dip100 EUT and the Dip250 EUT by using ANSI C63.5 AFs are depicted in Figure 3.15 and Figure 3.16, respectively. The deviations of radiated emission results obtained by using ANSI C63.5 AFs are listed in the Tables 3.3 and 3.4. Observing these deviations of the radiated emission results, we can conclude that the deviation caused by using the biconical antenna is at most 1.7 dB. So, the deviations, caused by the biconical antenna are somewhat larger using the ANSI C63.5 AF, than using the free-space AF. The deviations, caused by the bow-tie antennas using ANSI C63.5 AFs, are somewhat smaller, i.e., the deviation is at most 1.9 dB in the operating bandwidth of 20-200 MHz.

From the results presented here, we cannot observe significant differences in the deviations of the radiated emission results achieved by using the free-space or ANSI C63.5 calibrated AFs. Both methods of calibration result in roughly the same substantial level of deviation (2 to 3 dB) relative to the tuned-dipole reference. The level of deviation due to the use of different types of receive antennas (2 to 3 dB) is defined as substantial relative to the $U_{\mathrm{CISPR}}$ value for 3 m SAR measurements, which is 5 dB [9][17]. In conclusion, the level of deviation due to the antenna type in radiated emission measurements is not affected by the way the receive antenna is calibrated.

It should be remarked that the $U_{\mathrm{CISPR}}$ value is a so-called expanded uncertainty value [17]. So, the comparison of the antenna-type deviation results with the $U_{\mathrm{CISPR}}$ value is limited. The root of the sum of various squared standard uncertainties determines the expanded uncertainty value. The standard uncertainty value for the antenna-type deviation can be determined when an approximation of the probability distribution can be made. The standard uncertainty is subsequently calculated by multiplying the standard deviation with the coverage factor. For example, a coverage factor of 1.96 is applicable to a normal distribution and a confidence level of 95%. This procedure is described in CISPR 16-4-2 [17].

In addition, it is observed that the deviation is not affected by the EUT size. This means that EUT size and associated directivity of the EUT has a negligible effect on the antenna-type deviation in this frequency range.
In Tables 3.5-3.8, the deviations of radiated emission results relative to the E-field reference are listed. These results are all obtained by using free-space AFs. The comparison between the E-field reference and the tuned-dipole reference is discussed in Subsection 3.5.4.

Table 3.1 Deviations in radiated emission of the Dip100 EUT (horizontal polarization) compared to the tuned-dipole reference using free-space antenna factors.

| Freq. [MHz] | Tuned dipole $E_{ref}$ [dB μV/m] | Biconical $\Delta E_{rad}$ [dB] | Bow-tie A $\Delta E_{rad}$ [dB] | Bow-tie B $\Delta E_{rad}$ [dB] |
|---|---|---|---|---|
| 100 | 105.7 | -0.3 | -0.1 | -0.6 |
| 200 | 103.0 | -0.7 | -0.6 | -2.5 |
| 300 | 101.6 | -1.2 | +3.2 | +3.3 |

Table 3.2 Deviations in radiated emission of the Dip250 EUT (horizontal polarization) compared to the tuned-dipole reference using free-space antenna factors.

| Freq. [MHz] | Tuned dipole $E_{ref}$ [dB μV/m] | Biconical $\Delta E_{rad}$ [dB] | Bow-tie A $\Delta E_{rad}$ [dB] | Bow-tie B $\Delta E_{rad}$ [dB] |
|---|---|---|---|---|
| 100 | 87.6 | -0.3 | -2.0 | -2.5 |
| 200 | 107.7 | -0.2 | -1.1 | -2.0 |
| 300 | 107.0 | -1.1 | -1.7 | +0.8 |

Table 3.3 Deviations in radiated emission of the Dip100 EUT (vertical polarization) compared to the tuned-dipole reference using ANSI C63.5 antenna factors.

| Freq. [MHz] | Tuned dipole $E_{ref}$ [dB μV/m] | Biconical $\Delta E_{rad}$ [dB] | Bow-tie A $\Delta E_{rad}$ [dB] | Bow-tie B $\Delta E_{rad}$ [dB] |
|---|---|---|---|---|
| 100 | 105.9 | +0.4 | +0.5 | +0.5 |
| 200 | 97.4 | +1.7 | -0.1 | +0.7 |
| 300 | 103.9 | +1.4 | +2.4 | +1.5 |

Table 3.4 Deviations in radiated emission of the Dip250 EUT (vertical polarization) compared to the tuned-dipole reference using ANSI C63.5 antenna factors.

| Freq. [MHz] | Tuned dipole $E_{ref}$ [dB μV/m] | Biconical $\Delta E_{rad}$ [dB] | Bow-tie A $\Delta E_{rad}$ [dB] | Bow-tie B $\Delta E_{rad}$ [dB] |
|---|---|---|---|---|
| 100 | 86.2 | +0.4 | -1.3 | -1.3 |
| 200 | 102.3 | -0.8 | -1.9 | -0.4 |
| 300 | 102.7 | +1.6 | +0.3 | +0.8 |

Table 3.5 Deviations in radiated emission of the Dip100 EUT (horizontal polarization) compared to the E-field reference using free-space antenna factors.

| Freq. [MHz] | Reference $E_{ref}$ [dB μV/m] | Tuned dipole $\Delta E_{rad}$ [dB] | Biconical $\Delta E_{rad}$ [dB] | Bow-tie A $\Delta E_{rad}$ [dB] | Bow-tie B $\Delta E_{rad}$ [dB] |
|---|---|---|---|---|---|
| 100 | 105.3 | +0.4 | +0.1 | -0.2 | +0.3 |
| 200 | 102.7 | +0.3 | -0.4 | -1.2 | -0.3 |
| 300 | 101.4 | +0.2 | -1.0 | +3.5 | +3.4 |

Table 3.6 Deviations in radiated emission of the Dip100 EUT (vertical polarization) compared to the E-field reference using free-space antenna factors.

| Freq. [MHz] | Reference $E_{ref}$ [dB μV/m] | Tuned dipole $\Delta E_{rad}$ [dB] | Biconical $\Delta E_{rad}$ [dB] | Bow-tie A $\Delta E_{rad}$ [dB] | Bow-tie B $\Delta E_{rad}$ [dB] |
|---|---|---|---|---|---|
| 100 | 105.7 | -0.5 | 0.0 | +0.1 | +0.2 |
| 200 | 97.2 | +0.1 | +0.1 | -0.3 | -0.7 |
| 300 | 104.4 | -0.2 | -1.2 | +0.6 | +1.5 |

Table 3.7 Deviations in radiated emission of the Dip250 EUT (horizontal polarization) compared to the E-field reference using free-space antenna factors.

| Freq. [MHz] | Reference $E_{ref}$ [dB μV/m] | Tuned dipole $\Delta E_{rad}$ [dB] | Biconical $\Delta E_{rad}$ [dB] | Bow-tie A $\Delta E_{rad}$ [dB] | Bow-tie B $\Delta E_{rad}$ [dB] |
|---|---|---|---|---|---|
| 100 | 86.9 | +0.7 | +0.4 | -1.8 | -1.3 |
| 200 | 107.9 | -0.2 | -0.4 | -2.2 | -1.3 |
| 300 | 106.8 | +0.2 | -0.9 | +1.0 | -1.5 |

Table 3.8 Deviations in radiated emission of the Dip250 EUT (vertical polarization) compared to the E-field reference using free-space antenna factors.

| Freq. [MHz] | Reference $E_{ref}$ [dB μV/m] | Tuned dipole $\Delta E_{rad}$ [dB] | Biconical $\Delta E_{rad}$ [dB] | Bow-tie A $\Delta E_{rad}$ [dB] | Bow-tie B $\Delta E_{rad}$ [dB] |
|---|---|---|---|---|---|
| 100 | 86.0 | -0.6 | -0.1 | -1.8 | -1.6 |
| 200 | 100.7 | -0.5 | -1.1 | 0.0 | -1.1 |
| 300 | 103.4 | -0.4 | -1.5 | +1.8 | +3.2 |

### 3.5.2 Frequency range 300-1000 MHz

Figure 3.17 A and B show simulation results in the 300-1000 MHz range for the radiated emission measurement of the Dip100 EUT and the Dip250 EUT in horizontal and vertical polarization, respectively. The deviations due to the use of the log-periodical antenna are listed in Tables 3.9-3.12, where the deviations are shown relative to the E-field reference. For comparison purposes, also the radiated emission results obtained by using the tuned dipole are listed in Tables 3.9-3.12. All the results in this frequency range are obtained by using free-space AFs. ANSI C63.5 AFs are not applied in this range.

In Tables 3.9-3.12, we observe that for horizontal polarization (Tables 3.9-3.10) the deviation is less than 1.6 dB at frequencies below 800 MHz and at 1000 MHz the deviation is 2.9 dB. In addition, in the vertical polarized configuration (Tables 3.11-3.12) the deviations are smaller than 1.1 dB up to 1000 MHz. The deviations become larger above 800 MHz because multilobing starts to develop above this frequency. At a frequency of 1000 MHz the maximum gain of the log-periodical antenna is no longer in the mechanical boresight direction of 90°, i.e., the direction for which the free-space AF was calibrated (see Section 3.2), but also near 60° and 120°, see Figure 3.12 B. Accordingly, above 1000 MHz the used log-periodical antenna is not suitable for radiated emission measurements performed in a 3 m SAR. However, the manufacturer has specified the antenna up to 2 GHz.

It must also be noted that the 10 cm height step of the receive antenna becomes more critical in the range 800-1000 MHz ($\lambda/4<10$ cm). In practice, the log-periodical antennas are often combined with bow-tie antennas. In the previous subsection, the maximum deviation in radiated emission results measured using the bow-tie antennas was 3.6 dB at 200 MHz (Table 3.4). The bilog antenna configured as a combination of a log-periodical part and a bow-tie part is expected to result in similar deviations of around 2 dB in the frequency range 20-200 MHz, because the interaction between the log-periodical part and the bow-tie part is negligible [77].

In addition, it is observed that the two EUTs result in similar deviations. It can be concluded that EUT size and corresponding directivity has a negligible influence on the antenna-type deviation in this frequency range.

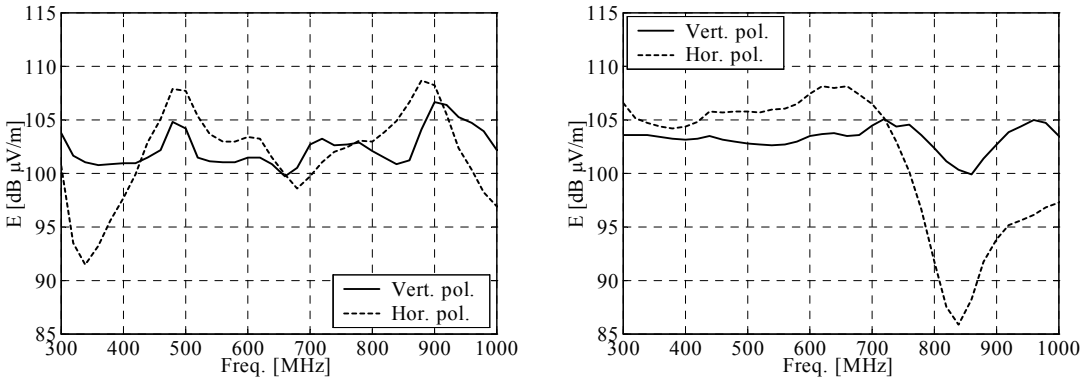


A. Dip100 EUT B. Dip250 EUT

Figure 3.17 Simulated radiated emission results obtained by using a log-periodic receive antenna with free-space AFs.

Table 3.9 Deviations in radiated emission of the Dip100 EUT (horizontal polarization) compared to the E-field reference using free-space antenna factors.

| Freq. [MHz] | Reference $E_{ref}$ [dB µV/m] | Tuned dipole $\Delta E_{rad}$ [dB] | Log-periodical $\Delta E_{rad}$ [dB] |
|---|---|---|---|
| 300 | 101.4 | +0.2 | -0.7 |
| 400 | 96.1 | +0.0 | +1.6 |
| 600 | 103.6 | +0.3 | -0.3 |
| 800 | 102.3 | +0.1 | +0.7 |
| 1000 | 99.8 | -0.1 | -2.9 |

Table 3.10 Deviations in radiated emission of the Dip250 EUT (horizontal polarization) compared to the E-field reference using free-space antenna factors.

| Freq. [MHz] | Reference $E_{ref}$ [dB µV/m] | Tuned dipole $\Delta E_{rad}$ [dB] | Log-periodical $\Delta E_{rad}$ [dB] |
|---|---|---|---|
| 300 | 106.8 | +0.2 | -0.3 |
| 400 | 103.7 | +0.0 | +0.6 |
| 600 | 106.7 | +0.2 | +0.7 |
| 800 | 93.1 | +0.1 | -1.4 |
| 1000 | 94.6 | -0.1 | +2.7 |

Table 3.11 Deviations in radiated emission of the Dip100 EUT (vertical polarization) compared to the E-field reference using free-space antenna factors.

| Freq. [MHz] | Reference $E_{ref}$ [dB μV/m] | Tuned dipole $\Delta E_{rad}$ [dB] | Log-periodical $\Delta E_{rad}$ [dB] |
|---|---|---|---|
| 300 | 104.4 | -0.2 | -0.6 |
| 400 | 101.1 | -0.5 | -0.1 |
| 600 | 101.8 | -0.5 | -0.4 |
| 800 | 101.8 | -1.1 | +0.2 |
| 1000 | 101.0 | -0.3 | +1.1 |

Table 3.12 Deviations in radiated emission of the Dip250 EUT (vertical polarization) compared to the E-field reference using free-space antenna factors.

| Freq. [MHz] | Reference $E_{ref}$ [dB μV/m] | Tuned dipole $\Delta E_{rad}$ [dB] | Log-periodical $\Delta E_{rad}$ [dB] |
|---|---|---|---|
| 300 | 103.4 | -0.4 | +0.2 |
| 400 | 102.4 | -0.3 | +0.7 |
| 600 | 103.3 | -0.1 | +0.1 |
| 800 | 103.1 | -0.7 | -0.8 |
| 1000 | 102.3 | -0.6 | +1.1 |

### 3.5.3 Validation by measurements

The analysis of the deviation due to the use of different types of receive antennas is based on simulations. It is, however, important to validate the simulations by measurements. Therefore, a limited number of measurements have been performed to validate the simulation model. For that purpose, the radiated emission of the Dip100 EUT, a 100 MHz resonant dipole, was measured by using a biconical antenna and a log-periodical antenna for horizontal and vertical polarization. For the measurements the bow-tie part of the bilog antenna was removed in order to achieve a configuration comparable with the simulation. In the lower frequency range (30-300 MHz), the biconical antenna was used and in the higher frequency range (300-1000 MHz) the log-periodical antenna was applied.
The radiated emission measurement results of the Dip100 EUT at the lower and higher frequency range are shown in Figure 3.18 A and B, respectively. If we compare these figures with the corresponding simulated radiated emission results in Figure 3.13 and Figure 3.17, we observe that the measurement results match the simulation results within ±3 dB. From these measurement results, it was concluded that the simulation model is valid for use.

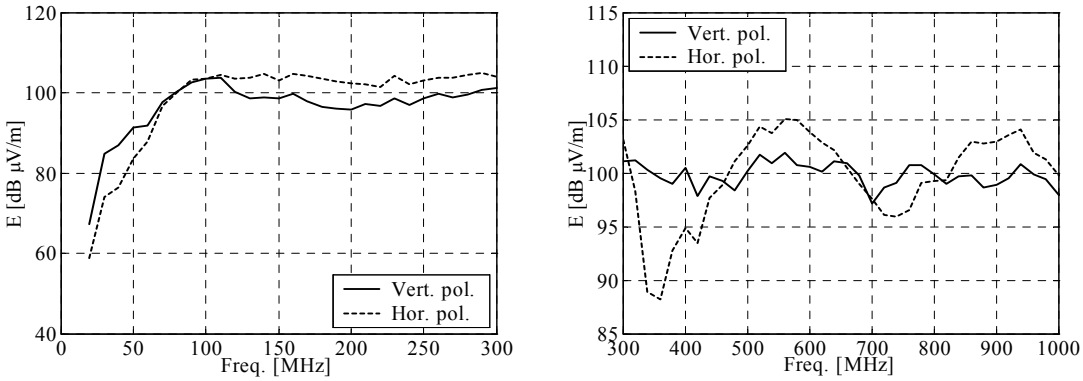


A. Biconical antenna B. Log-periodical antenna

Figure 3.18 Measured radiated emission results of the Dip100 EUT obtained by using receive antennas with free-space AFs.

### 3.5.4 Comparison of E-field and tuned-dipole reference

In this subsection, the comparison of the application of the (electric) E-field reference and the tuned-dipole reference is discussed. The E-field reference is determined numerically in absence of the receive antenna and was explained in Subsection 2.6. In Table 3.13, the maximum deviations in radiated emission results are presented of each of the used receive antennas for each of the two EUT configurations (two EUTs at two polarizations). From this table, it is clear that the deviation due to use of different types of receive antennas can be significant. All simulated receive antennas can result in a maximum radiated emission deviation (relative to E-field reference) of approximately 3 dB. In Table 3.14, the maximum deviations in radiated emission results relative to the tuned-dipole reference results are listed. Comparison of the deviations summarized in Table 3.13 with the deviations in Table 3.14 leads to the conclusion that the maximum levels of the deviations are comparable. However, we can observe that the maximum deviations of both the biconical antenna and the log-periodical antenna are somewhat larger in the E-field reference case (Table 3.13). In particular, the maximum deviation is -1.5 dB for the biconical antenna, -2.2 dB for the bow-tie antennas, and -2.9 dB for the log-periodical antenna. In the tuned-dipole reference case the maximum deviations of these antennas are: -1.2 dB for the biconical antenna, -2.5 dB for the bow-tie antennas, and -2.8 dB for the log-periodical antenna.

So, we can conclude that by using the E-field reference the maximum deviations due to the use of different types of receive antennas are comparable within 0.3 dB to the maximum deviations obtained by using the tuned-dipole reference. Considering the uncertainties, the E-field reference as adopted in CISPR/A is therefore neither an improvement nor a degradation compared with the tuned-dipole reference. However, the choice of taking the E-field reference makes sense when we keep in mind that most of the radiated emission limits are expressed in electric-field values.

Table 3.13 Maximum deviations $\Delta E_{rad}$ of the four EUTs with E-field reference.

| | Dip100 EUT Hor. [dB] | Dip100 EUT Vert. [dB] | Dip250 EUT Hor. [dB] | Dip250 EUT Vert. [dB] |
|---|---|---|---|---|
| Tuned dipole | +0.4 | -1.1 | +0.7 | -0.7 |
| Biconical | -1.0 | -1.2 | -0.9 | -1.5 |
| Bow-tie Green | -1.2 | -0.3 | -2.2 | -1.8 |
| Bow-tie Purple | 0.3 | -0.7 | -1.3 | -1.6 |
| Log-periodical | -2.9 | +1.1 | +2.7 | +1.1 |

Table 3.14 Maximum deviations $\Delta E_{rad}$ of the four EUTs with tuned-dipole reference.

| | Dip100 EUT Hor. [dB] | Dip100 EUT Vert. [dB] | Dip250 EUT Hor. [dB] | Dip250 EUT Vert. [dB] |
|---|---|---|---|---|
| Biconical | -1.2 | -1.1 | -1.1 | -1.1 |
| Bow-tie Green | -2.5 | +0.6 | -2.5 | -1.2 |
| Bow-tie Purple | -0.6 | -0.8 | -2.0 | -1.0 |
| Log-periodical | -2.8 | +1.4 | +2.8 | +1.7 |

### 3.5.5 Discussion and conclusions

In Section 3.4, it was observed that all types of antennas have a certain frequency, above which the antenna patterns start to deteriorate, i.e., the antenna patterns exhibit multilobing. This observation led us (in Subsection 3.5.1) to formulate a guideline for the operating bandwidths of antennas, i.e., that a receive antenna must have its maximum directivity in the same direction of the incident wave used during the free-space calibration as shown in Figure 3.2. The justification of the use of different types of antennas as stated in Section 3.1 has been investigated by considering the deviations in radiated emission results. In the operating bandwidths of the investigated antennas, a considerable antenna-type deviation is found of around 2 dB. The level of deviation due to the use of different types of receive antennas (2 to 3 dB) is judged as substantial relative to the $U_{CISPR}$ value for 3 m SAR measurements, which is 5 dB [17]. However, the $U_{CISPR}$ value is a so-called expanded uncertainty value as was explained in Subsection 3.5.1. The budgets presented in CISPR 16-4-2 should therefore be reconsidered and extended by including the antenna-type standard uncertainty value. For that purpose, an approximation of both the probability distribution and the standard deviation of the antenna-type deviation should be made first. From this standard deviation, a coverage factor can be determined for a corresponding confidence level. The standard uncertainty value of the deviation can be calculated by multiplying the standard deviation with the coverage factor. The approximation of the standard deviation can be performed when more antenna-type deviation data become available.

The antenna-type deviations found using the large and small EUT (Dip100 EUT and Dip250 EUT) exhibit no significant deviations. This means that the EUT size and the associated directivity of the EUT is not of large influence.
We have investigated the deviation due to the use of different types of receive antennas in a 3 m OATS/SAR test site. However, radiated emission measurements are often performed in 10 m test sites. So, future uncertainty analyses should also include the 10 m configuration. We expect a smaller antenna-type uncertainty at 10 m measurement distance because the deviations in the radiation patterns of the receive antennas are smaller due to the smaller elevation angles. In Section 3.1, we questioned whether the AF adequately defines the antenna behavior, since deviations (up to 3 dB) had been observed in radiated emission results [40]. In its operating bandwidth of 20-300 MHz the biconical antenna shows a radiated emission deviation relative to the tuned-dipole reference of at most 1.2 dB. It was concluded that the operating bandwidth of the bow-tie antennas is 20-200 MHz. In this bandwidth the bow-tie antennas exhibit a radiated emission deviation relative to the tuned dipole of at most 2.5 dB. The log-periodical antenna exhibits a maximum deviation of 2.8 dB relative to the tuned-dipole reference in its operating bandwidth (200-1000 MHz). These deviations, which are achieved using a 3 m measurement distance, confirm the antenna-type uncertainty suggested in [40].

## 3.6 Antenna-type deviation 1-18 GHz

Up to now, the antenna-type deviation has been investigated in the frequency range 30-1000 MHz. In Section 1.1, the trend was indicated that an increasing number of products operate at frequencies above 1 GHz. For that reason, the antenna-type deviation is investigated in the frequency range 1-18 GHz. It was explained in Chapter 2 that CISPR/A published a new radiated emission method for frequencies above 1 GHz based on a FAR. However, in the USA, radiated emission measurements above 1 GHz frequencies have been performed at an OATS or in a SAR for many years [36]. In this section, the OATS/SAR method is used for the simulations in the range 1-18 GHz as well.

### 3.6.1 Simulation model

For the simulations, the geometrical-optics approximation [78] was used instead of the time-consuming full-wave approximation used by FEKO. Besides time saving also the complexity of the antenna modeling is an important reason to use a geometrical-optics model, where only the antenna patterns are needed as input. The geometrical-optics model is used to simulate the radiated emission measurement configuration of an OATS or SAR (1 - 4 m height scan and 3 m measurement distance) in the frequency range 1-18 GHz. The antenna patterns of the receive antennas are available from the manufacturers and are incorporated in the model. The E-field reference is taken for comparison purposes. The maximum E-field is calculated in absence of the receive antenna. This yields the E-field reference. Subsequently, the calculated E-field is simulated when the receive antenna in

place and described by its free-space AF only. The availability of antenna patterns gives the opportunity to compare the deviation due to the use of different types of antennas with typical antenna pattern properties, e.g., the beamwidth. The same approach is followed as described for frequencies below 1 GHz (Section 3.3).

### 3.6.2 Simulated antennas

Three types of receive antennas are considered in this experiment: the commonly used double-ridged waveguide horn antenna, a special double-ridged waveguide horn antenna ETS 3117 developed by ETS-Lindgren, and a log-periodical antenna with radome HL050 developed by Rohde & Schwarz. These antennas are shown in Figure 3.19. The double-ridged waveguide horn antenna is the most commonly used receive antenna in EMC measurements above 1 GHz. Recent simulation results [13] have demonstrated that this antenna shows inferior behavior in the antenna pattern at frequencies above roughly 10 GHz. It was shown that multilobing of the antenna pattern will occur above 10 GHz. For that reason, a completely new type of double-ridged waveguide horn antenna was developed by ETS-Lindgren, i.e., the ETS 3117. This antenna does not show any multilobing up to 18 GHz. The HL050 log-periodical antenna developed by Rohde & Schwarz is of a quite different type. The HL050 log-periodical antenna is a very broadband antenna (850 MHz-26.5 GHz) with low mismatch and excellent specifications of the beamwidth and gain. It is interesting to investigate a possible relation between the beamwidth property of a receive antenna and the antenna-type uncertainty. In Tables 3.15-3.16, the beamwidth specifications of the receive antennas are summarized. The E-plane and H-plane antenna patterns of the receive antennas are shown in Figure 3.21 at 2 GHz and in Figure 3.22 at 16 GHz. The antenna patterns are normalized to the maximum directive gain. The antenna pattern of the common double-ridged waveguide horn antenna is only plotted in the range of angles 0-180°, assuming symmetrical behavior around 0°. It can be observed that at 2 GHz all antennas show a proper beamwidth of roughly 60°. At higher frequencies, the beamwidths of both the common double-ridged waveguide horn antenna and the special double-ridged waveguide horn antenna ETS 3117 show a tendency to decrease. The log-periodical antenna HL050 retains a large beamwidth of roughly 60° over the entire frequency range.

Figure 3.19 Antennas used in the simulations from left to right: double-ridged waveguide horn, the special double-ridged waveguide horn, and the log-periodical antenna with radome.

It is important to emphasize that the special double-ridged waveguide horn antenna ETS 3117 does not suffer from multilobing, but the beamwidth decrease is faster compared to the log-periodical antenna HL050 for increasing frequency.

Two types of EUTs are used in this simulation. The EUTs are both variations of a metallic box (1.0 m × 0.92 m × 0.72 m) with five holes randomly located on each of the six faces of the box, which were also used in [38]. The holes have a radius of 1 cm. The metal box was excited by using a dipole antenna with a length of two times the applicable wavelength. A picture of the metal box and its 3D radiation pattern are shown in Figure 3.20.

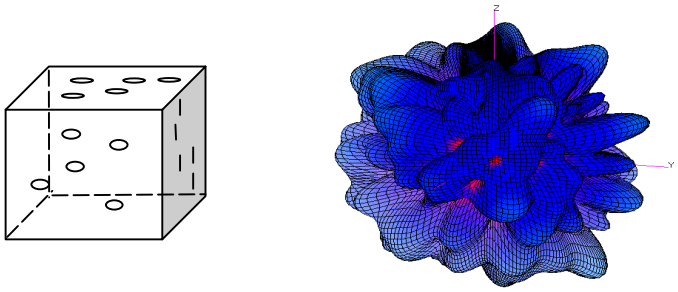

Figure 3.20 Metal box EUT and its 3D radiation pattern at 1 GHz (source: [38]).

The antenna patterns (linear directivity) of the EUTs, EUT A and EUT B, are plotted in Figure 3.23. Actually, these antenna patterns were simulated (by using FEKO) at 2 GHz for EUT A and at 4 GHz for EUT B. In the geometrical-optics simulation, however, the same antenna patterns will be used over the entire frequency band (1-18 GHz) as input in the model. In other words, two typical antenna patterns are used in the geometrical-optics model, which are typical for EUT radiation patterns above 1 GHz.

Table 3.15 Half power beamwidth (E-plane / vertical polarization)

| Freq. [GHz] | HL050 [°] | ETS 3117 [°] | Double-ridged [°] |
|---|---|---|---|
| 1 | - | 90 | 100 |
| 2 | 66 | 60 | 56 |
| 4 | 60 | 60 | 58 |
| 6 | - | 65 | 49 |
| 8 | 60 | 48 | 55 |
| 10 | - | 42 | 67 |
| 12 | 60 | 48 | 71 |
| 15 | - | 50 | 13 |
| 16 | 57 | 49 | 10 |

Table 3.16 Half power beamwidth (H-plane / horizontal polarization)

| Freq. [GHz] | HL050 [°] | ETS 3117 [°] | Double-ridged [°] |
|---|---|---|---|
| 1 | - | 150 | 75 |
| 2 | 71 | 116 | 54 |
| 4 | 68 | 78 | 50 |
| 6 | - | 59 | 33 |
| 8 | 61 | 54 | 41 |
| 10 | - | 38 | 47 |
| 12 | 65 | 44 | 43 |
| 15 | - | 38 | 9 |
| 16 | 62 | 37 | 18 |

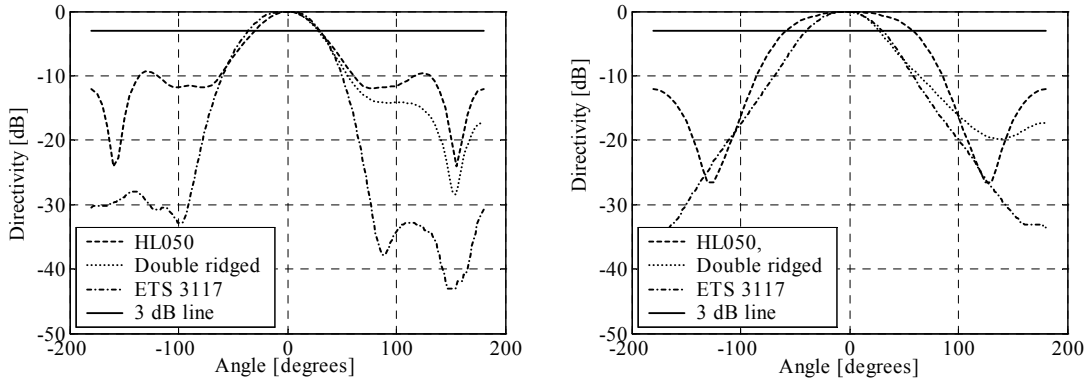


A. E-plane B. H-plane

Figure 3.21 Antenna patterns (E-plane (A) and H-plane (B)) of normalized directivity of three receive antennas at a frequency of 2 GHz.

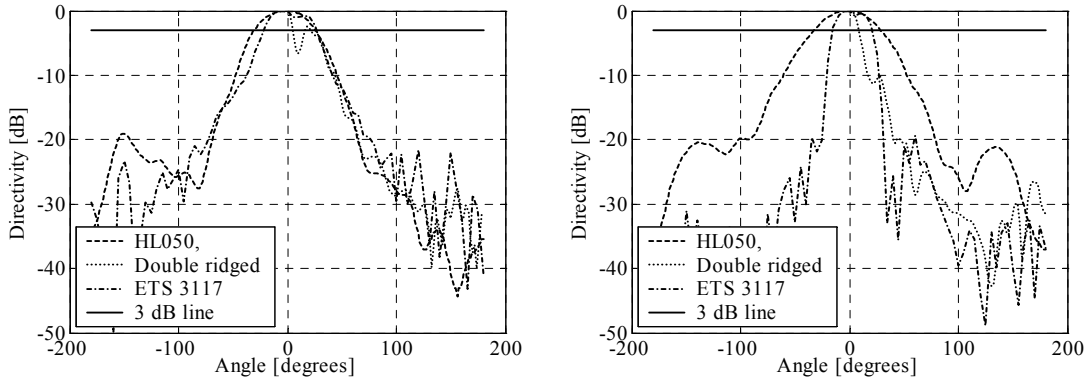


A. E-plane B. H-plane

Figure 3.22 Antenna patterns (E-plane (A) and H-plane (B)) of normalized directivity of three receive antennas at a frequency of 16 GHz.

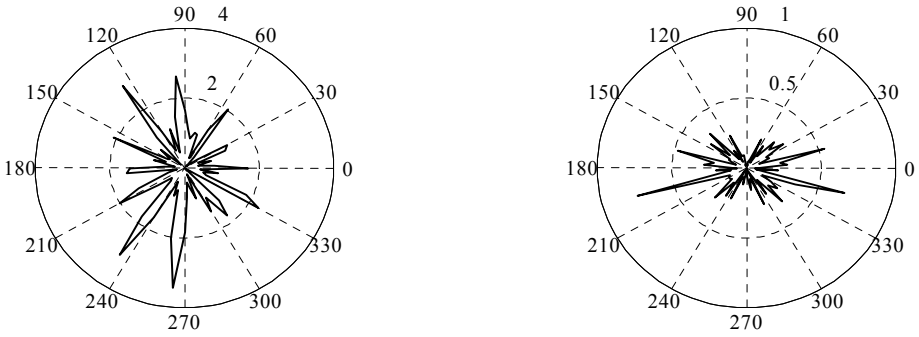


A. EUT A (2 GHz) B. EUT B (4 GHz)

Figure 3.23 Antenna patterns (linear directivity) of EUT A (A) and EUT B (B).

### 3.6.3 Discussion of the deviation results

In Tables 3.17-3.20, the deviations in radiated emission results of EUT A and EUT B are summarized with respect to the E-field reference for the three different types of receive antennas. In Tables 17 and 18, the deviations for vertical polarization are listed, whereas the deviations for horizontal polarization are presented in Tables 3.19 and 3.20. In general, the E-field reference results of EUT A and EUT B differs approximately by 3 dB.

It can be observed that the deviations for the two EUTs are similar, although the radiation patterns of the EUTs are different as shown in Figure 3.22. A possible explanation is that the antenna-related properties are more important than the EUT radiation properties in this specific case. Furthermore, it can be observed that the deviations are somewhat larger for horizontal polarization (Tables 3.19 and 3.20). First, this can be explained by the fact that the beamwidths of the receive antennas in the H-plane (Tables 3.15 and 3.16) are in general smaller. Secondly, the deviations for horizontal polarization are somewhat larger due to the larger reflection of the ground plane. In general, we can conclude that the ETS 3117 and the common double-ridged horn antenna show deviations up to approximately 3 dB (vertical polarization) and 5 dB (horizontal polarization). The log-periodical antenna (HL050), however, shows excellent performance with a maximum deviation up to 1.7 dB (horizontal and vertical polarization). Therefore, it can be concluded that a large beamwidth is equally important as the absence of multilobing. Approximately, a 60° beamwidth yielded 1 dB deviation and a 30° beamwidth yielded 4 dB deviation.

Table 3.17 Deviations in radiated emission results of the vertically polarized EUT A for different types of receive antennas (free-space AF).

| Freq. [GHz] | Reference $E_{rad}$ [dB μV/m] | HL050 $\Delta E_{rad}$ [dB] | ETS 3117 $\Delta E_{rad}$ [dB] | Double-ridged $\Delta E_{rad}$ [dB] |
|---|---|---|---|---|
| 1 | 117.6 | - | -0.4 | -0.3 |
| 2 | 118.2 | -1.1 | -1.3 | -1.4 |
| 4 | 118.2 | 1.6 | -1.4 | -1.3 |
| 6 | 118.2 | - | -1.5 | -1.9 |
| 8 | 118.2 | -1.5 | -2.0 | -1.8 |
| 10 | 118.2 | - | -3.3 | -0.8 |
| 12 | 118.2 | -1.1 | -3.2 | -0.0 |
| 15 | 118.2 | - | -2.5 | -3.1 |
| 16 | 118.2 | -1.7 | -2.6 | -3.1 |

Table 3.18 Deviations in radiated emission results of the vertically polarized EUT B for different types of receive antennas (free-space AF).

| Freq. [GHz] | Reference $E_{rad}$ [dB μV/m] | HL050 $\Delta E_{rad}$ [dB] | ETS 3117 $\Delta E_{rad}$ [dB] | Double-ridged $\Delta E_{rad}$ [dB] |
|---|---|---|---|---|
| 1 | 115.4 | - | -0.4 | -0.2 |
| 2 | 115.4 | -0.8 | -1.1 | -1.3 |
| 4 | 115.4 | -1.4 | -1.5 | -1.2 |
| 6 | 115.4 | - | -1.3 | -1.7 |
| 8 | 115.4 | -1.2 | -2.0 | -1.5 |
| 10 | 115.4 | - | -3.1 | -0.8 |
| 12 | 115.4 | -1.0 | -2.8 | +0.2 |
| 15 | 115.4 | - | -2.6 | -2.8 |
| 16 | 115.3 | -1.5 | -2.6 | -2.3 |

Table 3.19 Deviations in radiated emission results of the horizontally polarized EUT A for different types of receive antennas (free-space AF).

| Freq. [GHz] | Reference $E_{rad}$ [dB μV/m] | HL050 $\Delta E_{rad}$ [dB] | ETS 3117 $\Delta E_{rad}$ [dB] | Double-ridged $\Delta E_{rad}$ [dB] |
|---|---|---|---|---|
| 1 | 117.9 | - | -0.2 | -1.1 |
| 2 | 118.5 | -1.1 | -0.4 | -1.8 |
| 4 | 118.6 | -1.2 | -1.2 | -2.2 |
| 6 | 118.6 | - | -2.8 | -3.8 |
| 8 | 118.6 | -1.5 | -3.0 | -3.5 |
| 10 | 118.6 | - | -5.0 | -3.1 |
| 12 | 118.5 | -1.4 | -5.3 | -2.5 |
| 15 | 118.6 | - | -4.1 | -4.7 |
| 16 | 118.5 | -1.7 | -4.3 | -4.5 |

Table 3.20 Deviations in radiated emission results of the horizontally polarized EUT B for different types of receive antennas (free-space AF).

| Freq. [GHz] | Reference $E_{rad}$ [dB μV/m] | HL050 $\Delta E_{rad}$ [dB] | ETS 3117 $\Delta E_{rad}$ [dB] | Double-ridged $\Delta E_{rad}$ [dB] |
|---|---|---|---|---|
| 1 | 115.8 | - | -0.2 | -1.0 |
| 2 | 115.7 | -0.9 | -0.3 | -1.7 |
| 4 | 115.7 | -1.2 | -1.1 | -2.1 |
| 6 | 115.8 | - | -2.7 | -3.6 |
| 8 | 115.7 | -1.4 | -2.7 | -3.3 |
| 10 | 115.8 | - | -4.9 | -3.5 |
| 12 | 115.7 | -1.3 | -4.7 | -2.7 |
| 15 | 115.7 | - | -4.5 | -4.1 |
| 16 | 115.6 | -1.4 | -4.5 | -4.0 |

## 3.7 Summary

In this chapter, extensive investigations have been presented about the role of the receive antenna in radiated emission measurements performed in a 3 m SAR. The results in this chapter clearly demonstrate that the deviation due to use of different types of receive antennas can reach a level of a few dBs depending on the frequency range. We have concluded that the calibration method, standard-site method or free-space method, has a negligible influence on the resulting uncertainty. In other words, the level of deviation due to the antenna-type in radiated emission measurements is not affected by the way the receive antenna is calibrated. The discussion concerning the reference was introduced. The deviation is investigated by using either the tuned-dipole reference or the E-field reference. We have concluded that the choice of reference has a minor effect on the final uncertainty. The E-field reference was shown to be more practical for comparison purposes performed by numerical or analytical simulations. We have concluded that it is very important to use the receive antennas in the design bandwidths defined by the manufacturers, where the receive antenna should have its maximum gain in the direction for which the AF was determined. It was concluded that multilobing, i.e., deterioration of the antenna pattern, increases the deviation due to the antenna-type significantly. Besides the multilobing property also the beamwidth property of the receive antenna appeared to be important. If the receive antenna has one main lobe in its applicable bandwidth, but the beamwidth is small, then still a substantial deviation can be expected, when different types of receive antennas are applied. However, when both antenna properties, a single main lobe and a large beamwidth, are satisfactorily met, then the antenna-type deviation can be kept small in 3 m SAR measurements. It was demonstrated that when a receive antenna with a large beamwidth of 60° without any multilobing is applied, the antenna-type deviation can be kept smaller than approximately 1.6 dB even at 16 GHz.

The EUTs used in the investigations described in this chapter cover a wide range of properties of realistic EUTs, e.g., horizontal and vertical polarization and different directional behavior. It may be useful to investigate other types of EUTs in future investigations. More deviation results, obtained by using other EUTs and other receive antennas, support the statistical analysis of the deviation caused by using different types of receive antennas. Statistical information enables the definition of an expanded uncertainty value including the antenna-type uncertainty.

# 4 Radiated emission measurements in the Reverberation Chamber

In this chapter, the radiated emission measurement performed in a Reverberation Chamber (RC) is the subject of investigation. As mentioned in Section 1.1, in the home environment an increasing number of multimedia products (unintentional radiators) and wireless communication systems (intentional radiators) are present, which use frequencies above 1 GHz. For that reason, radiated emission measurement methods specifically suitable for frequencies above 1 GHz and corresponding emission limits are required. In Chapter 2, the new radiated emission measurement method for measuring above 1 GHz based on the FAR was already reviewed. The RC is another example of a facility which is suitable for measuring at high frequencies. An overview of the RC developments for EMC testing of the last decades can be found in [20]. Test facilities that use the same concept can be found in other physical domains, e.g., a resonance chamber in acoustics [58]. This chapter starts with a brief overview of the concept and theoretical background of the RC in Sections 4.1 and 4.2. Subsequently, we focus on a standardized comparison method in order to derive radiated emission limits based on established limits (e.g., CISPR 22) in Sections 4.5 and 4.6. The directivity of the EUT plays an important role in the comparison of results obtained within an RC and a FAR/SAR. Therefore, this chapter concludes with an evaluation of the directivity aspects and the associated uncertainties.

## 4.1 Reverberation chamber concept

Before we look at some basic aspects and the theory of the RC, it is appropriate to obtain a better view of the RC configuration and measurement method. A general overview of such a configuration is given in Figure 4.1. A RC consists of a shielded enclosure of certain dimensions in which one or more conductive stirrers are positioned. Figure 4.1 shows an RC with two stirrers. A stirrer is a conductive paddle wheel which is used to change the electromagnetic boundary conditions. The number of applied stirrers can be chosen arbitrarily, but effective stirring can already be achieved by one stirrer. The RC configuration can be used for both radiated emission measurements and radiated immunity tests. In this chapter, we focus on radiated emission measurements and the conversion of radiated emission measurement results. However, the theoretical overview in this section is valid for both emission measurements and immunity tests. For a radiated emission measurement, the chamber is fed by the radiated power generated in the EUT. This radiated power is measured by using a receive antenna and an EMI receiver. An overview of the measurement configuration for emission measurements is shown in Figure 4.2 A. Vice versa, a signal generator and transmit antenna is applied for feeding the chamber in the case of a radiated immunity test. This configuration is shown in Figure 4.2 B. The behavior and description of the electromagnetic field inside the RC is the same for both cases.

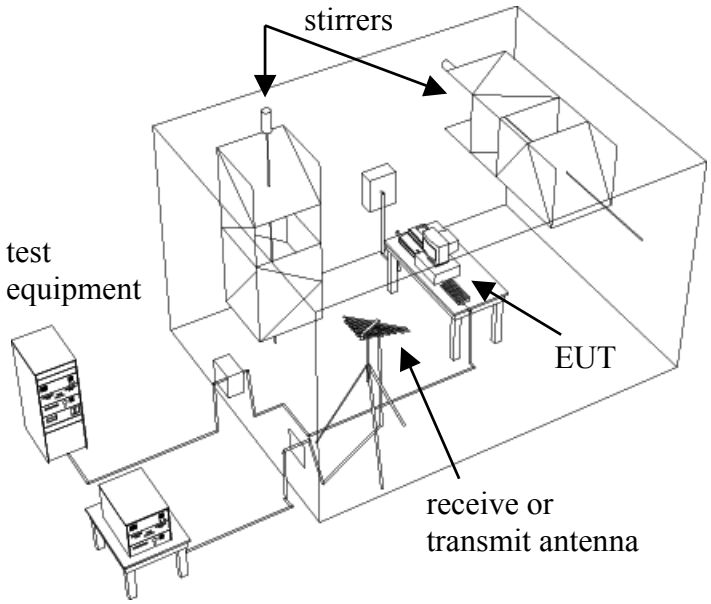


Figure 4.1 Overview of the RC measurement configuration.

Conventional measurement methods like the OATS/SAR or the FAR are deterministic methods and based on straightforward wave propagation. These methods aim to measure the maximum electric field of an EUT at a certain measurement distance in a free-space or semi-free space environment. The RC method is a statistical method and utilizes multiple reflections in a shielded enclosure. This method aims to find the total radiated power of an EUT by taking samples at various stirrer positions.
The concept of the mode-stirred reverberation chamber is the realization of a statistical average uniform and isotropic field inside the test volume over a full stirrer rotation. This means that the field obtained in the test volume of the chamber must be sufficiently uniform for three rectangular components (isotropic). The test volume is defined as the volume inside the RC with a sufficient distance ($>\lambda/4$) from the walls or other metallic objects, e.g., stirrer(s). This requirement is necessary because of the boundary conditions at the walls or other metallic objects where the field can never be isotropic.

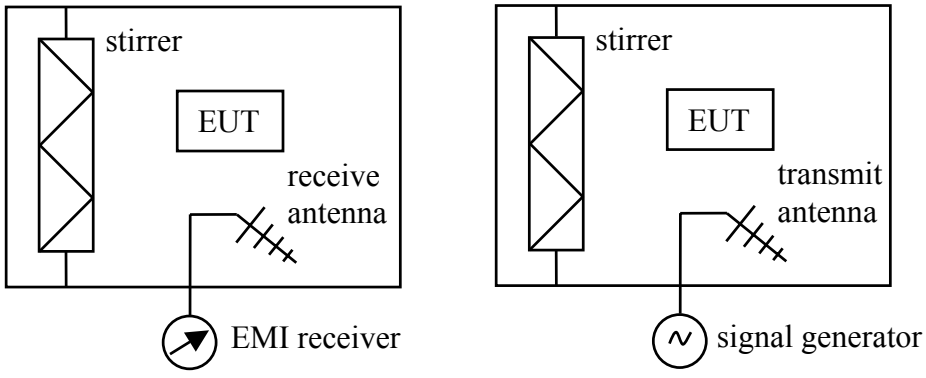


A. Radiated emission B. Radiated immunity

Figure 4.2 RC configurations for emission measurements (A) and immunity tests (B).

At the electrically conducting walls and objects, only the normal component of the electric field can be present. Useful insights concerning the behavior of the field in the vicinity of a metal surface can be found in [4]. The RC works as an electromagnetic resonant cavity. Above a certain frequency, which is called the cut-off frequency, resonances appear at discrete frequencies determined by the dimensions of the RC. The density of these resonances or modes (=number of modes/freq. range) increases with increasing working frequency. The frequencies of the resonances can be changed by rotating the mode stirrer. In other words, the rotating stirrer changes the standing wave patterns inside the chamber, which are caused by the multiple reflections. This standing-wave stirring, caused by the rotating stirrer, must be performed in such a way that at all locations inside the test volume a statistically uniform field is obtained over a full stirrer rotation. This can be realized if the stirrer is sufficiently effective, i.e., the frequency shift of the resonances is sufficiently large such that all frequencies are covered.

There is a statistical measure which can be used to check the stirrer effectiveness. This measure is based on the maximum-to-minimum ratio (measured over a full stirrer rotation) of the received power based on a statistical distribution (see [65][76] and Figure 4.3). In order to cover all frequencies of interest, the distance between successive resonances shall be small enough. Therefore, an effective stirrer is applied. As a consequence, the mode density must be sufficiently large, so that the limited frequency shift of the resonances, caused by the limited stirrer effectiveness, results in a frequency test sweep covering all (resonance) frequencies completely inside the sweep. The mode density $D$ can be determined using the following equation:

$$D(f) = \frac{dN(f)}{df} = 8\pi abc\frac{f^2}{c_0^3} - \frac{a+b+c}{c_0}, \tag{4.1}$$

where $N$ is the number of modes, $a$, $b$ and $c$ are the dimensions of a rectangular chamber, $f$ is the frequency, and $c_0$ is the free-space wave velocity. In general, 1 mode/MHz is the criterion for obtaining a suitable RC, i.e., the chamber shall be over-moded. The combination of a large mode density $D$ (large chamber) in combination with an effective stirrer (large stirrer) yields an RC, which can be used starting from low frequencies. The uniformity requirement is defined in Annex B of the IEC 61000-4-21 standard [54] and is explained in Subsection 4.3.2.

Concerning the uniformity, it must be noted that the chamber quality factor $Q$ is also an important parameter. In general, the higher the $Q$ the higher the field strength (emission or immunity), and the more difficult it becomes to comply with the uniformity requirement. When the $Q$ is high, the resonance peaks have a small bandwidth and as a consequence the stirring effectiveness is important. When the required field strength permits a lower $Q$, we can increase the uniformity by lowering the chamber $Q$ by placing absorbing material inside the chamber. A discussion concerning the effective use of loaded and unloaded RCs for wireless multimedia testing can be found in [51]. Furthermore, it is important that both the transmit and the receive antenna are not directed into the test volume and not directed towards each other. As was stated in the concept defined above, it is the goal to realize a statistically isotropic and uniform field within the entire test volume of the RC. For that reason, directivity and distance influences caused by either the transmit or receive antenna should be eliminated by directing these antennas to the walls or the stirrer(s).

## 4.2 Theory of reverberation chamber

After the introduction of the concept of the RC as EMC measurement facility, we now consider some theoretical aspects. Only that part of the theory is discussed that is needed in this chapter. An extensive treatment of the theory of RCs can be found in [46][65]. The electric field vector in the chamber is defined as follows:

$$\vec{E} = E_x \cdot \vec{e}_x + E_y \cdot \vec{e}_y + E_z \cdot \vec{e}_z, \tag{4.2}$$

where $E_x$, $E_y$, $E_z$, are complex numbers, i.e., six basic field variables are involved. The basic assumption for an ideal RC is that the six field variables are normally distributed with zero mean and variance $\sigma^2$. This situation is called a well-stirred RC. The statistics of the RC method is based on this assumption. The magnitude of the total electric field $E_T$ is defined as:

$$E_T = \left|\vec{E}\right| = \sqrt{E_x^2 + E_y^2 + E_z^2}. \tag{4.3}$$

Now that the basic field assumptions have been introduced, we are able to compute the average total electric field which will be realized within the test volume when a certain level of RF power is fed into the chamber. This average (denoted as $\langle\rangle$) total squared electric field over all stirrer steps $N$ can be calculated as follows:

$$\left\langle E_T^2 \right\rangle_N = \frac{QP_t}{\omega\varepsilon V}, \tag{4.4}$$

where $E_T$ is the magnitude of the three rectangular electric field components (Eq. (4.3)), $N$ is the number of stirrer steps, $Q$ is the quality factor of the chamber, $P_t$ is the transmitted power of the antenna or EUT, and $V$ is the volume of the chamber. The probability density function describing the magnitude of the total electric field, $E_T$, is a so-called $\chi$ (chi) distribution with six degrees of freedom (see [46]). This is defined as:

$$\begin{aligned} f(E_T) &= \frac{E_T^5}{8\sigma^6} e^{-E_T^2/2\sigma^2} \\ \sigma^2 &= \frac{E_T^2}{6}, \end{aligned} \tag{4.5}$$

where the $\sigma^2$ denotes the variance of either a real or imaginary part of a rectangular component of the electric field (Eq. (4.2)). A $\chi$-distribution will be realized by summation of a number of standard normal distributions, where the number of variables defines the degrees of freedom (see [46] and [76]). The real and imaginary parts of each rectangular component of the electric field are normally distributed inside a well-stirred chamber. Consequently, the magnitude of the total electric field, $E_T$, is a summation of six normally distributed field parts and, therefore, this becomes a $\chi$-distribution with six degrees of freedom.

Besides the electric field also the average received power over all stirrer steps $N$ at a certain location inside the test volume is of relevance, which is given by [46]:

$$\langle P_r \rangle_N = \frac{1}{2} \cdot \frac{\langle E_T^2 \rangle_N}{\eta} \cdot \frac{\lambda^2}{4\pi}, \tag{4.6}$$

where the last term on the right-hand side can be recognized as the effective area of an isotropic antenna. As mentioned in Section 4.1, the field within the RC is ideally isotropic. As a consequence, also a realistic antenna (with directivity) illuminated by an isotropic field can be described by the effective area of the isotropic antenna. In other words, the directivity information of the antenna is lost because of the isotropic behavior of the incident field. The factor ½ in the equation accounts for the polarization mismatch error correction. When Eq. (4.4) is substituted into Eq. (4.6), we obtain an expression which relates the received power and the transmitted power. Performing this substitution yields:

$$\langle P_r \rangle_N = \frac{\lambda^3 Q}{16\pi^2 V} P_t. \tag{4.7}$$

The latter equation brings us to another parameter which is often used as a chamber quality parameter namely the chamber gain. The chamber gain $\langle G_c \rangle$ is defined as:

$$\langle G_c \rangle_N = \frac{\langle P_r \rangle_N}{P_t} = \frac{\lambda^3 Q}{16\pi^2 V}, \tag{4.8}$$

where $Q$ is actually an average quality factor in this case, because the presence of the rotating stirrer(s) causes a small variation in $Q$. However, the $\langle G_c \rangle$ defined as the received power divided by the transmitted power is a more physical parameter. In the IEC 61000-4-21 standard, different types of the chamber gain are used as calibration parameters. These parameters will be introduced in the next section.

The average received power (Eq. (4.7)) is statistically described by a $\chi^2$ (chi-squared) distribution with two degrees of freedom; this is equal to an exponential distribution:

$$f_{\chi_2^2}(x) = \frac{1}{2\sigma^2} e^{-x/2\sigma^2} \cdot U(x), \tag{4.9}$$

where $U(x)$ is Heaviside's function. The mean of an exponential distribution is $2\sigma^2$. When a radiated emission measurement is performed in an RC we can measure the maximum or the average value of a quantity, e.g., the maximum or average received power. In practice, measuring the maximum value is beneficial when a limited dynamic range is available, which is typical for emission measurements at frequencies above 1 GHz. However, the maximum, taken from a series of $N$ samples (stirrer steps) of a certain variable, is a different statistical distribution than the original distribution of the variable [76]. This will be explained now for the received power. In the following equations, the variable $x$ stands for the received power $P_r$.

When the Probability Density Function (PDF) of a statistical variable $x$ is $f_A(x)$, then the PDF for the maximum value (denoted as $\lceil\ \rceil$) can be defined as:

$$f_{\lceil A \rceil_N}(x) = N \cdot [F_A(x)]^{N-1} f_A(x). \tag{4.10}$$

This can be interpreted as the PDF of the maximum value, when the experiment of taking the maximum from $N$ samples (stirrer steps) is repeated. When Eq. (4.10) is used for the received power ($\chi^2$-distribution with two degrees of freedom), then the following PDF for the maximum received power is obtained:

$$f_{\lceil \chi_2^2 \rceil_N}(x) = \frac{N}{2\sigma^2}\left[1 - e^{-x/2\sigma^2}\right]^{N-1} e^{-x/2\sigma^2}. \tag{4.11}$$

The mean of the maximum can be determined by:

$$\left\langle \lceil \chi_2^2 \rceil_N \right\rangle = \int_0^\infty x \cdot N\left[1 - e^{-x/2\sigma^2}\right]^{N-1} \frac{1}{2\sigma^2} e^{-x/2\sigma^2} dx. \tag{4.12}$$

Equation (4.12) can be transformed to a finite sum by using binomial expansion and integrating by parts (see Annex A1). Subsequently, the mean of the maximum can be determined by approximation of a finite sum (by using Eq. (0.131) in [42]):

$$\begin{aligned} \left\langle \lceil \chi_2^2 \rceil_N \right\rangle &= 2\sigma^2 \sum_{i=1}^{N} \frac{1}{i} \approx 2\sigma^2\left(\gamma + \ln(N) + \frac{1}{2N}\right) \\ &= \left\langle \chi_2^2 \right\rangle\left(\gamma + \ln(N) + \frac{1}{2N}\right), \end{aligned} \tag{4.13}$$

where $\gamma \approx 0.57721$ is the Euler-Mascheroni constant and $\left\langle \chi_2^2 \right\rangle = 2\sigma^2$ is the mean of the received power (exponential distribution) as given in Eq. (4.9). From Eq. (4.13), an important parameter called maximum-to-average ratio for an exponential distribution can be determined, denoted as $\xi_N$:

$$\xi_N(P_r) = \xi_N\left(\chi_2^2\right) = \frac{\left\langle \lceil \chi_2^2 \rceil \right\rangle}{\left\langle \chi_2^2 \right\rangle} = 0.577 + \ln(N) + \frac{1}{2N}. \tag{4.14}$$

During RC measurements, the maximum-to-average ratio can be used to estimate the average received power when the maximum received power was measured:

$$\left\langle P_r \right\rangle_N = \frac{\lceil P_r \rceil_N}{\xi_N(P_r)}. \tag{4.15}$$

The transformation from the maximum to the average received power as presented in Eq. (4.15) is also an important underlying principle in the calibration of the RC in accordance with the IEC 61000-4-21 standard. This will be highlighted during the

discussion of the calibration in Section 4.3. Statistics of either the maximum or the minimum of other field quantities inside the RC are derived in [65]. For example, the theoretical value of the maximum-to-minimum ratio of the received power is determined by applying this kind of statistics. As mentioned in Section 4.1, the maximum-to-minimum ratio of the received power can be used as a measure to evaluate the stirrer effectiveness.
The stirrer effectiveness, defined as the maximum-to-minimum ratio of the received power, of a compact RC (1.27 m × 0.95 m × 0.8 m, see Figure 4.4) is depicted in Figure 4.3. In this figure, the measured stirrer effectiveness is compared with the theoretically expected value based on the statistical distribution (exponential) of the received power. The minimum recommended stirrer effectiveness is 20 dB, which originates from practical experience. It is interesting to notice that this small RC has an excellent statistical correlation with other RCs, which have other dimensions [65].

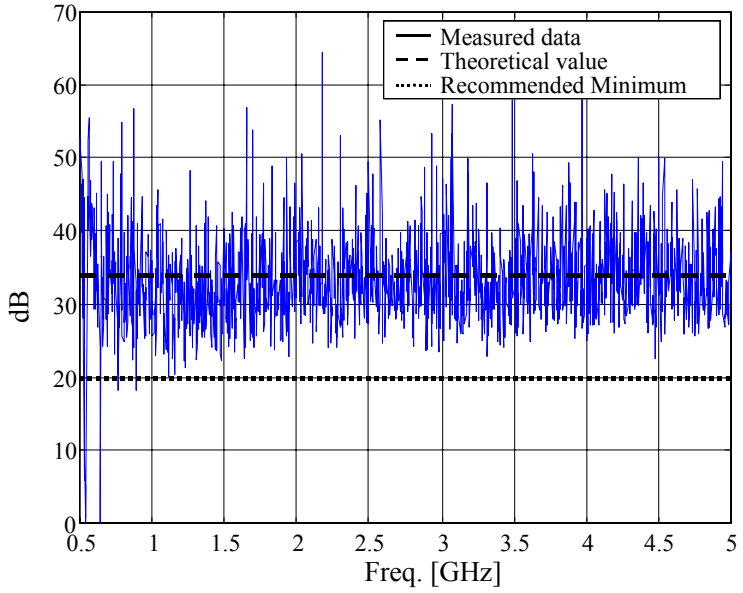


Figure 4.3 Maximum-to-minimum ratio in dBs of the received power for $N$=225.

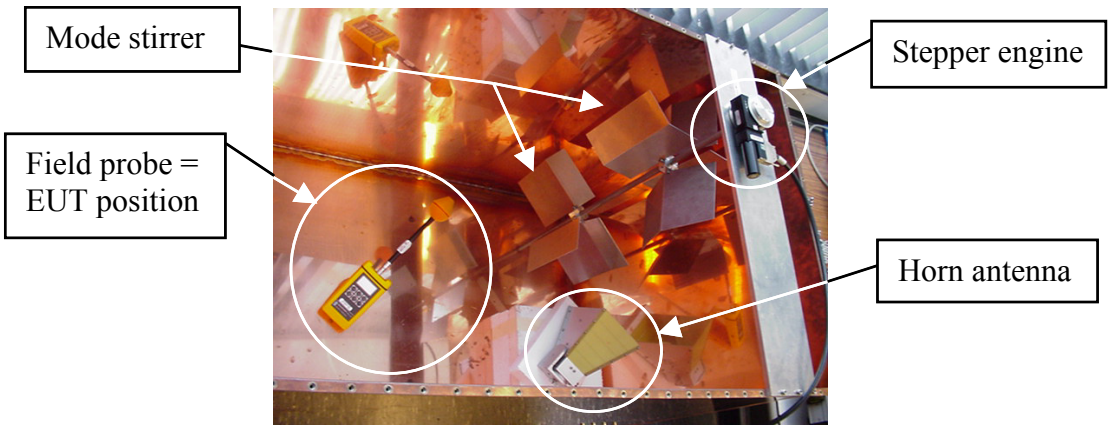


Figure 4.4 Inside view of a compact RC configuration (top cover is removed).

## 4.3 Summary of calibration process

### 4.3.1 Calibration factors for power conversion

In Annex B of the IEC 61000-4-21 standard [54], the RC calibration procedure is described. This calibration includes the field uniformity validation as well as a power transfer calibration. The power transfer calibration is necessary to determine the power loss of the chamber. Moreover, the power-loss information is needed for immunity testing where a certain input power is applied in order to realize a certain field-strength level. When the emission of an EUT is measured, the power transfer calibration parameters are necessary to compute the radiated power of the EUT from the measured power. The Antenna Calibration Factor (*ACF*) and the Insertion Loss (*IL*) are measured in the empty RC (no EUT load) using either at least eight (<1 GHz) or at least three (>1 GHz) field probe readings measured at different locations, respectively. The *ACF* and *IL* are defined as:

$$ACF = \left\langle \frac{P_{\text{Ave Rec}}}{P_{\text{input}}} \right\rangle, \qquad IL = \left\langle \frac{P_{\text{Max Rec}}}{P_{\text{input}}} \right\rangle, \tag{4.16}$$

where $P_{\text{Ave Rec}}$ and $P_{\text{Max Rec}}$ are, the average and the maximum received power over one stirrer rotation, respectively, and where $P_{\text{input}}$ is the power transmitted into the chamber. The *ACF* is the spatial average of the power transfer between the transmit and receive antenna within the whole test volume of the chamber, defined by the eight field probe locations. In other words, the inverse *ACF* describes the spatial average ratio of power loss measured over the whole test volume of the empty chamber. When the *IL* is divided by *ACF* we end up with the maximum-to-average ratio $\xi_N$ as already derived in Eq. (4.14).

$$\xi_N = \frac{IL}{ACF}. \tag{4.17}$$

The Chamber Calibration Factor (*CCF*) is similar to the *ACF*, but now of a chamber including the EUT and its associated equipment and with the receive antenna at a single location. It is defined as follows:

$$CCF = \left\langle \frac{P_{\text{Ave Rec}}}{P_{\text{input}}} \right\rangle. \tag{4.18}$$

The *CCF* defines the power transfer ratio in the same manner as the *ACF*, but now only at a single receive antenna location. This location should be preferably the same as in the final measurement after the calibration procedure. The inverse *CCF* describes the ratio of power loss measured within the chamber including the EUT and its supporting equipment. When the *ACF* is divided by *CCF*, a new factor is obtained which is called the Chamber Loading Factor (*CLF*) and is defined as:

$$CLF = \frac{CCF}{ACF}. \tag{4.19}$$

The *CLF* expresses the power loss by placing the EUT and its supporting equipment in the RC.

### 4.3.2 Field uniformity calibration

The field uniformity in the RC will be expressed in terms of the standard deviation of the field inside the chamber. As a first step in the calibration, the normalized maximum electric field-strength measurement $\ddot{E}$ is calculated for different locations in the test volume:

$$\ddot{E} = \frac{E_{\max}}{\sqrt{P_{\text{input}}}}, \tag{4.20}$$

where $E_{\max}$ is the maximum electric field-strength reading of one location over all stirrer steps and $P_{\text{input}}$ is the input power. The $\ddot{E}$ is determined for three rectangular components (x,y,z) of the electric field separately as well as for the magnitude (total) of the electric field (Eqs. (4.2) and (4.3)). Subsequently, the arithmetic mean of the normalized electric field over the locations ($N_{\text{loc}}$) is calculated:

$$\left\langle \ddot{E} \right\rangle = \frac{\sum_{N_{\text{loc}}} \ddot{E}_{N_{\text{loc}}}}{N_{\text{loc}}}. \tag{4.21}$$

Because of the fact that mostly a cubical test volume is calibrated, typically a number of 9 locations is taken, $N_{\text{loc}}$=9, in this way, the corners and the center of the cubical test volume can be defined. Finally, the standard deviations of the three rectangular field components and the magnitude of the field can be calculated as follows:

$$\sigma = \sqrt{\frac{\sum_{N_{\text{loc}}} \left( \ddot{E}_{N_{\text{loc}}} - \left\langle \ddot{E} \right\rangle \right)^2}{N_{\text{loc}} - 1}}. \tag{4.22}$$

The standard deviation can be normalized and expressed in dBs:

$$\sigma_{dB} = 20 \cdot \log\left( \frac{\sigma + \left\langle \ddot{E} \right\rangle}{\left\langle \ddot{E} \right\rangle} \right), \tag{4.23}$$

which shall be smaller than 3 dB to comply with the IEC 61000-4-21 standard at frequencies above 200 MHz. At frequencies in the range 80-200 MHz, the requirement that defines the maximum standard deviation of the field components decreases linearly from 4 dB to 3 dB.

## 4.4 Emission measurement procedure

In radiated emission measurements, we need to determine the *CCF*, *CLF*, or *IL* (Eq. (4.18)-(4.19)) in order to take the losses of the RC and EUT into account. The output of the RC emission measurement, the total radiated power of the EUT, $P_{\mathrm{Rad}}$, can be obtained by determining either the average $\langle P_{\mathrm{AveRec}} \rangle_N$ or the maximum $\langle P_{\mathrm{MaxRec}} \rangle_N$ value of the measured received power:

$$P_{\mathrm{Rad}} = \frac{\langle P_{\mathrm{AveRec}} \rangle_N \cdot \eta_{Tx}}{CCF}, \qquad P_{\mathrm{Rad}} = \frac{\langle P_{\mathrm{MaxRec}} \rangle_N \cdot \eta_{Tx}}{CLF \cdot IL}, \tag{4.24}$$

where the parameter $\eta_{Tx}$ is the antenna efficiency, which is typically 0.9 for a horn antenna and 0.75 for a log-periodical antenna. If we consider the denominator of the second term of Eq. (4.24) and substitute Eq. (4.17) in Eq. (4.24), then we end up with:

$$CLF \cdot IL = CCF \cdot \frac{IL}{ACF} = CCF \cdot \xi_N . \tag{4.25}$$

Equation (4.25) indicates the underlying use of the maximum-to-average ratio. Evaluating Eq. (4.24) again, it becomes clear that the measured average received power will be corrected by both the chamber losses and the EUT losses. The result of the radiated emission measurement is the total radiated power of the EUT. From the total radiated power (Eq. (4.24)), a radiated electric field can be derived using the free-space formulation:

$$E_{\mathrm{Rad}} = \sqrt{\frac{G \cdot P_{\mathrm{Rad}} \cdot \eta_0}{4\pi d^2}}, \tag{4.26}$$

where $G$ is the EUT's directivity, $\eta_0 = 377\,\Omega$ is the wave impedance of free space, and $d$ is the distance of the point for which the field was calculated from the EUT's position. It is noted that $G$ is the directivity of the EUT. We use the symbol $G$ for the directivity because the symbol $D$ is used for the deviation in the following sections.

We have now arrived at the difficult issue of the EUT's directivity $G$. This is difficult because the EUT's $G$ is *a priori* not known and it is also not measured during the radiated emission measurement. In the standard IEC 61000-4-21, a note was included which describes the recommendation of using a directivity $G$=1.7 (equivalent to the directivity of a small dipole radiator) unless the product committee can supply a more appropriate value. The tuning effect in the RC causes a statistical (over the stirrer steps) uniform and isotropic field in a well-performing chamber. The effective directivity of the EUT in an RC seems to become $G_{\mathrm{eff}}$ =1, because the field (radiated emission) are stirred and will be incident on the receive antenna in an isotropic way. Because of the lack of knowledge about the EUT's directivity, investigations have been performed in order to determine average directivities for certain classes of EUTs [64], [92]-[94]. Further considerations of the aspects of the directivity of EUTs are given in Section 4.7.

## 4.5 Conversion method

In this Section, an overview is given of a procedure to convert and compare reverberation chamber results to OATS/SAR results. The development of a standardized conversion method is essential to accelerate the proliferation of alternative measurement methods such as the RC. Several of these alternative test methods are advantageous in terms of either reduced measurement time or better reproducibility. Moreover, also company-specific bench-test or pre-compliance measurement methods can be validated in the future by using the standardized conversion method. The 10 m OATS/SAR measurement is considered as the measurement method for which the radiated emission limit is established. CISPR/A has published a technical report in CISPR 16-4-5 that describes a conversion method [18][61][62]. This conversion method is intended for comparing results obtained from established and alternative test methods. An established test method (EM) is a measurement method which is described in a basic standard and for which limits have been established for many years. On the other hand, an alternative test method (AM) is a measurement method which is described in a basic standard as well, but without established limits. In [61][62], examples are given of a comparison between the 10 m OATS/SAR and 3 m FAR measurements as well as a comparison between the 10 m OATS/SAR and 3 m OATS/SAR measurements. In this Section, the conversion procedure described in CISPR 16-4-5 is applied to compare results obtained from an RC measurement and an OATS/SAR measurement. The method described in [61][62] is not only suitable for radiated emission measurements, but can also be used for other types of EMC emission measurements. An introduction of the conversion method as described in CISPR 16-4-5 is given in Subsections 4.5.1-4.5.3.

### 4.5.1 Selection of a reference quantity

The comparison procedure starts with an apparently trivial but essential step, namely, the choice of the reference quantity *X*. This is the reference in which the essential requirement of radio protection is expressed, e.g., a maximum electric field-strength level at a certain distance from the EUT. After the definition of the reference quantity, the specific measurement can be performed. Each measurement method leads to a set of results denoted by *M*, which can deviate from the reference quantity *X*. The deviation *D* of both the alternative method and the established method (AM & EM) for a specific EUT (index *i*) is defined as (in dBs):

$$D_{AMi}(f) = X_i(f) - M_{AMi}(f), \quad D_{EMi}(f) = X_i(f) - M_{EMi}(f). \tag{4.27}$$

The deviations depend on the specific measurement methods of the comparison. For example, on a 10 m OATS/SAR the radiated emission measurement of the maximum electric field is estimated by application of the height-scanning antenna (1 - 4 m) at a 10 m measurement distance, and by the rotation of the EUT. However, by using this procedure

the actual maximum might not be captured. Consequently, also an established method might suffer from a deviation compared to an ideal reference.

### 4.5.2 Determination of the standard and inherent uncertainties

If a general conversion factor of emission results is needed rather than for a specific EUT only, the average deviation should be computed by testing many different EUTs. For example, it is useful to define conversions for specific classes of EUTs. The measurement results of all different EUTs, (index *i*) in the specific class of EUTs for which we want to determine the conversion factor, will result in the average and the standard deviation of *D*. The averages of the deviations of both the established method and alternative method are defined as:

$$\tilde{\mu}(D_{AM}) = \frac{1}{N}\sum_{i=1}^{N} D_{AMi}, \qquad \tilde{\mu}(D_{EM}) = \frac{1}{N}\sum_{i=1}^{N} D_{EMi}. \tag{4.28}$$

Subsequently, also the standard deviation can be calculated, which will be called the inherent uncertainty $u_{\text{inherent}}$. The inherent uncertainty is caused by the different radiation behavior of the different EUTs exhibited in either the alternative or established method and can also be defined as 'measurement method uncertainty'. The relevant quantities are defined as:

$$u_{AM,\text{inherent}} = s(D_{AM}) = \sqrt{\frac{\sum_{i=1}^{N}\left(D_{AMi} - \tilde{\mu}(D_{AM})\right)^2}{N-1}}, \tag{4.29}$$

$$u_{EM,\text{inherent}} = s(D_{EM}) = \sqrt{\frac{\sum_{i=1}^{N}\left(D_{EMi} - \tilde{\mu}(D_{EM})\right)^2}{N-1}}. \tag{4.30}$$

If both instrumentation and measurement method uncertainties are present, the combined uncertainty can be calculated as follows:

$$u_{AM} = \sqrt{u_{AMm}^2 + u_{AM,\text{inherent}}^2}, \qquad u_{EM} = \sqrt{u_{EMm}^2 + u_{EM,\text{inherent}}^2}, \tag{4.31}$$

where $u_{\text{m}}$ includes both the instrumentation and the measurement method uncertainties. The expanded uncertainty *U* can be calculated by using the coverage factor *k* which depends on the probability distribution, the number of experiments *N* (degrees of freedom), and the level of confidence (usually 95%). Assuming a normal probability distribution, we can find the coverage factor *k* in a *t*-distribution table (sampled normal distribution) [76]. This yields the expanded uncertainty of the established and the alternative test method:

$$U_{AM} = k \cdot u_{AM}, \qquad U_{EM} = k \cdot u_{EM}. \tag{4.32}$$

### 4.5.3 Computation of the conversion factor

The final step in the conversion method is the determination of the actual conversion factor *C*. For each individual EUT the conversion factor can be calculated by subtracting the deviations *D* (in dBs) of the established and the alternative test method. This results in:

$$C_i(f) = D_{AMi}(f) - D_{EMi}(f). \tag{4.33}$$

As a subsequent step the average conversion factor of all EUTs (index *i*) can be calculated:

$$\tilde{\mu}(C(f)) = \tilde{\mu}(D_{AM}(f)) - \tilde{\mu}(D_{EM}(f)), \tag{4.34}$$

where $\tilde{\mu}(C(f))$ is the (estimated) average of the conversion factor *C(f)*. The (estimated) averages $\tilde{\mu}(D_{AM}(f))$ and $\tilde{\mu}(D_{EM}(f))$ are values which were calculated earlier, see Subsection 4.5.2. When the $\tilde{\mu}(D_{AM}(f))$ and $\tilde{\mu}(D_{EM}(f))$ are represented by their expressions as introduced in Eqs. (4.27)-(4.28), the following expression for the average conversion factor is obtained:

$$\begin{aligned}\tilde{\mu}(C) &= \frac{1}{N}\sum_{i=1}^{N}(X_i - M_{AMi}) - \frac{1}{N}\sum_{i=1}^{N}(X_i - M_{EMi}), \\ &= \frac{1}{N}\sum_{i=1}^{N}(M_{EMi} - M_{AMi}).\end{aligned} \tag{4.35}$$

With the achieved average conversion factor $\tilde{\mu}(C(f))$ the limit of the established test method (e.g., CISPR 22 radiated emission limit) can be translated into a limit for the alternative test method. If the $L_{EM}$ denotes the limit of the established method, the limit for the alternative test method ($L_{AM}$) is found as follows:

$$L_{AM}(f) = L_{EM}(f) - \tilde{\mu}(C(f)). \tag{4.36}$$

However, it is necessary in accordance with the conversion method [61][62] to correct the alternative limit by the difference $\Delta$ between the uncertainties $U_{EM}$ and $U_{AM}$ (Eqs. (4.29)-(4.32)) of the measurement methods:

$$\Delta(f) = U_{AM}(f) - U_{EM}(f). \tag{4.37}$$

Using this difference we end up in the final definition of the limit for the alternative measurement method:

$$L_{AM,U}(f) = \begin{cases} L_{AM}(f) - \Delta(f) & \text{if } \Delta(f) > 0 \\ L_{AM}(f) & \text{if } \Delta(f) \le 0. \end{cases} \tag{4.38}$$

In other words, a penalty $\Delta$ is applied only when the total uncertainty $U_{AM} > U_{EM}$.

## 4.6 Derivation of emission limit applicable for the RC

In this section, the conversion method is demonstrated by the derivation of an RC limit, based on the established CISPR 22 measurement method and class B limit. Large products or systems can include various small emission sources. The conversion of such products can be approximated by the simulation of various isotropic point sources distributed over a grid of nodes. The grid size emulates the size of the product. The derivation of the conversion is performed by simulations based on geometrical-optics [78]. In this analysis, 25 isotropic point sources have been used. The point sources are located at nodes of a 5-by-5 equally spaced grid (0.4 m separation) and are simulated separately. The EUT height is varied from 0.4 m to 2.0 m in 0.4 m steps and the measurement distance is varied from 9.2 m to 10.8 m again in 0.4 m steps. Figure 4.5 shows the simulated OATS/SAR configuration. In this figure, the depicted antenna is only symbolic. The electric field-strength is simulated in points along the height-scan track without antenna. The isotropic point source EUTs are not rotated in this simulation. Furthermore, the results obtained for horizontal and vertical polarization are considered separately. This deviates from the actual OATS/SAR measurement procedure and is performed to gain insight.

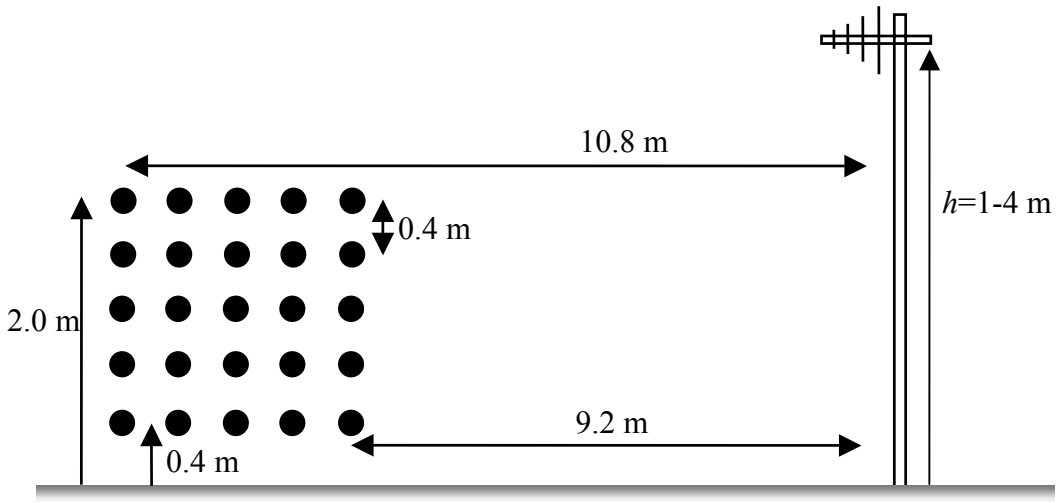


Figure 4.5 Overview simulation configuration.

### 4.6.1 Choice of the reference quantity

Radio services are protected by posing limits to the radiated emission of an EUT. Therefore, the maximum of the radiated (free-space) electric field of an EUT at a reference distance of 10 m in any direction is an appropriate choice to be the reference quantity $X$. This results in:

$$X = E_{\text{ref}} = 20 \cdot \log\left|\frac{A}{d_{\text{ref}}} e^{-jkd_{\text{ref}}}\right| = 20 \cdot \log\left(\frac{A}{d_{\text{ref}}}\right), \tag{4.39}$$

where $d_{ref}$=10 m is the measurement distance at which the quantity $X$ is determined, $k$=2π/λ, and $A$ is a factor which includes the directivity (directivity=1 in this case) and power information. This information is usually unknown in real measurements of practical EUTs.

### 4.6.2 Determination of the deviation

Before we can calculate the deviation $D$ (Eq. (4.27)), we need to define the measurand $M$ for both the established (10 m OATS/SAR) and the alternative (RC) measurement method. The measurand $M$ for the 10 m OATS/SAR measurement in the case of an isotropic point source EUT can be calculated as:

$$M_{oats} = 20 \cdot \log \left| \frac{A}{\sqrt{d_{oats}^2 + h_1^2}} e^{-jk\sqrt{d_{oats}^2+h_1^2}} + \rho \cdot \frac{A}{\sqrt{d_{oats}^2 + h_2^2}} e^{-jk\sqrt{d_{oats}^2+h_2^2}} \right|_{\max h=1-4\,\mathrm{m}} \quad (4.40)$$

where $h_1$=$h$-$o$, $h_2$=$h$+$o$, $h$ is the height of the receive antenna and the offset $o$ is the height of the EUT, $d_{oats}$=10 m, $\rho$ is the reflection coefficient of the ground plane (i.e. $\rho$≈1 and $\rho$≈-1 for vertical and horizontal polarization, respectively) and $A$ is a factor related to radiated power. Subtracting the reference quantity $X$ and the measurand $M_{oats}$, $D_{oats}$=$X$-$M_{oats}$, yields the deviation $D_{oats}$. Because of the condition that we have one EUT at 25 positions in this comparison, 25 $M$ and $D$ curves are obtained.

The deviations $D_{oats}$ are depicted in Figure 4.6 for both horizontal and vertical polarization ($A$=1). The corresponding inherent or 'measurement method uncertainty' (Eqs. (4.30)-(4.32)) is depicted in Figure 4.7. In this figure the $k$=1.96 factor (95%) was already taken into account. This means, the dashed solid line in Figure 4.7 is an expanded uncertainty of the inherent uncertainty.

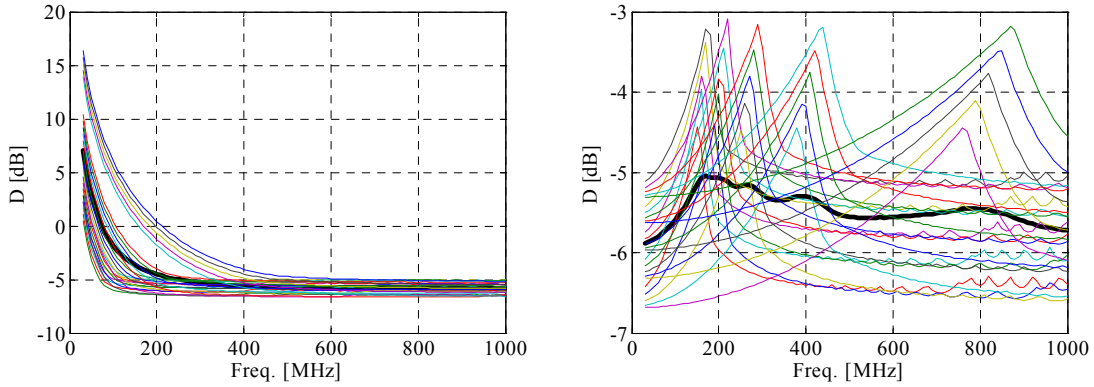


A. Horizontal polarization B. Vertical polarization

Figure 4.6 Deviation $D_{oats}$ for horizontal polarization (A) and vertical polarization (B). The average is the bold solid line.

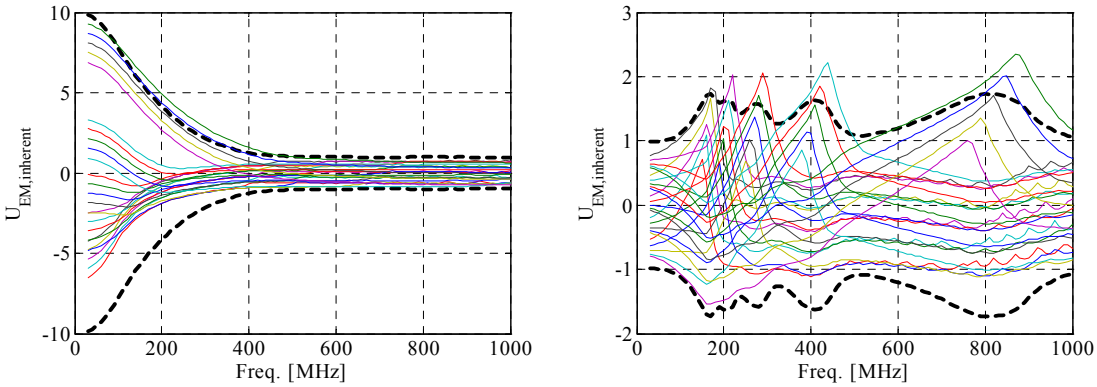


A. Horizontal polarization B. Vertical polarization

Figure 4.7 Inherent uncertainty (normalized to average) of $D_{oats}$ for horizontal polarization (A) and vertical polarization (B). The bold dashed line is the expanded uncertainty ($k$=1.96).

Subsequently, we need to determine the deviation $D_{reverb}$ of the RC. Due to the fact that we have chosen a hypothetical isotropic point source as EUT, the problem of the unknown directivity is avoided, i.e., $G$=1. The measurand of the radiated emission measurement performed in an RC is defined as:

$$M_{reverb} = 20 \cdot \log\left(\sqrt{\frac{G \cdot P_{\mathrm{Rad}} \cdot \eta_0}{4\pi d^2}}\right) = 20 \cdot \log\left(\frac{A}{d}\right), \tag{4.41}$$

where $G$=1 is the EUT's directivity, $d$=$d_{ref}$=10 m, $\eta_0$=377 Ω, $P_{Rad}$ is the measured radiated power and $A$ is the same factor as mentioned above and in Subsection 4.6.1.

Because of the fact that in an OATS/SAR radiated emission measurement the electric field is measured (by using the AF of the receive antenna) and in an RC the radiated power, the mentioned factor $A$ can be determined:

$$A = \sqrt{\frac{G \cdot P_{\mathrm{Rad}} \cdot \eta_0}{4\pi}}. \tag{4.42}$$

Moreover, we can observe that the factor $A$ depends on the EUT's directivity, the total radiated power, and the wave impedance $\eta_0$=377 Ω. Observing the measurand $M_{reverb}$ discussed above, the deviation $D_{reverb}$ of the RC becomes 0 dB:

$$D_{reverb}(f) = X(f) - M_{reverb}(f) = 0 \text{ dB}. \tag{4.43}$$

It must be emphasized that $D_{reverb}$=0 dB for all EUTs for which the directivity approximation $G$=1.7, in accordance with the standard, is an appropriate approximation. However, if we do not use an isotropic point source EUT the $X$, $M_{oats}$ and $M_{reverb}$ cannot be calculated as easily as it was done above from Eqs. (4.39)-(4.41). However, 3-D full wave

numerical results of an actual RC measurement configuration are presented in [14]. Such numerical simulations can be used to simulate more complex EUTs in SARs and RCs as well as to perform uncertainty assessments. The directivity as influence factor in limit conversion will be discussed in Section 4.7.

### 4.6.3 Determination of the conversion

The deviations $D$ of both the established and the alternative method are determined for a simple type of EUT, i.e., an isotropic point source, the conversion $C$ of this specific class of EUTs (isotropic point sources) can be calculated as well (Eq. (4.33)):

$$C(f) = D_{reverb}(f) - D_{oats}(f). \tag{4.44}$$

From Eq. 0, we know that $D_{reverb}$=0. This results in the following conversion factor:

$$C(f) = -D_{oats}(f). \tag{4.45}$$

This calculation should be performed after all quantities have been translated into dBs. In Figure 4.8, the result of the conversion procedure is depicted for both horizontal and vertical polarization. For actual EUTs, the conversion will only be determined by the maximum of both vertical and horizontal polarization, i.e., one conversion curve is obtained in practice.

### 4.6.4 The limit *L* for the alternative measurement method

As a final step the determination of the limit for the alternative test method, in our case an RC, can be accomplished.

$$L_{reverb}(f) = L_{oats}(f) - C(f). \tag{4.46}$$

From Eq. (4.45), we know that $C$=-$D_{oats}$. This results in the new limit for the alternative test method:

$$L_{reverb}(f) = L_{oats}(f) + D_{oats}.$$

In Subsection 4.5.3, it was explained that also the uncertainty considerations must be taken into account for the limit definition Eqs. (4.37)-(4.38). In Figure 4.7, the inherent uncertainty of the 10 m OATS measurement was presented for this hypothetical class of EUTs. For more realistic EUTs, uncertainty aspects will be discussed in Sections 4.7 and 4.8.

The new limit for the radiated emission measurement of the isotropic point source EUT in the RC is shown in Figure 4.9 in relation to the CISPR 22 radiated emission limit. Finally, it must be noted that $D_{oats}$ was calculated using $A$=1, see step 2 Subsection 4.6.2. If $A$=1 then $P_{rad}$ of the RC measurement was apparently 1/30 W according to Eq. (4.42).

From the two polarizations (horizontal and vertical) of this class of EUTs, it can be concluded that the limit for radiated emission measurements in an RC must be reduced by approximately 5 dB. In Figure 4.9, it can be observed that in the frequency range 80-250 MHz the difference between the CISPR 22 limit and the horizontal RC limit is less than the average 5 dB. This is due to the well-known OATS/SAR relaxation for low frequencies at horizontal polarization. This is explained from the observation that the maximum constructive interference cannot be found for the limited height scan from 1 m to 4 m.

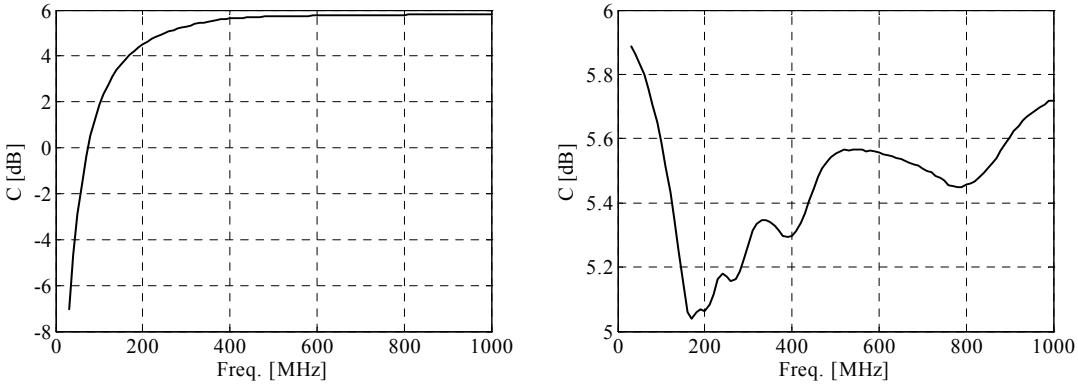


A. Horizontal polarization B. Vertical polarization

Figure 4.8 Conversion factors for RC results towards 10 m OATS results applicable to a set of isotropic point sources for horizontal polarization (A) and vertical polarization (B).

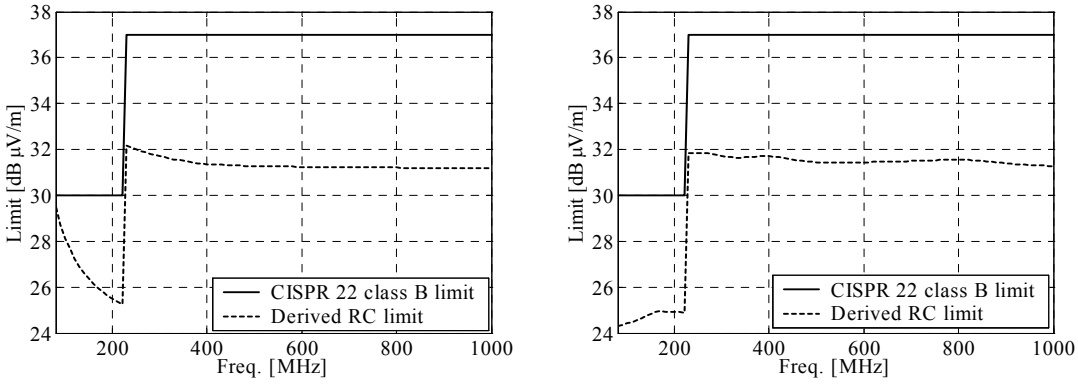


A. Horizontal polarization B. Vertical polarization

Figure 4.9 Existing CISPR 22 class B limit and the new limit for RC radiated emission measurement of a set of horizontally (A) and vertically (B) polarized isotropic point sources.

Up to now, we have discussed the conversion method described in [61][62]. This method has been developed by CISPR/A. The conversion method is straightforward in the application. In this section, the attention was on the conversion of radiated emission measurements performed at an OATS/SAR and within an RC. In Section 4.5, we have discussed the problem of the lack of knowledge of the EUT's directivity in the translation of the total radiated power measured in an RC into radiated electric field-strength. Hence, we have chosen an isotropic point source EUT, because the directivity of such a radiator equals one for all radiation angles.

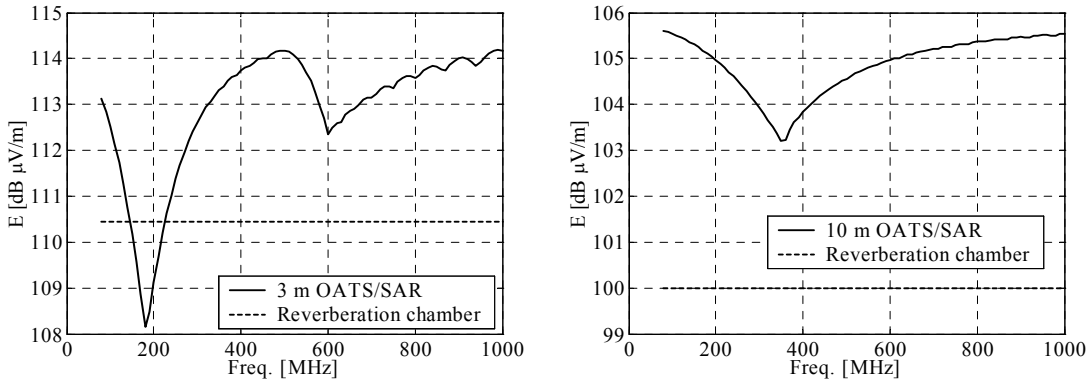


A. 3 m results B. 10 m results

Figure 4.10 Radiated emission results of a vertically polarized tuned dipole powered with 20 mW measured in an RC, 3 m SAR (A) and 10 m SAR (B).

In addition, also some simulations are performed by using tuned dipoles from which the directivity is known as well, i.e., $G$=1.65. It is noted that actually two established methods are applied here, i.e., the 10 m OATS/SAR method and the 3 m OATS/SAR method. Also for the 3 m OATS/SAR method, radiated emission requirements have been available for many years (e.g., CISPR 13 and FCC 15). Therefore, it is useful to consider both as reference methods. In Figure 4.10, simulated radiated emission results are shown of vertically polarized tuned dipoles obtained from an RC compared to results obtained from a 3 m SAR and 10 m SAR, respectively. The electric field-strength results of the RC are obtained by using Eq. (4.26).

We observe approximately 5 dB lower results in an RC as also observed in Figure 4.9. This difference is caused by the free-space transformation of the radiated power measured in the RC. In this way, the radiated emission results obtained from an RC emission measurement are actually free-space results. In the OATS/SAR a ground reflection is present which can cause a maximum constructive interference of 6 dB. Accordingly, the RC measurement method and the FAR measurement method are both free-space methods, i.e., the same limit can be used apart from possible corrections due to uncertainty differences. It is finally interesting to observe that the 'constructive interference gain' is roughly 1 dB smaller in a 3 m SAR than within a 10 m SAR, see Figure 4.10. This is caused by the different antenna height-scanning (1 - 4 m) in proportion to the different measurement distances (3 m and 10 m), which results in a different elevation angle between EUT and receive antenna. A

larger elevation angle will subsequently cause a larger propagation distance of the emission and accordingly more attenuation.

It is clear that the conversion of limits of different emission measurement methods needs statistical considerations, which can be simplified somewhat if very specific classes of EUTs are considered. From considering isotropic point sources and tuned dipoles, it can be concluded that the limit for radiated emission measurements in an RC should be reduced by approximately 5 dB in relation to the 10 m OATS/SAR measurement and reduced by approximately 4 dB in relation to the 3 m OATS/SAR measurement.

## 4.7 Evaluation of the uncertainty caused by the directivity of EUTs

### 4.7.1 Review of statistical EUT modeling

In the previous Section, limits for radiated emission measurements in the RC were derived. This was performed by considering EUTs for which the directivity is known, in particular an isotropic point source and a tuned dipole. A conclusion could be drawn, namely, the conversion factor for RC results to SAR results is approximately 4 to 5 dB, for 3 m and 10 m measurement distance, respectively. It was already stated in Section 4.5 that the directivity of the EUT is an important parameter in radiated emission measurements performed in the RC. The field emitted by the EUT is stirred and will accordingly illuminate the receive antenna isotropically so that the directivity information of the EUT is lost. The directivity is an important parameter in transforming the measured radiated power to a radiated electric field as defined in Eq. (4.26). For that reason, the directivity issue of EUTs is evaluated in this section in more detail. A theoretical model to approximate the maximum directivity, $G_{\max}$, of an unintentional radiator is introduced which is based on statistics [64][92]. Actually, the model describes the maximum-to-average ratio of the received power of an arbitrary EUT. The expression of this model is presented in Eq. (4.47):

$$\frac{\lceil P_r \rceil}{\langle P_r \rangle} = \begin{cases} 1.55, & \text{if } ka \le 1 \\ 0.577 + \ln(N) + \dfrac{1}{2N} & \text{if } ka > 1, \end{cases} \tag{4.47}$$

where $N$ is the number of independent samples and can be approximated by the number of spherical or cylindrical wave modes. The $N$ is different for either a cylindrical scan (planar cut) ($N_c$) or a spherical ($N_s$) scan of the EUT:

$$\begin{aligned} N_S &= 4(ka)^2 + 8ka, \\ N_c &= 4(ka) + 2, \end{aligned} \tag{4.48}$$

where $k$ is the wave number and $a$ is defined as the radius of a sphere that encompasses the EUT. The background of this model can be found in [43][92] and only a brief explanation

will be given here. The model is based on a $\chi^2$-distribution with two degrees of freedom, which is equal to an exponential distribution. In [65], the standard deviation of such a distribution is listed as a function of the number of samples. When the maximum is estimated, the standard deviation lies between 2.0 and the limit value 2.6, which results in a 95% spread of approximately 2 dB.
Equation (4.47) can be explained by considering the maximum-to-average ratio for the received power in the RC as presented in Eq. (4.14). Both ratios (Eqs. (4.14) and (4.47)) are actually the same if $N>1$, i.e., they have the same underlying assumption that the three rectangular electric field components (real and imaginary parts) comply with a standard normal distribution. The received power measured in the RC and the directivity of an EUT (maximum versus average received power) are both quantities weighted over all angles of incidence (isotropic). In the RC measurement, that weighting is realized by stirring. The number of independent samples for determining the approximated directivity of an EUT is estimated by considering the number of spherical or cylindrical wave modes. From [43], it is known that the electric field received by an EUT can be described by:

$$\vec{E}(r,\theta,\varphi) = \frac{k}{\sqrt{\eta}} \sum_{smn} Q_{smn} \vec{F}_{smn}(r,\theta,\varphi), \tag{4.49}$$

where $\vec{F}_{smn}$ are dimensionless wave functions and $Q_{smn}$ are the corresponding wave coefficients. Equation (4.49) is the solution of the spherical wave equation. In our analysis, we need Eq. (4.49) for the determination of the number of spherical wave modes. That number can be evaluated by considering the sum in Eq. (4.49):

$$\sum_{smn} = \sum_{s=1}^{2} \sum_{n=1}^{N} \sum_{m=-n}^{n} = 2N(N+2), \tag{4.50}$$

where $s$ defines either a TE or TM mode and $n$ and $m$ originate from the combined solutions of the spherical wave equation. Actually, the $N$ in Eq. (4.50) goes to infinity. However, for directivity analysis, only those modes are important which propagate to the far-field region. From [43] and [64], we know that the number of modes $N$ propagating to the far-field can reasonably be approximated by $N \approx ka$. The number of independent samples is twice the number of spherical wave modes (Eq. (4.50)), because the field solutions are assumed to consist of independent real and imaginary parts; this explains Eq. (4.48) for a spherical scan. For planar scans, the same analysis can be performed by considering cylindrical wave modes.
In [64], it is stated that the model is a proper estimation of the maximum directivity when transforming radiated power measurements (RC) to free-space electric field-strength. In addition, it is also stated that it is difficult to determine the actual electrical size of the EUT. The electrical size of an EUT is the size of that part of the EUT which really radiates. This means that taking the maximum EUT dimension, as estimate of the electrical size of the EUT, is a worst-case approximation. Moreover, it is expected that the directivity will be smaller in practice when (mains and connection) cables are used, which is typical for most multimedia applications. In Figure 4.11, maximum directivity curves, based on

Eq. (4.47) and spherical scan $N_s$, are shown for two frequency ranges (30-1000 MHz and 1-18 GHz). These curves are computed by taking the EUT sizes (radius) in the range $a$=0.1-1 m, because these are typical sizes of multimedia products. From the curves, it becomes clear that the maximum directivity of an unintentional radiator is approximately in the range 2-8 dB, depending on the frequency range and EUT size. In the range 30-1000 MHz, the maximum directivity is between 2-6 dB, while a maximum directivity range of 4-8 dB can be found in the range 1-18 GHz.
In [64], a comparison is presented between the radiated electric field-strength obtained by applying an RC measurement and a FAR measurement in the frequency range 800 MHz-2 GHz. The comparison is performed by using a PC cabinet (without cable) including an RF-generator as EUT. The RC measurement delivers the radiated power, which is converted to electric field-strength by using a directivity estimated from Eq. (4.47). The FAR measurement is performed with three orthogonal positions of the EUT in two polarizations of the receive antenna where the maximum is taken after the EUT rotation (100 turntable steps). The conclusion of the comparison is that the RC result and the maximum FAR result are similar within approximately 2 dB. The RC measurements are repeated resulting in approximately 2 dB spread in the maximum emission results. The six FAR measurements, however, demonstrate a spread of approximately 10 dB in the maximum emission results.

Based on the directivity model (Eqs. (4.47)-(4.48)) and the conversion method introduced in Sections 4.5 and 4.6, a theoretical comparison of the directivity effect will now be performed. In this comparison, the radiation behavior of the fictitious EUT is described by Eqs. (4.47)-(4.48). The radiated emission of this fictitious EUT needs to be determined in terms of maximum electric field-strength. So, the reference quantity is the maximum electric field-strength at a certain distance and in any direction.
Let us first consider the radiated emission measurement using the RC method. This measurement yields the radiated power of the EUT. The IEC 61000-4-21 standard already describes a default directivity of 1.7 (2.3 dB). A fictitious EUT of size $a$=0.25 m has a theoretical directivity of 4-7 dB (Eqs. (4.47)-(4.48)) in the range 1-6 GHz. So, for the transformation to electric field-strength, a deviation (under estimate) of approximately 2-5 dB with respect to the reference quantity is expected.

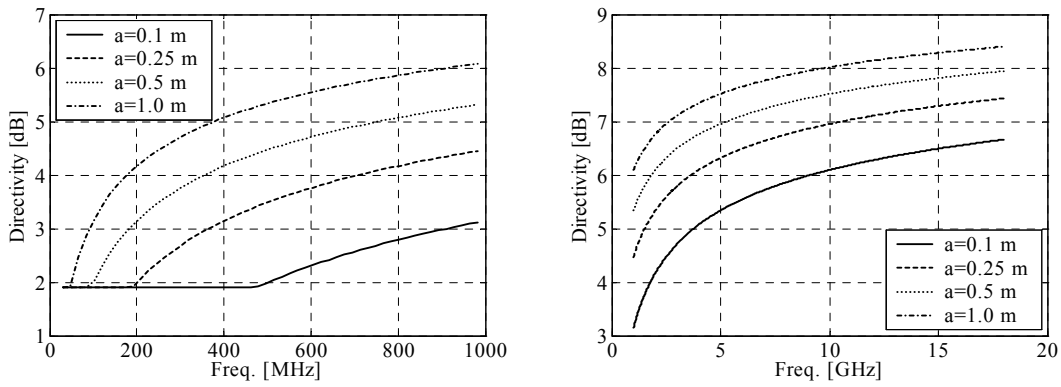


Figure 4.11 Computed maximum directivities for EUTs of different sizes.

Subsequently, the radiated emission of the fictitious EUT is measured in a FAR. In this method, only a planar cut (azimuth scan) with limited turntable steps is scanned in two polarizations. From [94], it is known that the deviation from the reference quantity due to the limited number of samples is approximately 2-4 dB. In addition, scanning a planar cut only instead of a spherical scan creates a deviation of approximately 1-3 dB. All the deviations are referred to as 'approximately' because they are all statistical quantities including some spread. As a consequence, the expected total deviation of a FAR measurement without height scan from the reference quantity is approximately 3-7 dB. Such deviations have been noticed before in FAR radiated emission measurements above 1 GHz [64][68].
The conclusion is that the lack of directivity application in the RC is of the same order of magnitude as the deviation caused by missing the maximum emission within the FAR in the range 1-6 GHz. The same conclusions are drawn in [47][75] for an immunity test configuration. This will be demonstrated also for a practical case in Section 4.9.

### 4.7.2 Simulations of the directivity effect

In this subsection, the effect of the directivity of EUTs is investigated by simulations. When we want to emulate EUTs that have significant (>5dB) directivity in the frequency range from 1 to 6 GHz, then a long-dipole antenna may be applied. An additional benefit of a long-dipole antenna is that it is calculable. Analytical expressions can be used in a geometrical-optics model [78]. In the simulations discussed here, a dipole antenna of a fixed length of 1.5 m is used. The total radiated power of the dipole antenna can be calculated using:

$$P_{rad} = \frac{\eta I_m^2}{4\pi} \int_0^{\pi} \frac{\left[ \cos\left( \beta \cdot \frac{L_{ant}}{2} \cdot \cos\theta \right) - \cos\left( \beta \cdot \frac{L_{ant}}{2} \right) \right]^2}{\sin\theta} d\theta, \tag{4.51}$$

where $I_m$ is the amplitude of the current which is taken 1/60 A, $L_{ant}$ is the antenna length of 1.5 m, $\beta$ is the wave number, and $\theta$ the elevation angle. The analytical expressions for dipole antennas assume sinusoidal current distributions. At higher frequencies, this assumption becomes questionable from a physical point of view. However, the analytical expressions remain useful for a model of a hypothetical EUT. Such an EUT can be used to compare the directivity effect on the emission results obtained from various measurement methods. The resulting total radiated power of the antenna is shown in Figure 4.12 A. The corresponding directivity of the antenna is shown in Figure 4.12 B. The directivity of this dipole antenna varies from 6 to 14 dB in this frequency range. Let us again take the maximum electric field-strength at a defined distance of the EUT in any direction as reference quantity. The reference quantity $X$ can accordingly be defined by using Eq. (4.26). The reference distance of 3 m is used in this investigation above 1 GHz. The reference quantity is shown in Figure 4.13. Subsequently, we use the dipole antenna as emulation for the EUT and calculate the radiated emission by using the RC method, the 3 m SAR method, and 3 m FAR method.

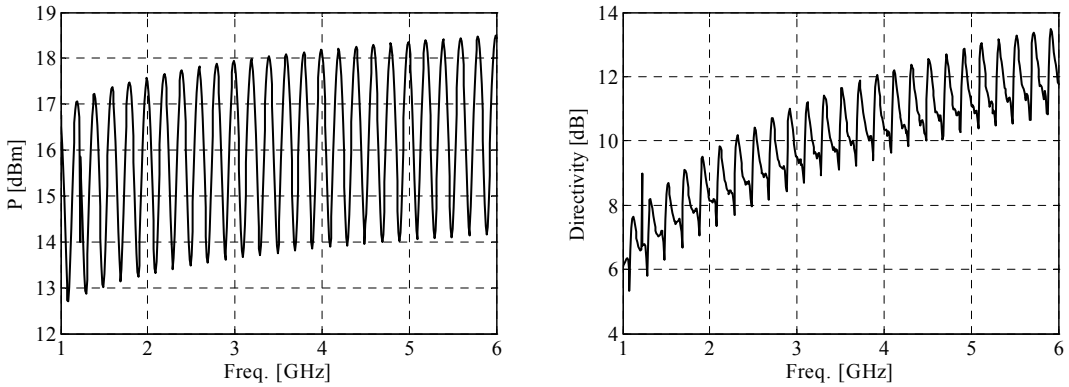


A. Total radiated power B. Directivity

Figure 4.12 The total radiated power (A) and directivity of a long-dipole antenna with a fixed length of 1.5 m.

For the SAR method we have calculated the electric field-strength by scanning from 1 to 4 m in 1 cm steps. A height scan of 1 to 2 m in 1 cm steps is applied for the FAR method. The limited height scan for the FAR method above 1 GHz is in accordance with a new proposal in CISPR/A. The FAR and SAR methods yield results for horizontal and vertical polarization, which are considered here separately. The dipole EUT in horizontal polarization is rotated 360° in 15° steps in the SAR and FAR simulations. Rotation of a vertically arranged dipole antenna is not relevant. Accordingly, the maximum emission is determined for the FAR and SAR method. The radiated emission obtained from the RC method is calculated by using the total radiated power and a directivity of 1.7 as defined in the IEC 61000-4-21 standard.

The radiated emission results obtained for the SAR method, the RC method, and the FAR method are given in Figure 4.14 A and B. The deviation results are presented in Table 4.1. The deviation $D_{\text{isotropic}}$ applicable to isotropic radiators are used to quantify the directivity effect on the deviation with respect to the reference quantity. The deviation for horizontal polarization ($D_{\text{Hor. pol.}}$) as simulated for the 3 m SAR is between -1 dB and -4 dB. The deviation of an isotropic radiator found for the 3 m SAR is -5 dB (Section 4.6). Therefore, the directivity effect is approximately 1-4 dB. The deviation result for the FAR method is approximately 0 dB, i.e., the directivity effect is 0 dB. At vertical polarization, a deviation of 1-6 dB is obtained for the SAR method. This results in a directivity effect of 6-11 dB. The deviation for the FAR method amounts 5-12 dB resulting in the same directivity effect at vertical polarization. The directivity causes a deviation of 3-9 dB for the RC method.

In conclusion, the directivity effect on the deviation with respect to the reference quantity depends on the polarization of the emission for the SAR and FAR methods for a long-dipole EUT (omni-directional). For horizontal polarization, the directivity effect of the used long-dipole EUT is negligible for the SAR and FAR methods. Therefore, the results confirm only partly the conclusion regarding directivity drawn in Subsection 4.7.1. The deviation due to the directivity of the EUT is approximately the same in the SAR method, FAR method, and RC method, but it depends significantly on the polarization of the emission. This influence should be investigated for realistic EUT configurations.

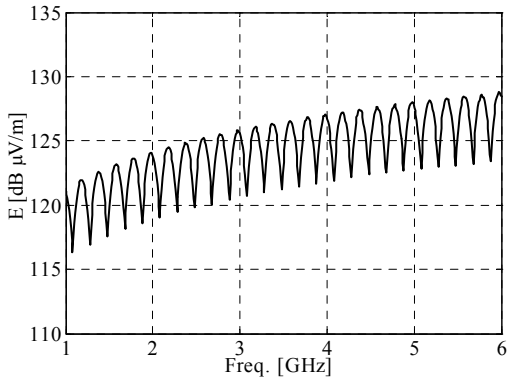


Figure 4.13 The reference quantity *X*: maximum emission at 3 m over the full sphere.

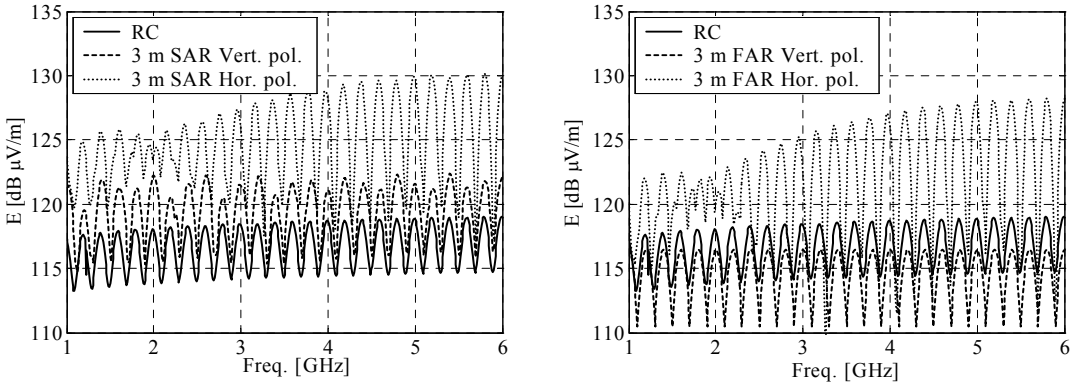


A.3 m SAR vs. RC B. 3 m FAR vs. RC

Figure 4.14 Radiated emission results.

In this section, the directivity of an EUT is discussed and its effect on radiated emission results is investigated. Based on a statistical model, it is found that the deviation due to the directivity effect is almost equal for the RC, SAR, and FAR methods. Simulations of a fixed-length dipole demonstrate that the deviation caused by the directivity depends on the polarization of the emission. However, EUTs emitting at frequencies above 1 GHz cause a lower interference risk in general. An interference problem can easily be solved by changing the position of the EUT slightly because of the narrow lobes in the radiation pattern. In conclusion, the directivity is not an important parameter for the conversion of emission results.

Table 4.1 Deviation *D* results.

| | $D_{\text{Hor. pol.}}$ [dB] | $D_{\text{Vert. pol.}}$ [dB] | $D_{\text{isotropic}}$ [dB] |
|---|---|---|---|
| 3 m SAR | -1 - -4 | 1 - 6 | -5 |
| 3 m FAR | 0 | 5 - 12 | 0 |
| RC | 3 - 9 | 3 - 9 | 0 |

## 4.8 Summary of comparison: uncertainty assessment

As mentioned in Subsections 4.5.2 and 4.5.3, also the uncertainties should be taken into account in the conversion method. Therefore, various uncertainty parameters are compared for the RC, FAR, and OATS/SAR methods in this section.

The uncertainties in the FAR radiated emission measurement due to limited step size of the turntable and lacking height scan were already included in the directivity evaluation (Section 4.7). Furthermore, the FAR measurement method suffers from geometrical tolerances. The uncertainties related to receive antennas can be substantial above 1 GHz (Chapter 3). The measurement facility validation for the FAR requires a Site Voltage Standing Wave Ratio (SVSWR) smaller than 6 dB, which is equivalent to an uncertainty of 3 dB. From practical evaluations, this appears to be a severe requirement

In the RC, the radiated power is measured with an expected uncertainty of 3 dB. This is based on radiated-power data obtained from the calibration procedure. In this example, the calibration procedure involves measurements at nine positions. When the average power is measured, this will result in 3.3 dB expanded uncertainty ($2\sigma$) and when the maximum power is measured the expanded uncertainty will result in 2.9 dB for the frequency range 80-1000 MHz. This can be demonstrated by depicting the differences of these received powers normalized to the mean value. The corresponding expanded uncertainty of one specific RC facility is shown in Figure 4.15. Based on the statistical equivalence of RCs [75], we can conclude that the reproducibility of measurements within one specific RC facility at different locations is equivalent to the reproducibility of RC measurements in different chambers. An expanded uncertainty of 3 dB is similar to the expanded uncertainty in the 10 m SAR [9]. In the RC, this uncertainty will be the same or even smaller at higher frequencies. All uncertainties related to the receive antenna are not applicable in the RC, because the receive antenna is part of the power-transfer calibration procedure as mentioned in Subsection 4.3.1. Different categories of uncertainty parameters of the RC, FAR, and OATS/SAR methods are summarized in Table 4.2.

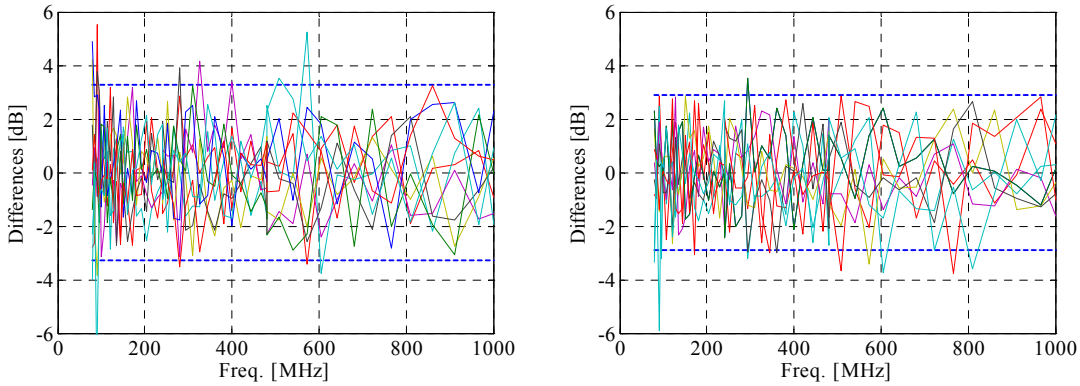


A. Average power B. Maximum power

Figure 4.15 Differences normalized to the mean value of average (A) and maximum (B) received power. The dashed lines are the $2\sigma$ expanded uncertainty levels.

Table 4.2 Comparison of uncertainty parameters.

| Uncertainty parameter | RC | OATS/SAR | FAR |
|---|---|---|---|
| Site | 4 dB (<200 MHz)<br>3 dB (>200 MHz) | 4 dB | 4 dB (<1 GHz)<br>3 dB (>1 GHz) |
| Antenna related (Type, mismatch, phase center, AF) | N.A. | 2 dB (<1 GHz)<br>4 dB (>1 GHz) | 1 dB (<1 GHz)<br>4 dB (>1 GHz) |
| Geometrical tolerances | N.A. | 1 dB (<1 GHz)<br>2 dB (>1 GHz) | 1 dB (<1 GHz)<br>2 dB (>1 GHz) |
| Near-field contributions | N.A. | N.A. | 2 dB (>1 GHz) |
| Directivity of the EUT | N.A. (<1 GHz)<br>2-5 dB (>1 GHz) | N.A. (<1 GHz)<br>3-7 dB (>1 GHz) | N.A. (<1 GHz)<br>3-7 dB (>1 GHz) |
| Deviation caused by EUT positioning tables | N.A. | 5 dB | 5 dB |
| Polarization error | N.A. | 3 dB | 3 dB |

N.A. = Not Applicable

The uncertainty parameters summarized in Table 4.2 include two main categories: instrumentation uncertainty and measurement method uncertainty (inherent). The uncertainty parameters listed in Table 4.2 are compared for the three methods. The different categories cause that Table 4.2 is unsuited to the purpose for calculating a total uncertainty. The values for uncertainty-parameter type site and antenna related, listed in Table 4.2, are based on uncertainty values presented in CISPR 16-4-2 [17]. The deviation values caused by the antenna type are based on the results presented in Chapter 3. The deviations related to geometrical tolerances (measurement distance and height of EUT) are based on results of a parameter study [24]. It should be noted that the number of turntable steps and the number of receive antenna height steps are not accounted for this type of uncertainty parameter. The uncertainties caused by the turntable step size, the height range, and the height step size are accounted for the class of deviations related to the directivity of the EUT. The uncertainty-parameter values caused by near-field contributions are based on the results of an uncertainty study [7]. The values of the uncertainty-parameter type directivity are based on the theoretical evaluation discussed in Section 4.8. Finally, the uncertainty-parameter values applicable to the influence of EUT positioning tables and antenna-polarization errors are based on [8] and [33], respectively.

Considering the uncertainty parameters of the RC method, the OATS/SAR method, and the FAR method, it can be concluded that the uncertainty due to the sites are almost the same. Furthermore, the OATS/SAR and FAR have uncertainty parameters which are not present in the RC. For that reason, an uncertainty penalty $\Delta$ for the derived RC limit as defined in Subsection 4.5.3 (Eqs. (4.37)-(4.38)) is not necessary, because it is obvious that the overall uncertainty of RC measurements is smaller than in OATS/SAR/FAR measurements.

## 4.9 Experimental evaluation of conversion factors

*CISPR 22 system-test configuration*

After the theoretical evaluation of the conversion factor, we will now discuss results of experimental evaluations of conversion factors. The first experiment is a system test of radiated emission in accordance with CISPR 22 in three configurations in order to investigate the reproducibility of measurements. CISPR 22 is a product standard for radiated emission of IT equipment and describes a so-called system test, which means that the product to be tested is combined with associated equipment to function as a system. The EUT in our experiment is a flat TV combined with a PC and a printer. The CISPR 32 standard under development applies the CISPR 22 system-test approach. In addition, CISPR 22 describes a 'scrolling-H' test mode of the display instead of the color-bar mode described in the current CISPR 13 standard for TVs. The PC generates the scrolling-H pattern which is connected to the flat TV using the VGA connector; the front view of the measurement configuration is depicted in Figure 4.16 A. Almost all connectors of the TV are connected with cables in this test as can be observed in Figure 4.16. These cables are not connected to other equipment and are bundled together as depicted in Figure 4.16.

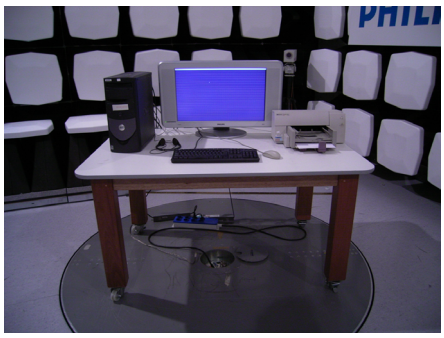

A. Front view in 3 m SAR

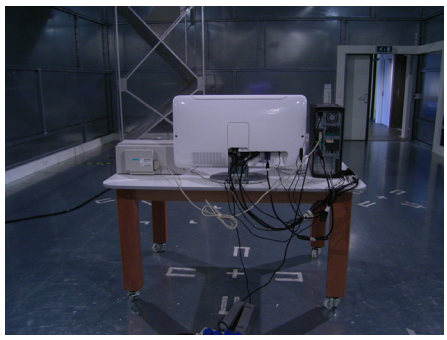

B. Configuration 1 in RC

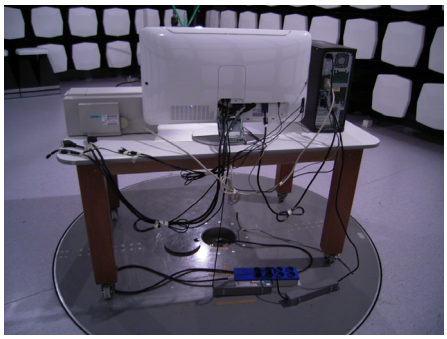

C. Configuration 2 in 3 m SAR

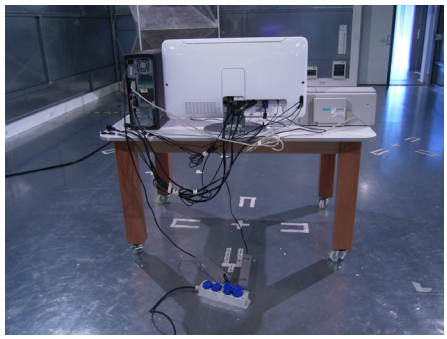

D. Configuration 3 in RC

Figure 4.16 Overview of the radiated emission configurations for a system test.

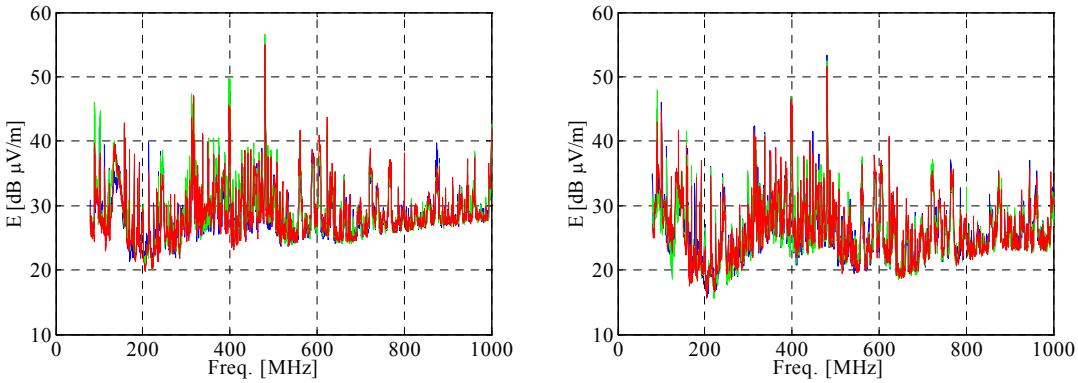


A. 3 m SAR results B. RC results

Figure 4.17 Radiated emission results (80-1000 MHz) of a system (flat TV/PC/printer) obtained from measurements in the 3 m SAR and RC for three EUT configurations.

Three configurations of the system have been measured, which all comply with the CISPR 22 standard. In the first configuration (config 1), the cables are routed to the right of the EUT table as shown in Figure 4.16 B. In the second configuration (config 2), the cables are routed to the left of the table as shown in Figure 4.16 C. Finally, the PC and printer locations are interchanged and the cables are routed to the left of the table in the third configuration (config 3, see Figure 4.16 D). The goal of this experiment is to investigate the conversion factor by considering the radiated emission results obtained from the 3 m SAR and the RC. However, a reference quantity cannot easily be determined for actual EUTs. Therefore, the conversion factor is determined here by comparing the emission results obtained from the 3 m SAR and RC directly (Eq. (4.35)). Moreover, the measurement results of the three configurations are used to investigate the reproducibility of both the 3 m SAR method and the RC method. These reproducibility measurements include EUT arrangement changes. The reproducibility here means the variation of the results when the EUT arrangement is changed and measured again in the same facility. Typical reproducibility investigations, e.g., Inter Laboratory Comparisons (ILC), assess the reproducibility also in different facilities.

The radiated emission results obtained from the 3 m SAR (A) and RC (B) for the three EUT configurations in the range 80-1000 MHz are shown in Figure 4.17. These results are obtained by using a resolution bandwidth (RBW) of 100 kHz and a video bandwidth of 300 kHz and a peak detector. After comparing the levels of narrowband emissions, it was found that the conversion factor could vary from -5 up to 10 dB as shown in Figure 4.18. The average of the conversion factor is calculated and depicted in Figure 4.18 as a solid line. The average value of the conversion factor is approximately 3 dB. Conversion factors of 4 dB were found from simulations of tuned dipoles in Section 4.6. The fact that smaller conversion factors are needed at lower frequencies (<100 MHz) confirms the simulated results obtained for isotropic point sources and tuned dipoles (Section 4.6). This effect was indicated as being caused by the limited height scan in the 3 m SAR.

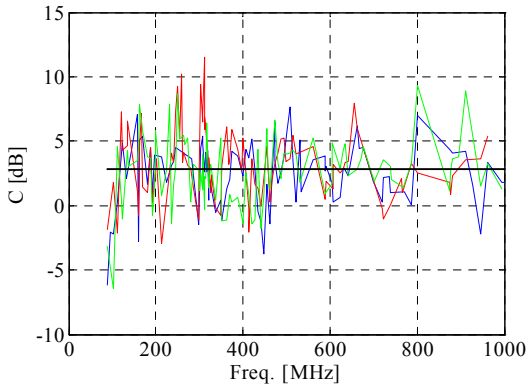


Figure 4.18 Conversion factors from three RC results to 3 m SAR results.

The EUT is measured in three configurations to investigate the reproducibility. The spread results for the three configurations for the 3 m SAR and RC method compared to the average are shown in Figure 4.19. From these figures, it is clear that the reproducibility due to variations in EUT arrangement is almost the same in the 3 m SAR method and the RC method. The expanded uncertainty is 2.6 dB.

However, it should be noted that the source of the spread is different in the SAR and RC measurements. The repeatability of the measurement in the RC is almost the same as the reproducibility. The reproducibility in the SAR is caused by the variations of the EUT arrangement and different cable routings. The same level of repeatability and reproducibility in the RC is caused by the statistical behavior. This property of the RC method causes that the RC method is less suitable for 'troubleshooting' measurements. Troubleshooting measurements are measurements where EUTs are repeatedly changed and measured in order to improve or investigate the emission behavior. So, troubleshooting measurements has more to do with repeatability. The spread results of both the RC method and the 3 m SAR method demonstrate that the reproducibility due to EUT arrangement variations is almost equal. Therefore, the RC method and the 3 m SAR method are equally suitable for performing compliance measurements.

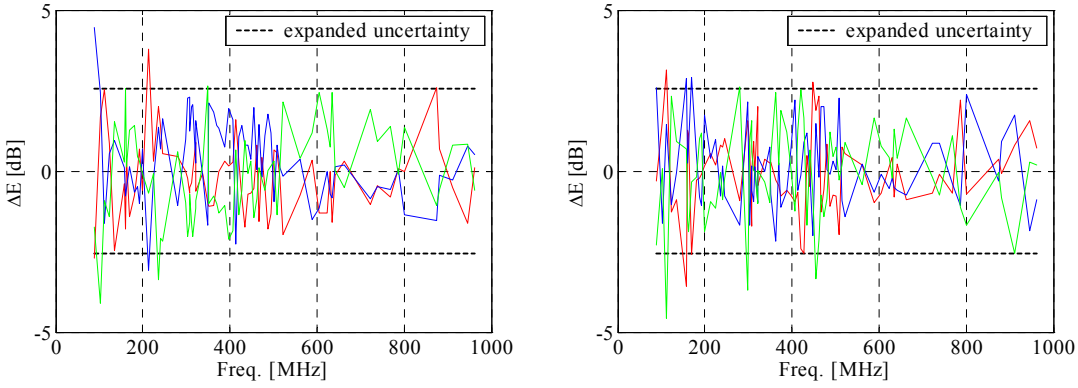


A. 3 m SAR results B. RC results

Figure 4.19 Spread of emission results for three reproduced measurements in 3 m SAR (A) and RC (B).

*PCB trace in combination with cable*

The second experiment uses an artificial EUT which represents a module with different types of PCB trace technologies. In this experiment, a PCB trace is applied that consists of two coplanar strips (strip width=0.5 mm gap=0.5 mm) terminated with 50 Ω. The PCB trace is excited by using a 2 m coaxial cable. The configuration of the PCB trace and its connection with the cable is shown in Figure 4.20. The simulated directivity of the EUT is shown in Figure 4.21. This directivity is simulated by using Microwave Studio of the company CST. The substantial directivity of this EUT makes it useful to experimentally investigate the directivity effect on radiated emission results obtained by applying the 3 m SAR method and the RC method. The conversion factors are determined by directly calculating the difference between 3 m SAR results and RC results in the frequency ranges from 80 to 1000 MHz and from 1 to 7 GHz. So, again no reference quantity is used.

The PCB trace is connected with a tracking generator of a spectrum analyzer by using a 2 m cable of which the shield is grounded after 2 m. For this configuration, it is expected that either the cable is the dominating radiator, roughly below 1 GHz, or the PCB trace (10 cm), roughly above 1 GHz. Three measurements in the 3 m SAR are performed for three orthogonal positions of the PCB board from which the maximum is considered.

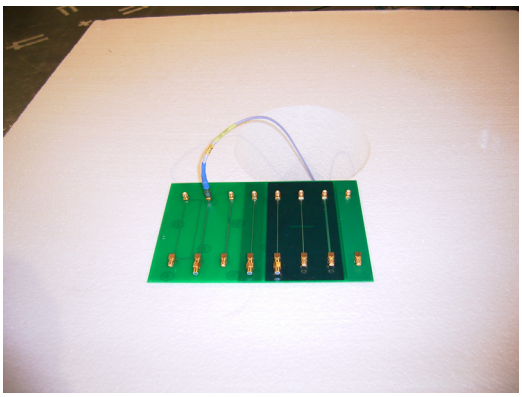

Figure 4.20 PCB configuration including a 2 m shielded cable.

The radiated emission results obtained from the 3 m SAR and RC measurements are given in Figure 4.22. From these results we can observe that at lower frequencies (<500 MHz) the results obtained from the RC are the same or even somewhat higher than obtained from the 3 m SAR. This effect has already been observed in the conversion factors for tuned dipoles as well as for the CISPR 22 system-test configuration. This is caused by the limited height scan in the SAR. Up to 1000 MHz, the SAR and RC results from this EUT are similar. The RC results are approximately 1 to 3 dB lower than the 3 m SAR results at frequencies above 1 GHz. In this frequency range, a conversion factor of roughly 3 to 5 dB is expected, based on the simulation results mentioned in Section 4.6. It should be noted here that the simulated conversion factors were obtained without applying the directional properties of the receive antenna.

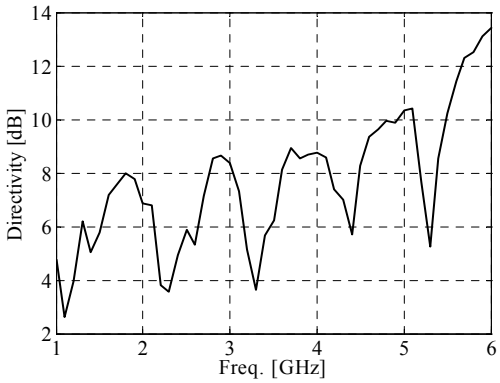


Figure 4.21 Directivity of the PCB and cable EUT configuration.

The beamwidth of typical receive antennas, e.g., the double-ridged waveguide horn antenna, are in general much smaller than the beamwidth of receive antennas below 1 GHz as investigated in Chapter 3. This provides a possible explanation for the observation that experimental conversion factors are measured (1 to 3 dB) which are (a few dBs) smaller than the simulated conversion factors (3 to 5 dB). This can be explained by the observation discussed in Chapter 3 that a small beamwidth of the receive antenna will result in lower measurement results in a SAR and consequently the conversion factors from RC to SAR results become smaller as well. Furthermore, this supports the conclusion stated in Section 4.7 that for EUTs with high directivity it will be very likely to miss the maximum emission in measurements performed within anechoic-type chambers.

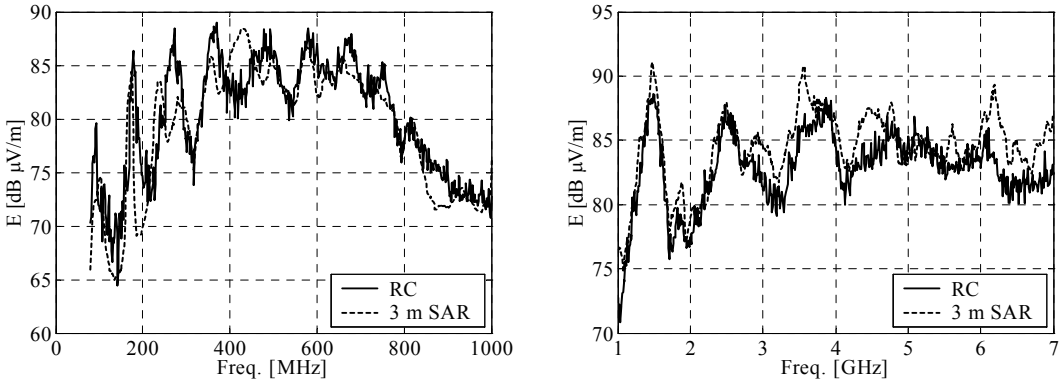


Figure 4.22 Radiated emission results of the PCB trace connected with a 2 m cable.

## 4.10 Evaluation

In this chapter, the RC as alternative facility for radiated emission measurements has been thoroughly discussed. The physical background is explained. An RC is a facility that creates a statistically isotropic and uniform field of a source inside the RC. By using a calibrated power transfer in the RC, the total radiated power of an unknown radiator, i.e., an EUT, can be measured accurately. The basic EMC standard for the RC is the IEC 61000-4-21. In this standard, the facility calibration and validation, an immunity test method, and an emission measurement method applicable to EMC are described. In Sections 4.2-4.5, the emission measurement procedure for measuring in the RC is summarized. During the emission measurement the total radiated power of the EUT is first determined and subsequently converted to radiated electric field-strength by using the free-space formulation.

In this chapter, much attention is devoted to the conversion of emission results or limits obtained either by using an RC or other facility like a SAR or FAR. A standardized conversion method is applied. The specific benefit of this method is that it is based on an independent reference quantity. This reference quantity is important for radio protection. The use of the reference quantity is also an additional advantage compared to the results presented in [15][49]. In these publications, the electric field-strength limit of the OATS/SAR method is transformed to a total radiated power limit. This is a valid approach, but the relation to a reference quantity for radio protection is lacking. However, one could argue that the use of the reference quantity based on maximum electric field-strength at a certain distance of the EUT is conventional. At frequencies above 1 GHz, EUT radiation-patterns typically show narrow lobes and substantial directivity. The narrow lobes cause a lower interference risk, because a small change in position of the EUT will solve the interference problem. For that reason, the total radiated power may be a suitable reference quantity as well. In that case, the RC method is preferable above the SAR and FAR methods.

In practice, the reference quantity is difficult to simulate for realistic EUTs and almost impossible to measure for any EUT. Therefore, calculable and simple EUTs are used to evaluate the conversion factor theoretically by using the standardized conversion method. In addition, practical emission experiments are compared in order to achieve insight into conversion factors for actual EUTs. Based on the theory and experiments, it is concluded that the conversion factor for emission results obtained from an RC towards SAR results is approximately 4 dB below 1 GHz, i.e., the results obtained by the SAR are in general 4 dB higher compared to the RC results. It is also concluded that, apart from uncertainty issues, the FAR and RC are both free-space methods and therefore equivalent.
The directivity of EUTs is discussed because it is an important factor when considering conversion factors. The directivity of an EUT is lost in an RC, which causes a deviation. It was found that if the directivity becomes higher, then the probability to miss the maximum emission in either a FAR or SAR becomes higher as well. Therefore, the conclusion could be drawn that the deviation due to the directivity of the EUT is approximately the same in

the SAR, FAR, and RC methods. In other words, the directivity of EUTs causes approximately similar inherent or 'measurement method uncertainty' in the SAR, FAR, and RC methods. However, it is also found that the directivity influence depends strongly on the polarization of the emission. For vertical polarization, the directivity effect is higher for the SAR and FAR method. The directivity effect is higher for the RC method if the emission is horizontally polarized. It is noted that the interference risk becomes lower for EUTs with narrow lobes and associated high directivity. Therefore, the directivity of EUTs is not an important parameter for the conversion of emission results.

# 5 Concepts of new immunity test-signals

As introduced in Section 1.1, many new types of wireless communications systems are present in the home environment. The intended and unintended radio signals of these new technologies may disturb other electronic products in a way different from the disturbance signals emulated in the present immunity tests. Present immunity tests are based on an Amplitude Modulated (AM) test-signal. This signal was developed for testing electronic products against interference from analog radio signals. The new broadcast and radio-communication signals are typically digitally modulated. For that reason, new immunity test-signals equivalent to digitally modulated radio signals will be derived and discussed in this chapter. First, some background concerning immunity tests is given and subsequently the principle of the Unified Disturbance Source (UDS) in standardized immunity tests will be explained in Section 5.1. The derivation of the new UDS signals is supported by simulations. Two main categories of radio-communication signals are considered, i.e., Time Division Multiplexing (TDM) signals and Frequency Division Multiplexing (FDM) signals. The disturbance properties of these signals are investigated for two interference scenarios, the conventional interference scenario and the coexistence interference scenario. The definitions of these interference scenarios are given in Section 5.2. Parts of this chapter were published earlier in [29][30].

## 5.1 Definition and background

It is important to apply representative test signals for immunity testing. This is important because the EU legislation demands a basic immunity of products to external electromagnetic disturbances in accordance with the EMC directive [32]. Requirements are defined for conducted and radiated immunity in harmonized standards. For a conducted immunity test, a current is injected into the EUT by using a coupling device. An electric field is applied for testing EUTs on radiated immunity.
As discussed in Chapter 1, many multimedia products are nowadays equipped with wireless technology. These radio-communication systems typically apply digital modulation. This trend in multimedia products causes new interference scenarios. The digitally modulated radio-communication signals may act as potential new disturbance sources. Vice versa, the radio-communication receivers in multimedia products are sensitive. It is important to investigate which specifications an immunity test-signal should have in order to emulate the interference potential of the new radio-communication signals in a representative manner.
The present immunity test-signal for conducted and radiated immunity is based on the analog AM broadcast signal. In addition, the current immunity tests are based on a conventional interference scenario. Without adaptations of the current immunity tests, quality issues for multimedia with wireless communication systems may be expected.

Current Audio and Video (AV) equipment is tested against immunity in accordance with the CISPR 20 standard. Information Technology Equipment (ITE) is tested on immunity in accordance with the CISPR 24 standard. These standards describe conducted and radiated immunity tests. Radiated and conducted immunity tests are performed by using the same AM test-signal. Both CISPR 20 and 24 prescribe a 1 kHz Amplitude Modulated (AM) test-signal with a modulation depth of 80%.
The 1 kHz 80% AM test-signal is representative for AM broadcast signals and was therefore a representative immunity test-signal in the past. The 1 kHz 80% AM test-signal has also been applied to represent disturbances of other analog radio services. Hence, the 1 kHz 80% AM test-signal for conducted and radiated immunity is one of the unified disturbance sources that is used today for immunity tests of electronic equipment. Other examples of current UDS implementations are surge currents, fast transients, and Electro Static Discharge (ESD) signals. These UDS implementations are described in the IEC 61000-4-# series. For example, the test field for radiated immunity testing with 1 kHz 80% AM is described in IEC 61000-4-3 [53]. The parameters of this UDS are the unmodulated field test-level in V/m and the carrier frequency (80 MHz-2 GHz). The modulation frequency (1 kHz) and the modulation depth (80%) are fixed parameters. This UDS implementation is depicted in Figure 5.1. The corresponding specifications are shown in Table 5.1.
The general UDS can be defined as follows.

A Unified Disturbance Source (UDS) is a (standardized) immunity test-signal which represents a number of actual disturbance signals. The interference potential of the UDS is equivalent to the interference potential of the actual disturbance signals.

In this chapter, only UDS implementations are considered for emulating radio-communication signals. These are typically applied for radiated immunity tests. The specifications of the UDS depend on which product or function is tested. The radio-communication signals (multimedia with transceivers) are considered as potential disturbance sources and other multimedia equipment (with and without transceivers) as the potential victims. Hence, two interference scenarios are applicable, which will be introduced in Section 5.2.

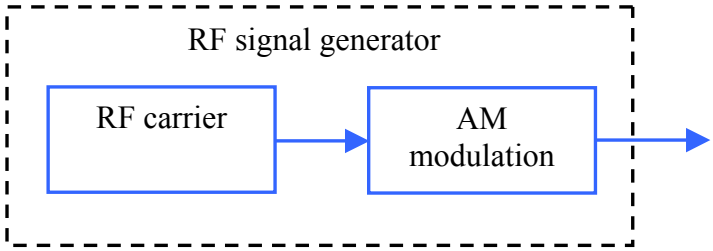


Figure 5.1 Current Unified Disturbance Source for radiated immunity measurements.

Table 5.1

| | |
|---|---|
| Level | 1 V/m (CISPR 20)<br>3 V/m (CISPR 24) |
| Carrier frequency | 150 kHz-150 MHz (CISPR 20)<br>80-1000 MHz (CISPR 24) |
| Modulation frequency | 1 kHz |
| Modulation depth | 80% |

## 5.2 Interference scenarios

The interference potential of a disturbance signal depends on which function of the product is evaluated and on the coupling mechanism. For example, an audio function of a product may be sensitive for other types of disturbance signals than a receiver function. Therefore, it is not sufficient to consider the disturbance properties of the radio-communication signals without taking typical characteristics of functions into account. In other words, the interference potential of a radio-communication signal can only be defined for a specific interference scenario. Two interference scenarios representative for multimedia products in the home environment are considered in this section.

### 5.2.1 Conventional interference scenario

The conventional interference scenario is based on an intentional radiator as disturbance source and the effect of nonlinear detection. The intentional radiator is reasonably far away from the victim in the conventional interference scenario, e.g., broadcast signals. Conventionally, these broadcast signals apply analog modulation. The linearity property of an EUT is especially important for AV equipment. The unintended demodulation due to the nonlinearity may cause a low Signal to Noise Ratio (SNR) in audio equipment or picture failures in video equipment [56]. For testing the nonlinearity of products, the AM test-signal including its 1 kHz modulation frequency is an appropriate UDS to cover this interference scenario. The 1 kHz modulation frequency was chosen because of the practical benefit that it is audible during immunity tests of audio equipment. In Annex A of the IEC 61000-4-3 standard, it is stated that TDM radio-communication signals can also be emulated by using the AM test-signal for this interference scenario. This statement becomes questionable if vulnerable digital equipment is considered, e.g., when the interference mechanism is clock jitter that may cause threshold failures [6].
As mentioned in Section 1.1, the analog broadcast systems will rapidly be replaced by digital systems. This replacement will cause a completely different interference scenario, because analog broadcast signals are relatively narrow-band whereas digital broadcast signals are typically broadband. This issue is discussed in Section 5.7, where the specifications of the UDS for OFDM radio-communication signals are presented.

### 5.2.2 Coexistence interference scenario

The second interference scenario that is considered is the coexistence interference scenario. This term is used for the interference scenario where the disturbance source is again a radio-communication signal of an intentional radiator and the victim is a receiver function of another radio-communication system. This radio-communication system could be integrated into a multimedia product. It should be noted that this definition of coexistence is different than from the one applied in technical committee IEEE 802.19. In that committee, coexistence is defined as the suitability of the radio-communication protocol to properly handle the parallel communication of the same systems. For example, multiple wireless networks of the same type in one environment. This kind of coexistence can be improved by algorithms in the higher Open Systems Interconnection (OSI) communication layers, e.g., Carrier Sense Multiple Access (CSMA) algorithms such as 'listen before talk' [21]. This kind of coexistence is what we call 'functional coexistence' and is not related to EMC.

In this chapter, we consider coexistence in the physical layer only, i.e., the radio-communication signal is a potential disturbance source for the receiver victim function. This means that the victim receiver has no information about the disturbance signal. Still, the receiver can be equipped with interference mitigation measures to improve the immunity. For example, the Bluetooth radio-communication system will avoid a certain channel when interference is measured in that channel. This has, however, nothing to do with the communication protocol. It is a preventive EMC measure. We use also the term coexistence immunity test to indicate testing of the coexistence interference scenario. Because of the fact that multimedia products are equipped with different radio-communication systems, the coexistence interference scenario and coexistence immunity tests are increasingly important. This coexistence interference scenario is not covered by the conventional interference scenario. Both the conventional and the coexistence interference scenarios are taken into account in order to determine the interference potential of radio-communication signals in this chapter. Subsequently, the specifications for a suitable UDS can be defined.

## 5.3 Approach

The specifications for suitable UDS signals are investigated by using simulations. By analyzing the time and frequency behavior of the radio-communication signals under test, the important properties that define the interference potential of the signals for a certain interference scenario can be determined. The Amplitude Probability Distribution (APD) is used as statistical evaluation of the time domain properties of the signal. The spectrum is simulated for investigation of the frequency domain properties of the signal. MatLab was applied for the simulations. In the investigation, we consider the following radio-communication signals:

1. GSM 900 and DCS 1800,
2. Wireless LAN IEEE 802.11a, b, g,
3. Bluetooth,
4. DECT,
5. Ultra Wide Band (UWB).

The types of modulation of the signals are summarized in Table 5.2. Multiplexing of digitally modulated data in the time or frequency domain is very common. Multiplexing the data means that the information is divided into time or frequency domain data frames. The type of multiplexing is important for the interference potential of the signal. Therefore, we will discuss both Time Division Multiplexing (TDM) signals and Frequency Division Multiplexing (FDM) signals separately and in more detail in the coming sections. General information concerning these communication techniques can be found in [21]. Both the conventional interference scenario and the coexistence interference scenario are considered for the interpretation of the simulation results.

Table 5.2 Radio-communication systems and their modulation schemes.

| Wireless communication system | Modulation scheme |
|---|---|
| Wireless LAN IEEE-802.11b | Various modulation and DSSS |
| Wireless LAN IEEE 802.11g | Various modulation and DSSS/OFDM |
| Wireless LAN IEEE 802.11a | Various modulation and OFDM |
| Bluetooth | GFSK and frequency hopping |
| DECT | GFSK and TDMA-duplex |
| GSM 900 and DCS 1800 | GMSK and TDMA-duplex |
| UWB (Multiband OFDM) | Various modulation and OFDM |

## 5.4 Time Division Multiplexing

### 5.4.1 Background of TDM communication systems

Time multiplexing systems divide the data into bursts in the time domain. The time span of a single burst is called a data frame. The data frame property is of high importance in the consideration of disturbance threats of these signals. The frame frequency will cause a low-frequency repetition in the transmission of the data. This low-frequency repetition may easily cause interference in the low-frequency (LF) range (audio) due to unintended nonlinear detection. A typical radio-communication signal that uses time multiplexing can be seen as a pulse-modulated RF carrier. A typical time scheme of a radio-communication signal as will appear in systems using the TDMA (Time Division Multiple Access) architecture is depicted in Figure 5.2. The data frames consist of time slots. GSM and DCS have 8 time slots and use frequency duplex, which means that a separate frequency band is used for transmitting and receiving. DECT has 24 time slots and uses time duplex. This

means that the transmitter and receiver (or master and slave) have alternate access to a time slot. The time-slot property determines the duty cycle of the radio-communication signal. Bluetooth combines Time Division Multiplex (TDM) duplex with Frequency Hopping (FH). FH is a simple technique, namely the carrier on which the data is modulated 'hops' at a certain time rate. For example, Bluetooth uses FH with a hop frequency of 1600 hops/s. We can simulate FH in measurements by using the frequency-sweep option of an RF signal generator. From an EMC point of view, FH may cause an on/off switching disturbance behavior in an Equipment Under Test (EUT) when this EUT is susceptible at a certain frequency, because the frequency at which the EUT is susceptible is not continuously present. FH has no effect on the RF amplitude as function of time. In Table 5.3, the frame period values and corresponding frame frequencies of GSM 900, DCS 1800, DECT, and Bluetooth are summarized.

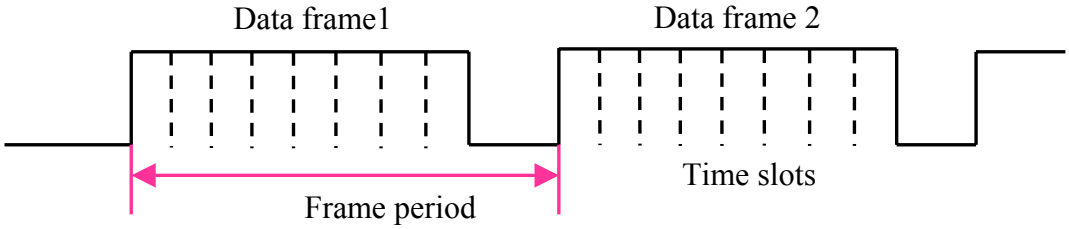


Figure 5.2 TDMA time signal including data frames and time slots.

Table 5.3 Overview of TDM frame periods and corresponding frequencies.

| | Frame period | Frame frequency | Number of time slots |
|---|---|---|---|
| Bluetooth | 625 μs | 1600 Hz | 1 |
| GSM 900 | 4.61 ms | 217 Hz | 8 |
| DCS 1800 | 4.61 ms | 217 Hz | 8 |
| DECT | 10 ms | 100 Hz | 24 |

### 5.4.2 Discussion of simulations

In order to derive a UDS concept for TDM types of radio-communication signals, some simulations are performed. The TDM systems investigated in this study all use (Gaussian filtered) Frequency Shift Keying (FSK) as modulation scheme combined with time multiplexing. Minimum Shift Keying (MSK) as implemented in GSM and DECT transceivers is a special case of FSK, i.e., FSK with modulation index m=0.5 [21]. MSK is also known as phase-continuous FSK. The time-slot property of TDM signals can be emulated by pulse modulation. The pulse frequency is equivalent to the relatively low-frequency (LF) data-frame frequency of TDM radio-communication signals. So, a TDM radio-communication signal can be seen as a FSK modulated carrier (sine wave) which is subsequently pulse modulated. To investigate the different aspects of such a signal, three signals are simulated:

1. pulsed sine wave signal,
2. unpulsed FSK modulated carrier,
3. pulsed FSK modulated carrier.

The three simulated signals give us insight into the individual properties of both the FSK modulation and the pulse modulation (time slots). FSK modulation is performed for a random bit stream. The carrier frequency is chosen to be 500 MHz and the modulation signal, representative for the bit stream, is a 50 kHz rectangular pulse signal with a duty cycle of 50% and 0-5 V level. A pulse frequency of 2.5 kHz is taken to simulate the TDM frame frequency. The three signals are statistically evaluated in the time domain by considering the simulated APD. The APD result is especially important to assess the conventional interference scenario. To investigate the interference potential for the coexistence interference scenario, the spectrum is evaluated as well.
In Figure 5.3 A, the Amplitude Probability Distribution (APD) of a pulsed FSK signal and a pulsed sine wave signal is shown. From this APD, we can observe that the FSK modulation aspect has only a minor influence in the amplitude distribution. For that reason, we might conclude that TDM radio-communication signals can be emulated well by using a pulse-modulated sine wave signal for the conventional interference scenario.
In other words, if unwanted demodulation due to nonlinearity is the important interference mechanism then a pulsed sine-wave can be used as UDS for TDM radio-communication signals. The specifications for such a UDS are defined by the duty cycle and the Pulse Repetition Frequency (PRF). The PRF is specified by the corresponding frame frequency. The duty cycle is determined by the time slot, i.e., frame period divided by the number of time slots. More details about the specifications are given in Section 5.7.
For the coexistence interference scenario not only the amplitude distribution in the time domain is important but also the spectrum of the disturbance. For that purpose, the spectra are computed of both a pulsed FSK signal and a pulsed sine wave signal shown in Figure 5.3 B. In this figure, we can observe that for a proper spectral emulation of the TDM radio-communication signal we need the FSK modulation, i.e., only a pulsed sine-wave signal is not representative for this interference scenario.

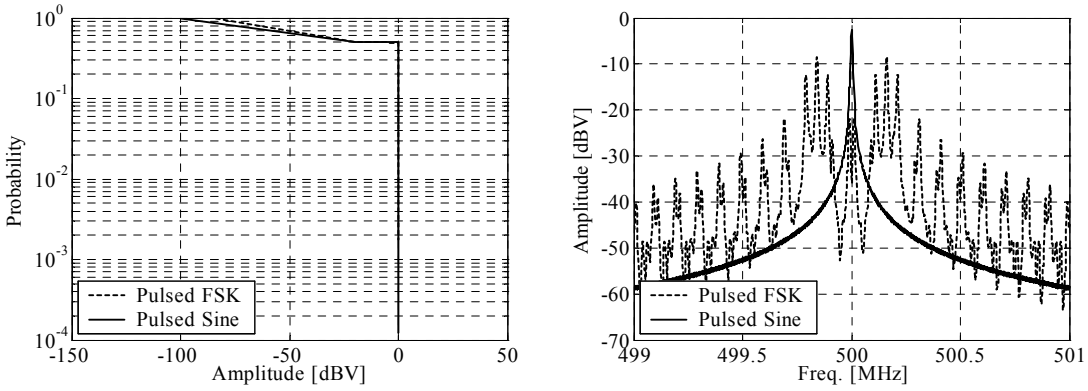


A. APD B. Spectrum

Figure 5.3 APD (A) and spectrum (B) of pulsed FSK signal and pulsed sine wave.

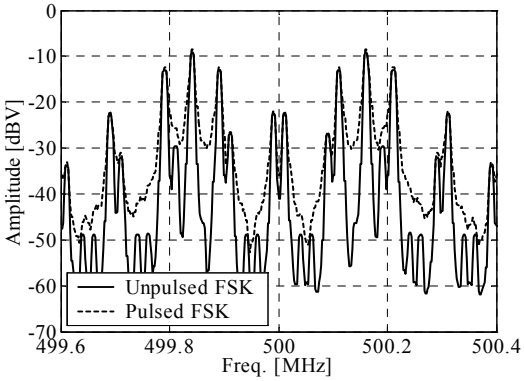


Figure 5.4 Computed spectra of a pulsed FSK modulated carrier and an FSK modulated carrier.

Subsequently, the effect of the pulse modulation is investigated for this coexistence interference scenario. In Figure 5.4, the spectra of both an FSK signal (unpulsed) and a pulsed FSK signal are depicted. From this figure, it is observed that the LF pulse, representing the TDM frame period, has a minor influence on the maximum levels of the spectrum signature. From this result, we might conclude that an (unpulsed) FSK modulated signal may be used as UDS to emulate TDM radio-communication signals for the coexistence interference scenario. Specifications for such an UDS for the TDM radio-communication signals considered in this study are given in Section 5.7.

## 5.5 Frequency Division Multiplexing

### 5.5.1 Background of FDM communication systems

In wireless communication systems based on Frequency Division Multiplexing (FDM), the data is divided and transmitted into data packets. A FDM algorithm which is used very often in current wireless communication systems is OFDM (Orthogonal FDM). OFDM is used in IEEE 802.11a and g. There are also OFDM implementations for Ultra Wide Band (UWB) applications; this will be discussed in Section 5.6. OFDM is a technique for transmitting data in parallel by using a large number of modulated carriers with sufficient spacing so that the carriers are orthogonal. Orthogonal in this aspect means that there is no overlap of the carriers at the sample positions. The orthogonal behavior of the various OFDM carriers can be realized by orthogonal sinc functions; where one carrier has its maximum all other carriers have a zero. OFDM is especially useful to decrease the effect of multipath effects [21]. In principle, FDM signals have time-continuous amplitude (unpulsed) and therefore the influence of demodulation effects due to nonlinear detection should be minor. However, also OFDM signals have a finite message length that depends on the data rate [55]. This time behavior of OFDM signals is discussed in the next subsection.

### 5.5.2 Time behavior of IEEE 802.11a/g OFDM signals

In Figure 5.5, the time schedule of an OFDM signal frame is shown which is typical for IEEE 802.11a and g. The frame starts with Long and Short preambles followed by a Signal symbol. The Long and Short preambles contain training symbols [55]. The OFDM mapping is realized by an inverse Fast Fourier Transformation (iFFT). The iFFT is performed after dividing the data into suitable symbol groups and randomizing the realized data. The channel width is 20 MHz and 64 OFDM subcarriers are used, which results in a subcarrier spacing $\Delta F$ of 0.3125 MHz (=20 MHz/64). This subcarrier spacing will result in an iFFT period of $T_{FFT}=1/\Delta F=3.2$ μs. This period is combined with a guard interval of $T_{GI}=0.8$ μs ($T_{FFT}/4$), which yields an OFDM symbol time of 4 μs. Subsequently, the output information of the OFDM mapping block is extended with training symbols in a preamble. The Signal OFDM symbol contains information about the data rate and the length of the TX vector, which corresponds to the number of OFDM symbols needed to transmit the data message. The TX vector will be determined by using 12 bits that indicate the number of octets (8 coded data bits) that the Medium Access Control (MAC) is currently requesting the physical layer (radio transceiver part) to transmit.

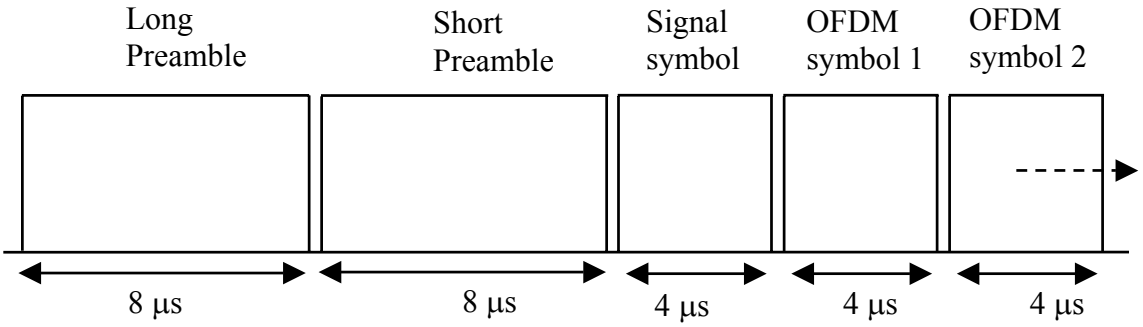


Figure 5.5 Time schedule of an OFDM frame.

For example, assume that a data message contains 6400 bits. This yields 6400/8=800 octets. When this data message is transmitted by using BPSK (consider Table 5.4), then 6400/48=134 OFDM symbols are needed, i.e., 48 coded bits per OFDM symbol. One OFDM symbol takes 4 μs, which will result in a message period of: Long preamble (8 μs) + Short preamble (8 μs) + Signal symbol (4 μs) + 134×OFDM symbols (134×4 μs), which adds up to 556 μs. The maximum number of octets is $2^{12}$=4096, which results in a maximum data length of 8×4096=32768 bits. From Table 5.4, we know that the coded data bits per OFDM symbol can vary depending on the data rate and the corresponding modulation scheme. The possible data rate depends on the channel quality as well as on the level of electromagnetic interference (EMI). Suppose that we can apply a bit rate of 54 Mbits/s, then the maximum number of OFDM symbols becomes 32768/288=114, which corresponds to a maximum message period (frame time) of 476 μs. On the other hand, if the maximum data length of 32768 bits needs to be transmitted with the lowest bit rate, 6 Mbits/s, then the maximum message period (frame time) becomes 2.752 ms. The duty cycle is 95-99%.

When we subsequently calculate the corresponding frame frequencies, then we arrive at the conclusion that the frame frequencies are in the range from 363 Hz to 2.1 kHz. This frame frequency may be demodulated by any nonlinear component in an electronic product and consequently may cause interference in the audio frequency range. Therefore, the frame frequency is an important OFDM signal property for the conventional interference scenario. However, the frame frequency of OFDM radio-communication signals is also important for the coexistence interference scenario since we know from weighting detectors (Subsection 2.2.1) that radio interference depends on the impulsive behavior [82].

For the derivation of a UDS, the frame frequency can be seen as more or less equivalent to the data-frame frequency in TDMA types of communication systems (see Section 5.4). Depending on the amount of data to be transmitted and the data rate, the frame frequencies in OFDM signals can vary from 363 Hz to 2.1 kHz, while the frame frequencies in TDMA systems are fixed and predefined quantities.

Table 5.4 Data rates and corresponding parameters (source: [55]).

| Data rate [Mbits/s] | Modulation | Coding rate | Coded bits per subcarrier | Coded bits per OFDM symbol | Data bits per OFDM symbol |
|---|---|---|---|---|---|
| 6 | BPSK | 1/2 | 1 | 48 | 24 |
| 9 | BPSK | 3/4 | 1 | 48 | 36 |
| 12 | QPSK | 1/2 | 2 | 96 | 48 |
| 18 | QPSK | 3/4 | 2 | 96 | 72 |
| 24 | QAM-16 | 1/2 | 4 | 192 | 96 |
| 36 | QAM-16 | 3/4 | 4 | 192 | 144 |
| 48 | QAM-64 | 2/3 | 6 | 288 | 192 |
| 54 | QAM-64 | 3/4 | 6 | 288 | 216 |

### 5.5.3 Direct Sequence Spread Spectrum signals

IEEE 802.11b wireless LAN is a widespread wireless communication system. In this system, Direct Sequence Spread Spectrum (DSSS) is used in combination with digital modulation. The spreader can be implemented by using shift registers [21]. The DSSS radio has a relatively high suppression of narrow-band disturbance signals. From an EMC point of view, radio-communication signals based on a DSSS algorithm have broadband noise interference potential for an unintended receiver, i.e., a receiver without information about the radio-communication signal. Broadband noise behavior justifies the use of a Gaussian-noise source as UDS.

### 5.5.4 Discussion of simulations

In this subsection, the OFDM radio-communication signal is simulated. The APD is calculated as well as the spectrum of the signal. The OFDM signal is simulated by using the block diagram shown in Figure 5.6. The OFDM transmitted time signal is depicted in Figure 5.7 A, from 0 to 1 µs. The total time range of the OFDM signal is 60 µs. We can compute the spectrum and the APD of the OFDM signal by using an EMI receiver simulation in MatLab.

First, the IF-output envelope signal is calculated. The result is depicted in Figure 5.7 B. The APD is calculated by using two Resolution Bandwidths (RBW), i.e., 10 and 20 MHz. The APD curves can be displayed in different ways. In Figure 5.8 A, the APD curves are depicted by using the so-called Rayleigh graph projection. Such a projection has the advantage that a Gaussian distributed signal corresponds to a decreasing straight line as APD curve. We use the Rayleigh graph for testing against a Gaussian distribution. As can be observed in Figure 5.8 A, the OFDM transmitted time signal results in a decreasing straight line APD curve. As explained above, this means that the IF-output envelope behaves like a Gaussian distributed signal. In Figure 5.8 A, the effect of bandwidth variation can be observed as well. A larger bandwidth will result in a proportionally higher APD level. This can be explained by the Gaussian behavior of the OFDM signal. Gaussian distributed signals are in general broadband and the received power scales linearly with the bandwidth.

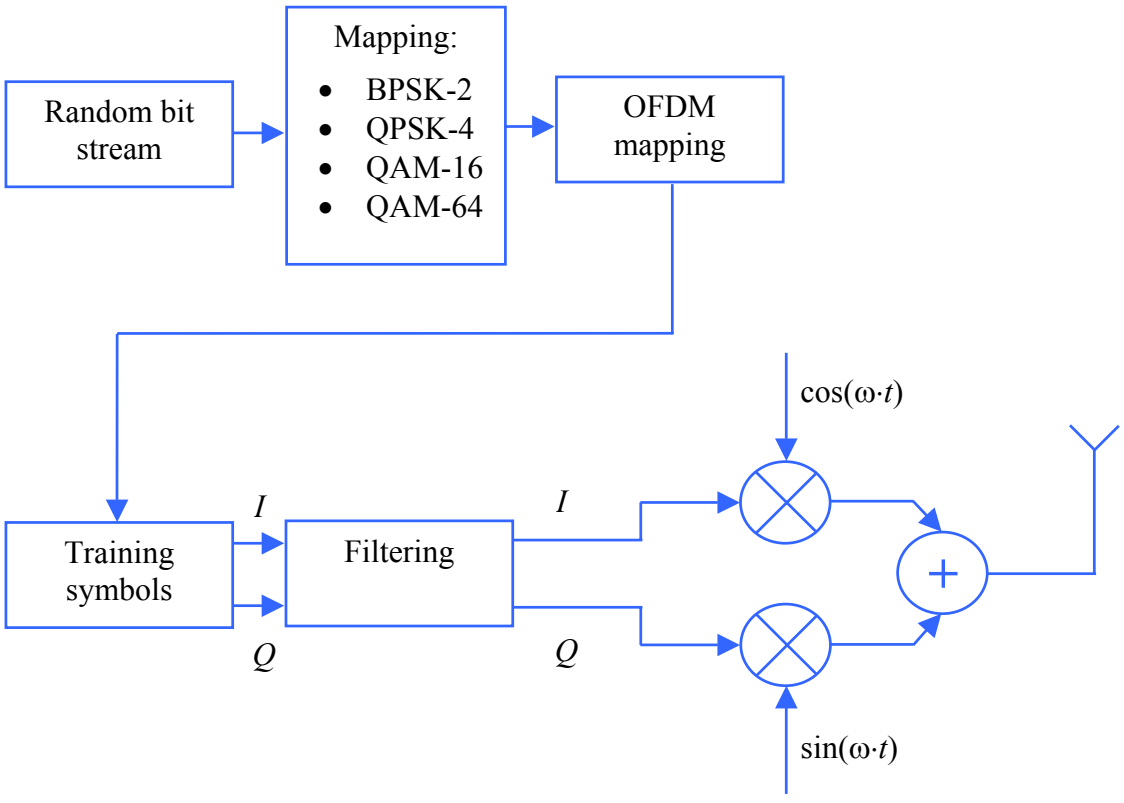


Figure 5.6 OFDM radio transmitter architecture used for the simulations.

In Figure 5.8 B, the Peak, Average, and RMS spectra of the OFDM signal are shown. The spectra are determined by applying a RBW of 1 MHz. Differences between these three spectra could be expected because of the time behavior of the OFDM signal and its corresponding IF output. It is known that the difference between RMS and Average results of a Gaussian signal is 1 dB. In Figure 5.8 B, we can observe this 1 dB difference in a large part of the transmitter range from 300 to 320 MHz. The differences between the weighting detector results are not important for the derivation of the UDS concepts.

In conclusion, the OFDM radio-communication signal can be emulated by a UDS based on Gaussian noise modulated on a RF carrier combined with pulse modulation. The pulse modulation is included to simulate the time behavior of OFDM signals as explained in Subsection 5.5.2. When the pulse modulation is included, the UDS can be applied for both the conventional interference scenario and the coexistence interference scenario. Specifications of this UDS are given in Section 5.7.

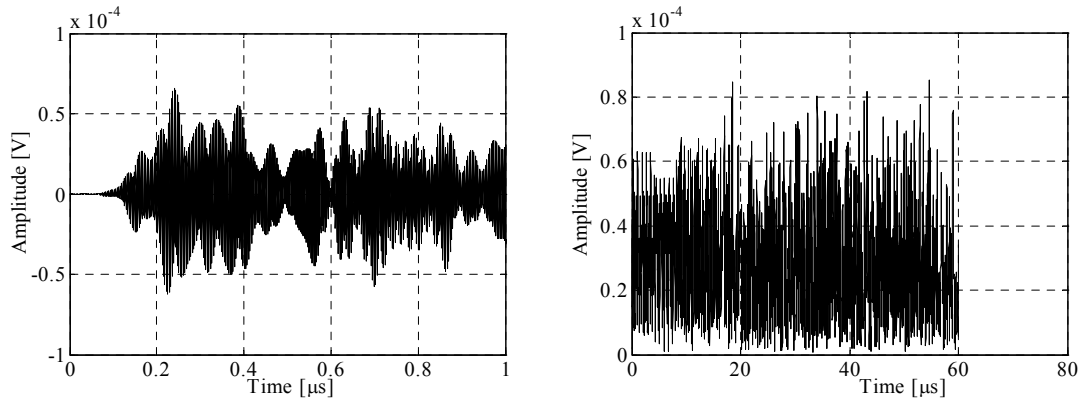


A. OFDM time signal B. IF-output

Figure 5.7 Transmitted time signal, from 0 to 1 µs (A) and IF-output signal of the received OFDM signal (B).

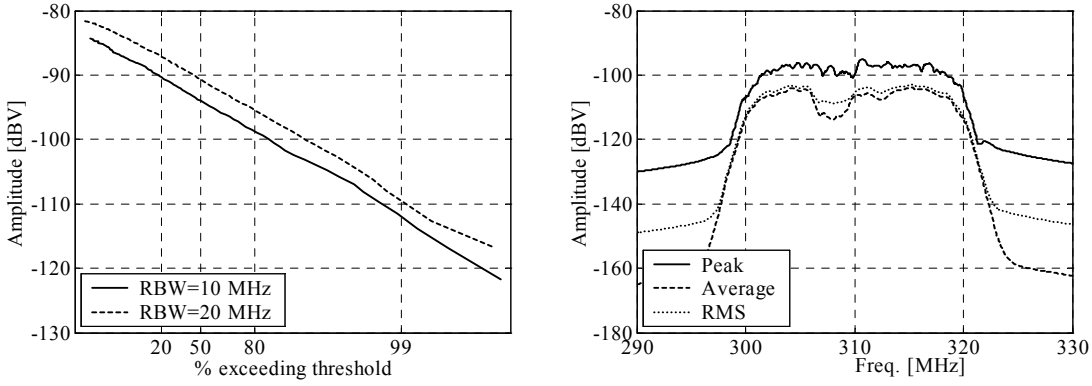


A. APD (Rayleigh graph) B. Spectra

Figure 5.8 APD of the OFDM transmitter signal in Rayleigh graph projection (A) and spectra of the OFDM transmitter signal (B).

## 5.6 Ultra Wide Band radio-communication signals

In this section, the signal behavior of Ultra Wide Band (UWB) signals is evaluated. UWB is a wireless technology that uses a low level signal (-41 dBm/MHz) over a broad frequency range. Because of the low level of the UWB communication signal, it is likely that it will not interfere with other communication systems and therefore UWB may be used in the same bands of other wireless technologies as depicted in the spectrum allocation overview of Figure 5.10. Two main categories of UWB technology are available nowadays. The first is the classical impulse radio technology known from radar applications in history.

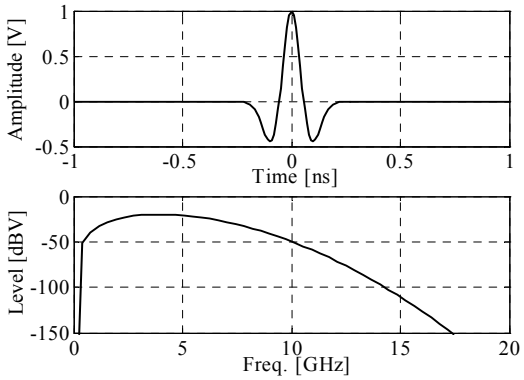


Figure 5.9 Ultra Wide Band (UWB) impulse signal in time and frequency domain.

The impulse radio technology is also suitable for determining the position of objects. An example of an impulse radio signal and its spectrum is given in Figure 5.9. Because of the low levels in the spectrum, it is expected that the impulse radio-communication signal has negligible influence on other radio-communication systems. The high amplitude and impulsive peaks in the time domain may possibly cause interference [6], but information about this is not available.

The second main category in UWB technology is based on (three or less) OFDM bands, which are activated by using frequency hopping. OFDM and frequency hopping (FH) are techniques that were already applied for Bluetooth and wireless LAN IEEE 802.11a/g. Therefore, it is expected that UWB radio-communication signals have negligible effect compared to the interference potential of FDM and TDM radio-communication signals.

The coexistence performance of UWB and other wireless LAN systems is moderate and was evaluated in [71]. Furthermore, an UWB receiver is predominantly susceptible to spurious emission originating from other radio-communication systems (coexistence interference scenario) and pulse modulation (TDM) due to nonlinearity. The linearity is difficult to realize because of the wide band (>500 MHz) in which the UWB receiver is operating. Especially the combination of two radio-communication signals (interferers) is critical for proper UWB radio-communication. Therefore, a coexistence immunity test with two UDS signals is recommended for testing UWB communication systems. For example, a combined radiated immunity test including a UDS for DECT/Bluetooth (1.9/2.4 GHz) and a UDS for wireless LAN (5.8 GHz).

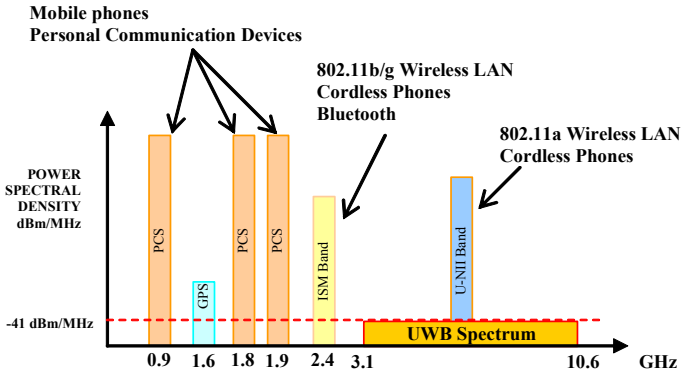


Figure 5.10 Comparison of frequency spectra of UWB and other wireless radio-communication technologies.

## 5.7 Specifications for the unified disturbance sources

From the results discussed in Sections 5.4 and 5.5, specifications for the different UDS implementations can be derived. The goal is to keep the implementations as simple as possible and therefore the use of basic signal generator functions are preferred.

### 5.7.1 UDS for TDM radio-communication signals

From the TDM results discussed in Section 5.4, we obtain two possible concepts for UDS implementation. The first is a simple pulse-modulated carrier for the conventional interference scenario where nonlinear detection is the dominating interference mechanism for a victim. The block diagram of this UDS implementation is depicted in Figure 5.11.
The specifications for the UDS are summarized in Table 5.5. The power levels are prescribed by the applicable standards for the radio-communication systems. For Bluetooth systems two classes of power levels are available. Bluetooth uses the frequency range from 2.402 to 2.48 GHz. This range is divided into 79 channels. As discussed in Subsection 5.4.1, Bluetooth uses Frequency Hopping (FH), i.e., it continuously changes the operational radio-communication channel. The channel is changed 1600 times per second. The duty cycle of a Bluetooth radio-communication signal, experienced by a victim receiver, is accordingly 1/79=1.3%.

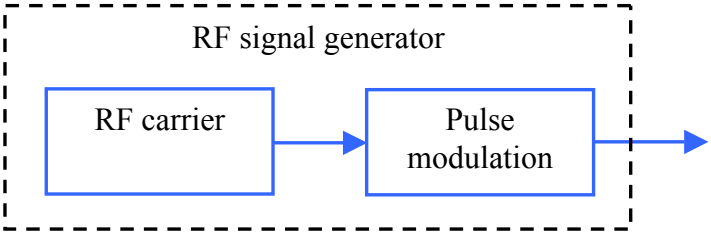


Figure 5.11 Diagram for generation of a pulse-modulated carrier for immunity tests.

Table 5.5 Specifications for narrowband pulsed modulated UDS.

| | Bluetooth | GSM/DCS | DECT |
|---|---|---|---|
| Level | Class I: 100 mW<br>Class II: 1 mW | 2 W | 250 mW |
| Carrier frequency | 2.4 GHz | GSM: 900 MHz<br>DCS: 1800 MHz | 1900 MHz |
| Pulse repetition frequency | 1600 Hz | 217 Hz | 100 Hz |
| Duty cycle | 1.3% | 12.5% | 2.1% |

The GSM and DCS radio-communication systems use frequency bands at 900 MHz and 1800 MHz, respectively. The properties of the physical layer of GSM and DCS systems are the same. They use both 8 time slots in combination with frequency duplex. This means that the transmitter (master) and the receiver (slave) use the time slot simultaneously, but at different frequencies. Therefore, the duty cycle is 1/8=12.5%. The pulse repetition frequency (PRF) is determined by the TDM frame frequency, which is 217 Hz for GSM and DCS systems. The DECT radio-communication system uses a frequency of 1900 MHz. The PRF is 100 Hz, which is the TDM frame frequency of DECT. The DECT system has 24 time slots in combination with time duplex. This means that the transmitter (master) and the receiver (slave) have alternate access to a time slot. This results in a duty cycle of 1/(2*24)=2.1%. It is suggested in Annex A of the IEC 61000-4-3 standard that TDM signals can be emulated also by using the conventional AM 80% 1 kHz test signal as a worst case for this conventional interference scenario. This becomes questionable for digital equipment, where clock jitter is a critical parameter [6].
The second UDS implementation of TDM signals is designed for emulating a coexistence interference scenario. In this case, also the spectral content of the UDS should be equivalent to the actual disturbance signal. Therefore, the FSK modulation should be present in such an implementation. The block diagram of this UDS implementation is depicted in Figure 5.12. This diagram illustrates that a RF signal generator and a LF arbitrary waveform generator are needed for this UDS. A combination of the UDS implementations for the two interference scenarios is also possible. The specifications of the UDS are summarized in Table 5.6.

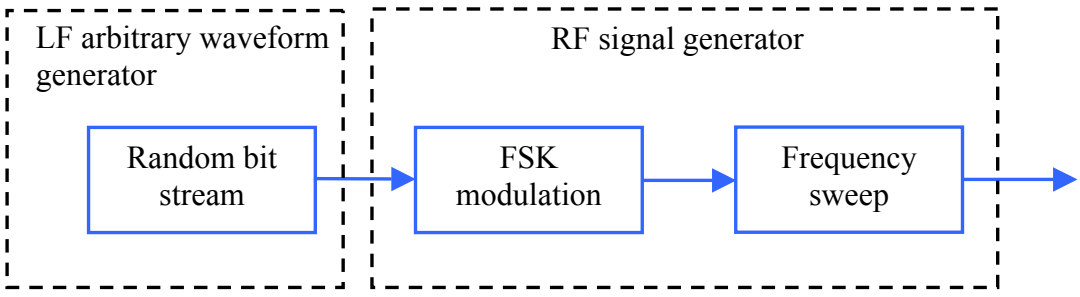


Figure 5.12 Diagram for generation of a Bluetooth simulation signal for immunity tests.

Table 5.6 Specifications for coexistence interference UDS.

| | Bluetooth | GSM/DCS | DECT |
|---|---|---|---|
| FSK deviation $\Delta f$ | 160 kHz | 67.8 kHz | 288 kHz |
| Bit time $T_b$ | 1.47 μs | 3.69 μs ($W \cdot T_b$=0.3) | 0.868 μs ($W \cdot T_b$=0.5) |
| Frequency sweep | 2.402-2.48 GHz | N.A. | N.A. |
| Frequency step size | 1 MHz | N.A. | N.A. |
| Dwell time | 625 μs | N.A. | N.A. |

The sweep function of the RF signal generator can be used for simulation of the FH of the Bluetooth radio-communication system. The frequency is swept in the operational band of Bluetooth, i.e., 2.402-2.48 GHz. The frequency step size equals the channel bandwidth of a Bluetooth radio-communication signal. The sweep frequency is equal to the FH frequency of 1600 Hz. This results in a dwell time of 1/1600=625 μs. A possible alternative for the use of the frequency sweep option is the use of a linear FM sweep. The frequency sweep is not applicable (N.A.) for GSM, DCS, and DECT. The bandwidth of a frequency modulated signal (FM or FSK) can be approximated by using the following equation known as Carson's rule [21]:

$$B_{\text{FM/FSK}} = 2 \cdot (\Delta f + W), \tag{5.1}$$

where $B_{\text{FM/FSK}}$ is the approximated bandwidth of the frequency modulated signal, $\Delta f$ is the FM/FSK frequency deviation which is 160 kHz for Bluetooth, and $W$ is the bandwidth of the LF data stream. For example, a Bluetooth channel has a bandwidth of 1 MHz and an FM/FSK frequency deviation of 160 kHz. This yields a $W$ of 340 kHz, the frequency of the random bit stream generated by the arbitrary waveform generator and a bit time $T_b$ of $1/(2W)$ =1.47 μs. The same calculations can be performed for GSM, DCS, and DECT.

### 5.7.2 UDS for FDM radio-communication systems

Finally, the simulations of the OFDM radio-communication signal in Section 5.5 resulted in one UDS implementation for the two interference scenarios (conventional and coexistence). This UDS implementation for OFDM/DSSS radio-communication signals is depicted in Figure 5.13. Broadband noise can be generated by using a relatively simple arbitrary waveform generator. Subsequently, the broadband noise is filtered to obtain the actual bandwidth. The noise is mixed on an RF carrier which is subsequently pulse-modulated to simulate the finite length of OFDM radio-communication signals. The specifications for this UDS are summarized in Table 5.7. The bandwidth of wireless LAN signals (IEEE 802.11a/b/g) is 20 MHz.

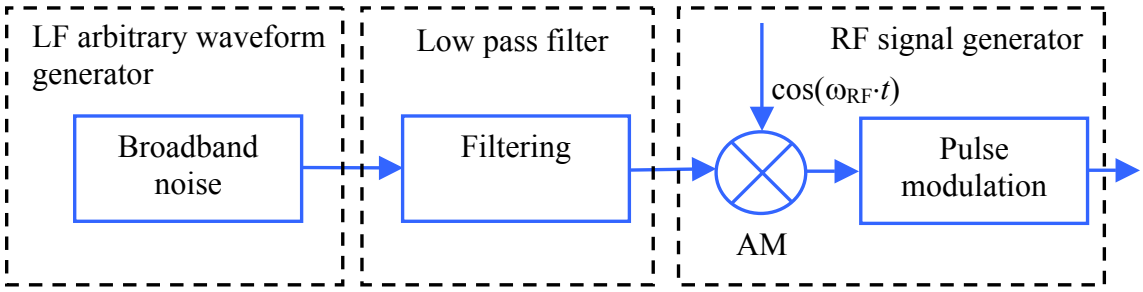


Figure 5.13 Diagram for generation of an OFDM simulation signal for immunity tests.

The RF power level of the UDS depends on national regulations, but can typically be specified in the range from 200 mW (EU) to 1 W (US). The PRF can vary in the range from 363 Hz to 2.1 kHz as derived in Subsection 5.5.2. The duty cycle of wireless LAN radio-communication signals is high and is approximately in the range 95-99%. This UDS can also be used to emulate other types of OFDM radio-communication signals, e.g., DVB broadcast, IEEE 802.11n, or WiMax signals.

Table 5.7 Specifications for the broadband (OFDM/DSSS) UDS.

| | |
|---|---|
| Broadband noise level | 0-5 V (TTL) |
| Filter bandwidth | 10 MHz (base band) |
| RF power level | 200 mW - 1 W |
| Carrier frequency | Applicable ISM bands |
| AM modulation depth | 100% |
| Pulse repetition frequency | 363 Hz - 2.1 kHz |
| Duty cycle | 95-99% |

## 5.8 Experimental evaluation

A few experiments by using the new UDS implementations have been performed.

*UWB wireless HDMI link*

An experiment was performed using a UWB radio-communication system for a wireless HDMI link. This experiment is discussed in more detail here. The EUT is an UWB radio-communication system for a HDMI link between a TV set and a DVD player as depicted in Figure 5.14. The antennas of the UWB system were placed in a compact FAR. Subsequently, the disturbance signal of the UDS was injected by using an antenna. The test

configuration and a picture of the compact FAR are shown in Figure 5.14. The test chain from the signal generator to the test antenna is depicted in Figure 5.15. The hardware used to realize the UDS is shown in Figure 5.16. This figure makes clear that one hardware configuration (19 inch rack) can be used for the new UDS implementations. The picture quality of the TV set was evaluated during the coexistence immunity test. We have injected signals equivalent to GSM signals, DECT signals, and wireless LAN signals (2.4 GHz). The UWB system was predominantly susceptible for GSM and DECT signals above 10 mW due to the pulse modulation. This confirms the nonlinearity problem of UWB receivers already mentioned in Section 5.6. The power was measured when the modulation was switched on.

*Coexistence immunity test on Zigbee radio-communication system*

Another experiment has been performed concerning the immunity of a Zigbee radio-communication system [73]. The Zigbee link was tested against the presence of Bluetooth Class I (100 mW) radio-communication signals. The Message Error Rate (MER) was determined for 100 messages per test-frequency.

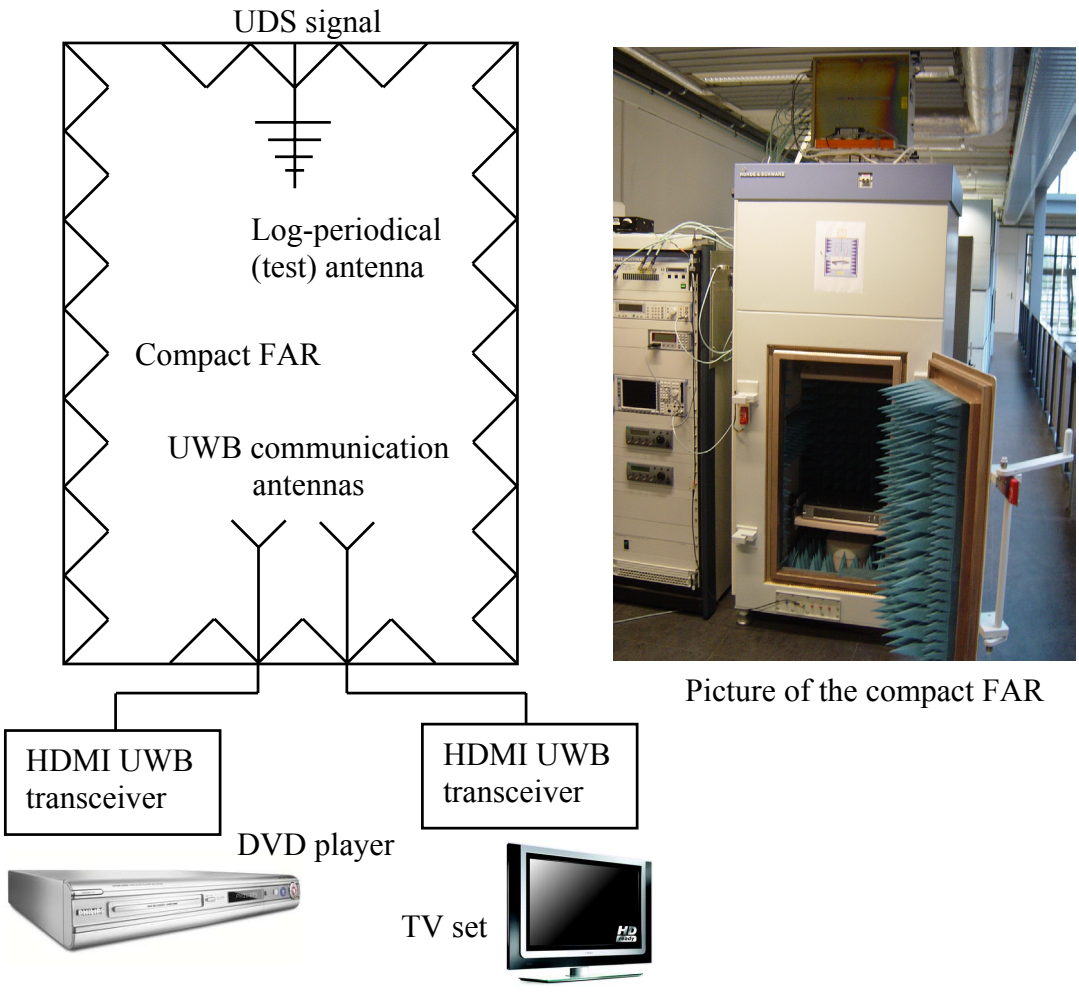


Figure 5.14 Coexistence immunity test configuration inside a compact FAR.

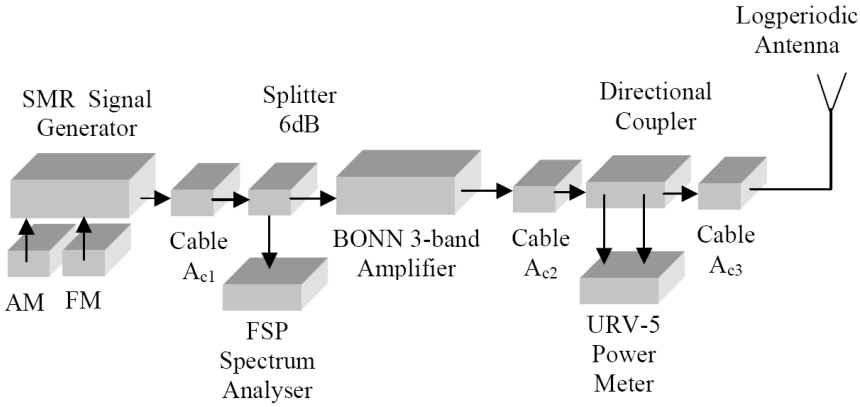


Figure 5.15 Block diagram of the test configuration.

The coexistence immunity test was performed in the frequency range from 2 GHz to 3 GHz. The frequency step was 1 MHz, which yields 1001 frequency points. The test configuration is similar to the configuration that was applicable to the above-mentioned immunity test of the wireless HDMI link (Figure 5.14). The Zigbee communication antennas were placed at the bottom of the compact FAR and the Bluetooth disturbance signal (UDS) was injected by using a log-periodical test-antenna at the top of the compact FAR. The Bluetooth-like signal was generated by applying the UDS implementation introduced in Subsection 5.7.1. The Zigbee communication channel was fixed to channel 8 (2.44 GHz). The operating band of Zigbee is from 2.4 GHz to 2.48 GHz including 16 channels of 5 MHz. The Zigbee link-distance was adjusted to 2.75 m by using attenuators. The distance between the log-periodical test-antenna and the Zigbee antennas is 1.4 m. The MER results as a function of the test carrier-frequency are shown in Figure 5.17. In Figure 5.17 A, the MER results are shown for the entire frequency range.

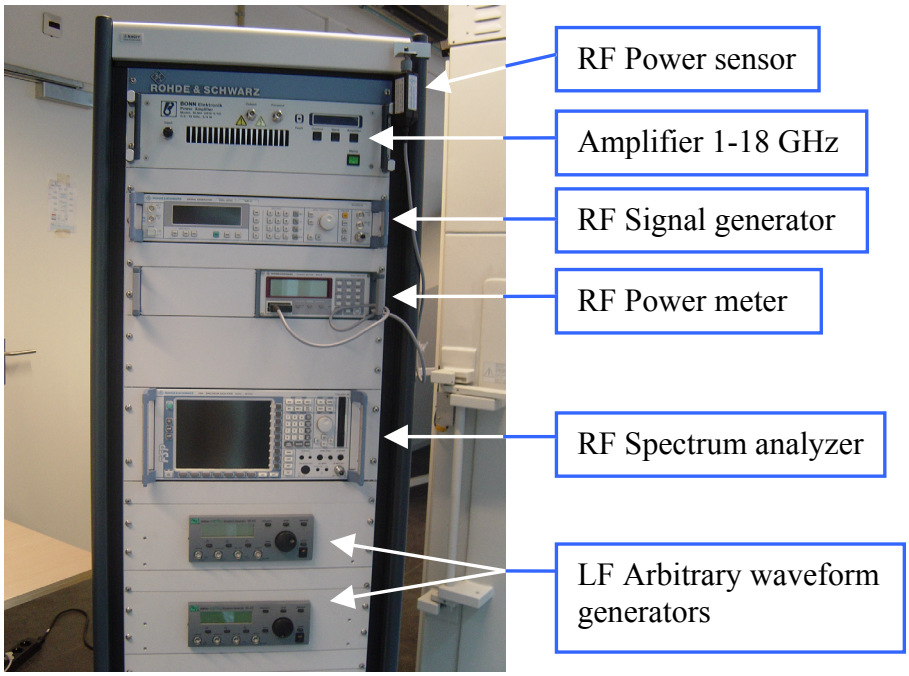


Figure 5.16 Test equipment for new UDS implementations.

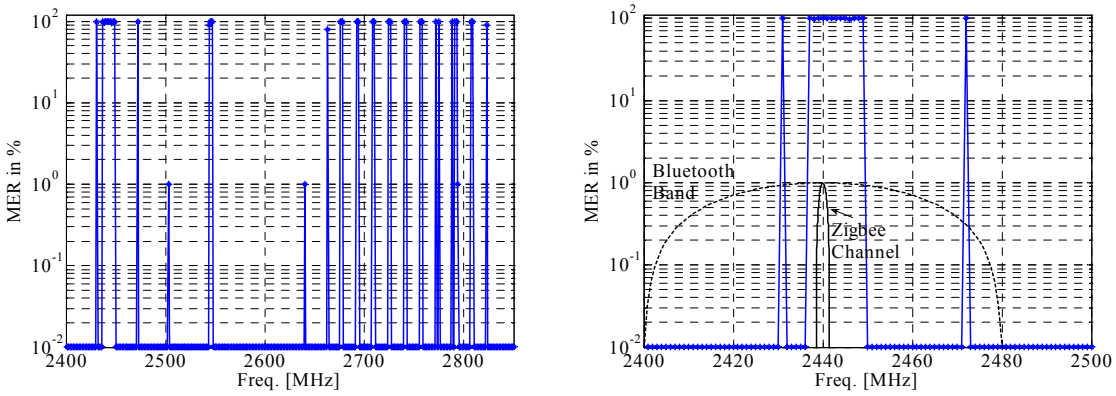


A. Entire frequency range B. Frequency range 2.4-2.5 GHz

Figure 5.17 Message Error Rate (MER) for a Zigbee link when disturbed by a Bluetooth-like test-signal (source: [73]).

The results are zoomed in from 2.4-2.5 GHz and shown in Figure 5.17 B. The MER results show that the Zigbee link can be shut down completely due to the Bluetooth disturbance signal. From Figure 5.17 B, it is observed that a 12 MHz interference bandwidth exists around the applicable Zigbee channel. This means that the Zigbee link does not only suffer from co-channel interference, but is also susceptible at other frequencies in the operating band of the Zigbee system. The Zigbee system is also susceptible at 2.431 GHz and 2.470 GHz. In conclusion, the Zigbee system is susceptible at 15 of the 79 Bluetooth channels.
From Figure 5.17 A, it is observed that the Zigbee link is also susceptible to a Bluetooth type of disturbance signal at higher frequencies. Some of these frequencies are equally spaced by 16 MHz. This is probably related to spurious frequencies of a local oscillator or the sampling IF used in the Zigbee radio. This observation demonstrates that radio-communication systems may have immunity problems also beyond their operating bands. This argues to perform coexistence immunity tests also beyond the operating bands of the radio-communication systems, when these radio-communication systems are being integrated into multimedia products.

The experiments demonstrate that by using the new UDS concepts practical coexistence immunity tests can be performed. The hardware setup (Figure 5.16) used for the UDS in the experiments includes test equipment commonly available. This means that special investments are not necessary. The experimental validation, whether the UDS signals have the same interference potential as the actual radio-communication signals, needs further investigations.

## 5.9 Summary and outlook

Concepts for possible implementations of a UDS were derived. The derivation is performed for TDM and FDM radio-communication signals. We have considered two interference scenarios for the UDS derivation, i.e., the conventional interference scenario and the coexistence interference scenario.

The UDS for TDM signals covering the conventional interference scenario is based on pulse modulation of an RF carrier. Specifications of this UDS are given for Bluetooth, GSM, DCS, and DECT. In addition, a UDS for TDM signals covering the coexistence interference scenario is derived. Specifications are defined for the same TDM systems.
Furthermore, a UDS for OFDM/DSSS types of signals like wireless LAN IEEE 802.11a/b/g signals is derived. This UDS is applicable for covering both the conventional interference scenario and the coexistence interference scenario. This UDS is based on mixed broadband noise, which is subsequently pulse-modulated. The UDS can also be applied to other types of OFDM radio-communication signals like DVB TV broadcast signals. From [79], it is expected that OFDM mapping techniques will extensively be used in future communication systems. Therefore, the new UDS concepts will be of high importance for future coexistence immunity tests.
The practical relevance of the new UDS concepts was demonstrated. The UDS implementations can be realized by using one hardware configuration of test equipment. The required test equipment is commonly available within EMC test laboratories. In conclusion, the use of UDS concepts will result in adequate and efficient (time+cost) immunity tests. Special investments are not anticipated.

The next step is to investigate the validity of the new UDS signals by testing multimedia products. This validation can be performed by comparing the interference effects of an EUT when subjected to both the UDS signal and the actual signal generated by a wireless-system tester. For every communication system a different wireless-system tester is needed.

Furthermore, it can be investigated whether the conventional 1 kHz 80% AM test-signal is really a worst-case signal for emulation of TDM signals as is suggested in Annex A of IEC 61000-4-3. From experimental experiences, it is known that especially for digital equipment a UDS based on pulse-modulation may be more severe than the conventional 1 kHz 80% AM UDS. For example, microcontrollers and high-speed busses are sensitive for impulsive disturbances because such disturbances can cause clock jitter, which can accordingly cause threshold failures [6].

# 6 Conclusions and outlook

## 6.1 Summary

In the first chapter of this thesis, the trends in electronic products were introduced. One of the consequences of these trends from an EMC point of view is the rapidly increasing development of all types of multimedia products, which have a high degree of integrated functionality. Moreover, these multimedia products use more and more wireless communication systems to establish a network with other multimedia products or to control peripheral equipment. An example of the latter is the implementation of wireless USB (Universal Serial Bus) by using Ultra Wide Band (UWB). All these new systems may act as potential new disturbance sources or may be potential new victims. This means that for EMC analysis new interference scenarios will appear. The wireless communication systems operate typically at frequencies above 1 GHz.
The results of three studies have been discussed in this thesis in the Chapters 3-5. These studies are preceded by a review of some developments in EMC standardization and corresponding technical issues in Chapter 2. In this standardization review, a list of seven topics was presented that are necessary for a proper adaptation of the standards towards modern multimedia products including wireless communication systems:

1. extension of radiated emission measurements above 1 GHz,
2. development of a new weighting detector for digital receivers,
3. development of new statistical techniques (e.g. Amplitude Probability Distribution (APD)) for processing of radiated emission measurement results,
4. extension of radiated immunity tests above 1 GHz,
5. extension of radiated immunity tests by using digitally modulated signals,
6. development of alternative measurement methods,
7. development of new multimedia standards.

The three studies discussed in this thesis have contributed to topics 1, 4, 5, and 6. In the standardization review of Chapter 2, developments concerning topics 2, 3, and 7 were clarified including a status overview of the development of the multimedia EMC product standards CISPR 32 and CISPR 35.

*The first study: Uncertainties due to the use of different types of receive antennas*

In the first study described in Chapter 3 of this thesis, the uncertainty source due to the use of different types of receive antennas was investigated. The receive antennas are characterized by their antenna factor (AF). The commonly used receive antennas in radiated emission measurements were included in the investigation:

- tuned dipole,
- biconical antenna,
- bow-tie antenna,
- log-periodical antenna,
- double-ridged waveguide horn antenna.

The main conclusion of the study is that the deviation (ΔE) in radiated emission results due to the use of different types of receive antennas can be substantial (below 1 GHz ΔE<3 dB, above 1 GHz ΔE<5 dB). This deviation is defined as the difference between the radiated emission result by using a specific antenna and the radiated emission result of two types of references. The radiated emission reference was determined by using the tuned-dipole reference and the E-field reference. In addition, the effect of the AF-calibration method on the deviation was investigated. The free-space method and the standard-site method (ANSI C63.5) were investigated.

An important guideline for the use of receive antennas could be defined, i.e., the receive antenna should have its maximum gain in the direction for which the antenna was calibrated. In general, multilobing of the antenna radiation-pattern does not exist when this guideline is adhered to. Multilobing of the receive antenna radiation-pattern increases the antenna-type deviation, because the beamwidth of the main lobe is in general small in such a situation. The smaller the beamwidth, the larger the antenna-type deviation will be. This was specifically demonstrated for the bow-tie antennas (30-300 MHz) and for two types of double-ridged waveguide horn antennas (1-18 GHz).
It was concluded that the level of deviation due to the antenna type in radiated emission measurements is not affected by the way the receive antenna is calibrated. This was investigated in the range 30-300 MHz.
Furthermore, we concluded that by using the E-field reference, the maximum deviations due to the use of different types of receive antennas are comparable within 0.3 dB to the maximum deviations obtained by using the tuned-dipole reference. Hence, the E-field reference as adopted in CISPR/A is therefore neither an improvement nor a degradation compared with the tuned-dipole reference. However, the choice of taking the E-field reference makes sense because the radiated emission limits are expressed in electric-field values.

At frequencies above 1 GHz, the antenna-type deviation can amount up to -5 dB. The deviation is always negative in this frequency range, i.e., the actual maximum could not be found. The radiated emission method above 1 GHz, based on a FAR, already requires information about the beamwidth of the receive antenna, namely, for the decision whether a height scan of the receive antenna is required. The results of the deviation study discussed in Chapter 3, also provide arguments for beamwidth specifications of receive antennas. It is shown that the beamwidth can be related to a specific deviation value. Approximately, a 60° beamwidth yields -1 dB deviation and a 30° beamwidth yields -4 dB deviation. Future standards can be adapted by including the requirement of beamwidth specifications and the corresponding deviations.

*The second study: Conversion factors for the RC radiated emission method*

In the second study, addressed in Chapter 4, the conversion of radiated emission results and limits was the topic of investigation. As indicated in the list of seven topics, alternative measurement methods are important in order to create optimal measurement methods for future applications, e.g., measurements above 1 GHz. A main issue in getting alternative measurement methods ready for introduction in product standards is the conversion of radiated emission results. This is a crucial issue because an unambiguous conversion method of radiated emission results obtained from alternative measurement methods for a class of EUTs can support the conversion of limits. Established methods are defined as being described in a basic standard and for which limits have been used for many years and that have proven adequate radio protection.
A standardized limit conversion method was applied for converting RC results to SAR results. The conversion is based on a four-step procedure, starting with the definition of a reference quantity. By the application of the conversion method also the uncertainty parameters of both the established method (SAR) and the alternative method (RC) were taken into account. The conversion method including the choice of the reference quantity can be applied to simulations of calculable EUTs only, because the reference quantity is difficult to derive for actual EUTs. We have used isotopic point sources, tuned dipoles, and a long-dipole for determining the conversion factor.
In addition, the conversion of radiated emission results was also investigated by using measurement results of system-test EUT arrangements in accordance with CISPR 22 including a TV, a PC, and a printer. This experiment demonstrated the suitability of the RC method for compliance measurements and the same level of uncertainty can be expected in the RC and in the SAR.

The directivity of EUTs was pointed out as a possible important influence quantity in the conversion factor, since the directivity of a half-wave dipole antenna (1.7) is taken as default in the transformation of received power to radiated electric-field. A statistical model for EUT directivity was reviewed and based on this model a comparison of the directivity effect was performed for a fictitious EUT measured within either a RC or a FAR in the frequency range 1-6 GHz. From the statistical review, we could conclude that the deviation resulting from the directivity effect of the EUT for the RC method and the FAR method is of the same order of 3-7 dB.
In addition, a long-dipole antenna of 1.5 m length was simulated to investigate the directivity effect for the 3 m SAR method, the 3 m FAR method, and the RC method in the frequency range 1-6 GHz. The reference quantity in this simulation was the maximum electric field-strength at 3 m distance of the EUT. The directivity effect is approximately 1-4 dB for the 3 m SAR at horizontal polarization. The directivity effect for the FAR method is approximately 0 dB. At vertical polarization, a directivity effect of 6-11 dB is obtained for the SAR method. The directivity effect for the FAR method amounts 5-12 dB at vertical polarization. The directivity causes a deviation of 3-9 dB for the RC method.
In conclusion, the directivity effect on the deviation with respect to the reference quantity depends on the polarization of the emission for the SAR and FAR methods for a long-dipole EUT. However, EUTs emitting at frequencies above 1 GHz cause a lower

interference risk in general. An interference problem can easily be solved by changing the position of the EUT somewhat because of the narrow lobes in the radiation pattern. In conclusion, the directivity is not an important parameter for the conversion of emission results.

In the range of 30-1000 MHz, a conversion factor of approximately 4 dB can be taken for the conversion of radiated emission results obtained from a RC towards SAR results. This conversion factor was determined by using measurement results and was confirmed by simulation of calculable EUTs. The conversion factors from RC to SAR results are of the same order of magnitude as the conversion factors from FAR to SAR results. This confirms that RC radiated emission measurements are equivalent to free-space measurements (FAR) from a conversion point of view.

*The third study: New immunity test-signals*

In Chapter 5, the third study concerning new concepts of immunity test-signals based on digitally modulated communication signals was addressed. In the strategic list of seven topics, topics 4 and 5 suggest the necessity of reconsidering the current immunity tests. An immunity test-signal, which covers a class of typical disturbance signals, is defined as a Unified Disturbance Source (UDS). The current immunity test-signal, a 1 kHz 80% AM modulated carrier, covers the class of analog radio signals and can be seen as the UDS for this class. However, more and more digitally modulated radio-communication signals are present in the home environment with multimedia products and integrated radio-communication systems. The radio-communication systems are applied for connecting multimedia applications to any kind of network as well as for wireless connection of peripheral equipment. This means that all types of digitally modulated radio-communication signals control essential parts of the functionality.
This trend has two consequences. Firstly, new concepts for immunity test-signals must be developed in order to cover the class of digitally modulated disturbance signals. Secondly, the currently lacking immunity tests for wireless communication systems should be reconsidered critically. This topic will be discussed further in the outlook, Section 6.2. The development of new concepts of immunity signals is discussed in the third study in this thesis, Chapter 5. Various communication signals have been considered: GSM 900, DCS 1800, DECT, Bluetooth, wireless LAN IEEE 802.11a/b/g, and UWB. A UDS should be representative for the relevant interference potential of a number of radio-communication signals. Moreover, it should be possible to generate the UDS signals in practice in a straightforward way. The latter point expresses the preference of using commonly used test equipment already available in EMC test laboratories. The investigated radio-communication signals were divided into two main categories: Time Division Multiplexing (TDM) signals and Frequency Division Multiplexing (FDM) signals. A relevant UDS depends also on the interference scenario. Two interference scenarios have been incorporated in this study, i.e., the conventional interference scenario (due to nonlinear detection) and the coexistence interference scenario. Three concepts of

immunity test-signals for TDM and FDM types of signals were formulated related to these interference scenarios.
The practical suitability of the UDS concepts was demonstrated by evaluating two experiments. The first experiment included a UWB link for a HDMI connection between a TV and a DVD recorder. The picture quality of the TV was evaluated when the UWB antennas were subjected to disturbance signals based on the UDS signals. The second experiment was a coexistence immunity test of a Zigbee communication system, when it was subjected to a Bluetooth-like signal based on a UDS concept. The Message Error Rate (MER) was measured during this experiment. The conclusion is that wireless communication systems can be sensitive to disturbances outside their operating band as well. This argues to perform coexistence immunity tests also beyond the operating bands of the radio-communication systems, when these radio-communication systems are being integrated into multimedia products. Furthermore, the UDS concepts can be implemented in a practical way by using commonly available test equipment. The concepts are based on fundamental radio principles (TDM and FDM), so that they will be able (with minor adaptations) to cover a wide scope of digital communication signals including future developments.

## 6.2 Outlook

In this thesis several issues concerning an adequate adaptation of the EMC standards for multimedia products were evaluated. These issues were summarized in a list of seven topics (see Section 6.1). Although most of the topics were addressed, still a lot of work has to be performed. In this outlook section, the following topics are discussed:

- coexistence immunity tests,
- uncertainties,
- conversion of immunity requirements,
- wireless coexistence in medical environments.

*Coexistence immunity tests*

The extension of radiated immunity tests above 1 GHz is a main issue for two reasons. The first reason is already indicated, namely, the increasing application of communication systems using frequencies above 1 GHz. This needs to be extended in due time. Secondly, wireless communication systems become an integral and essential function of the multimedia products. This means that the conventional separation between intentional and unintentional radiation should be reconsidered critically; it is becoming meaningless for, e.g., multimedia products that communicate with their peripheral equipment by using radio communication. An actual case reflecting the issue is the UWB technology for wireless USB or wireless HDMI. The UWB radio can be susceptible for interferers at 2.4 GHz (Bluetooth, IEEE 802.11b/n) and 5.8 GHz (IEEE 802.11a) that is caused by nonlinearity of

the UWB receiver. Sufficient linearity is difficult to realize because of the wide band (>500 MHz) in which the UWB receiver should perform. In accordance with CISPR 22, a combination of a PC and a printer using USB connection should be tested by performing a system immunity test. When an USB connection is implemented by applying UWB, the same system should be tested against the possible and ubiquitous threats of above 1 GHz interferers originating from other wireless communication systems. In conclusion, when immunity tests are performed in order to guarantee a basic immunity of products against external disturbances, then the integrated radio functions should have such an intrinsic immunity as well, because it fulfils an essential function of the product.

The use of statistical assessment tools can be supportive in the immunity tests of the radio function of the multimedia products. In Chapter 2, the Amplitude Probability Distribution (APD) was already indicated as a useful statistical function to characterize disturbance signals. State-of-the-art developments have shown that APD information of a disturbance signal can be related to the Bit Error Probability (BEP) of a digital radio receiver [41][90][91]. Proper 'coexistence algorithms' for the application of all kinds of wireless communication systems integrated into multimedia products should be developed by using APD assessments in combination with up-to-date interference scenarios. This can be realized by setting up an EMC matrix including modulation scheme and corresponding transmitter power level necessary for a specific throughput at the disturbance source side. Vice versa, power sensitivity levels and corresponding throughput must be defined at the victim side of the interference scenario. Based on the relation between APD and BEP of digital radios, it is possible to optimize the modulation scheme and corresponding transmitter power level and the duty cycle of a digital radio-communication signal in order to prevent disturbance with another digital communication system. We can envisage a priority trade-off based on APD and BEP of coexistence 'wireless jobs'. It is obvious that physical limitations of such a priority trade-off are present. However, proper assessments of wireless technology used in multimedia products should result in a more architectural approach of the arrangement of multimedia and radio-communication systems in the home environment.

*Uncertainties*

Another open issue related to the list of seven areas, is the unknown uncertainty sources in radiated emission measurements above 1 GHz as well as in alternative measurements. In order to apply the new methods properly in the near future, these uncertainty sources should be identified and quantified. Availability of uncertainty budgets is also important for the accreditation of test laboratories, which use the newly developed methods. Numerical simulations can be supportive in quantifying uncertainty sources [14][24]. Efficient numerical algorithms, like marching-on-in-anything, may be useful for the quantification of the uncertainties [10].

*Conversion of immunity requirements*

AV systems are currently tested in a 'Jacky' TEM waveguide test configuration as shown in Figure 6.1. This test configuration is limited to test frequencies up to 150 MHz and only suitable for small equipment. The FAR or the RC can be used when immunity tests should be performed up to 1 GHz or higher frequencies. This means that conversion of immunity test-requirements constitute an important issue, because the new immunity standard CISPR 35 will allow compliance demonstration by using different immunity-tests.
An investigation about immunity conversion between RC and FAR test levels can be found in [75], where a conversion factor is found of approximately 1-2 dB based on measurement results. This immunity conversion factor should be investigated further and numerical simulations as described in [14] can be supportive for such a study. In addition, the uncertainty of immunity test methods is an important topic when different methods are compared. Useful insights in the uncertainty of the maximum test field in a RC configuration are presented in [47][48].

Figure 6.1 TEM waveguide (Jacky) immunity test configuration.

*Wireless coexistence immunity tests in medical environments*

A picture of a Magnetic Resonance Imaging (MRI) scanner and its application environment is shown in Figure 6.2. Such a medical environment is nowadays equipped with many multimedia and wireless products. For example, beamers are used in order to create a patient-friendly environment. Wireless communication is applied for patient monitoring and for communication with the patient. The environment where the MRI scanners are placed is typically an electromagnetically shielded environment. Application of multimedia products and wireless communication systems within a medical environment create new EMC challenges, and offer opportunities for the concepts presented in this thesis. The application of wireless communication systems in an environment with sensitive medical equipment causes a high interference-risk. Extensions of immunity tests are needed in order to reduce this risk to levels suitable in a medical environment. The new UDS concepts derived in Chapter 5 can be useful to emulate the digital communication signals adequately and efficiently. Moreover, the application of a

statistical risk-evaluation approach based on analysis of variances (ANOVA) seems promising [5]. In such an approach, the EUT is subjected to various types of disturbance signals and their impact on the performance degradation of the product is evaluated statistically. This type of statistics is also known as the method of Design of Experiments (DoE). The benefit of a statistical risk-evaluation is that the susceptibility properties of the EUT become quantitative in a regression model. In such a model possible interactions between different disturbance signals can be expressed as well. The various UDS concepts, as representative test-signals of a class of wireless communication signals, can excellently be combined with the statistical risk-evaluation. For typical multimedia products of the home environment such extensive risk-assessments could be overdone in practice. However, for multimedia products applied within professional medical environments, an extensive risk-evaluation is useful because critical medical diagnostics, care of patients, and safety are important issues.

Figure 6.2 MRI scanner configuration equipped with multimedia and wireless technology.

Another issue is the reflective behavior of the environment. The propagating fields in such an environment will result in many reflections and accordingly in standing waves. It is known that inside reflective indoor environments the communication channels will statistically behave as Rayleigh or Rician distributed [44]. A very interesting property of the Reverberation Chamber (RC), presented in Chapter 4, is the possibility to emulate such statistical communication channels. In [51], interesting insights are presented about this RC application. An important issue for emulating Rayleigh or Rician communication channels within a RC is the loading of the chamber. The loading determines the quality factor $Q$ of the chamber. By bringing absorbing material within the RC, the quality factor $Q$ can be adjusted to values applicable to, e.g., medical environments. The same type of RC test is also useful for so-called Multiple Input Multiple Output (MIMO) communication systems, e.g., IEEE 802.11n. Such MIMO systems utilize the reflective behavior of their environments. The performance of MIMO systems can be tested in a RC that emulates the various communication channels.

# A1 Statistical distribution of the maximum received power in the RC

In this annex, the statistical distribution is derived for the maximum power received in a RC of a series of $N$ samples [65]. In Chapter 4, only the major steps in this derivation were presented. It was explained that the received power in the RC could be described by an exponential probability distribution ($\chi^2$-distributions with two degrees of freedom):

$$f_{\chi_2^2}(x) = \frac{1}{2\sigma^2} e^{-x/2\sigma^2} \cdot U(x), \tag{A1.1}$$

where $U(x)$ is Heaviside's function, $\sigma^2$ is the variance of either a real or imaginary part of a rectangular component of the received electric field, and $x$ is the received power. When a radiated emission measurement is performed in a RC, we can measure the maximum or the average value of a field quantity, e.g., the maximum or average received power. The maximum, taken from a series of $N$ samples (stirrer steps) of a certain variable, is a different statistical distribution compared to the original distribution of the variable [76]. Such a distribution is derived for the maximum received power. In the following equations $x$ stands for the received power $P_r$.

When the probability density function (PDF) of a statistical variable $x$ is $f_A(x)$ along with the cumulative distribution function (CDF) $F_A(x)$, then the PDF for the maximum value (denoted as $\lceil\ \rceil$) can be defined as:

$$f_{\lceil A \rceil_N}(x) = N\left[F_A(x)\right]^{N-1} \cdot f_A(x). \tag{A1.2}$$

This can be interpreted as the PDF of the maximum value, when the experiment of taking the maximum from $N$ samples (stirrer steps) is repeated. When Eq. (A1.2) is used for the received power ($\chi^2$-distribution with two degrees of freedom), then the following PDF for the maximum received power is obtained:

$$f_{\lceil \chi_2^2 \rceil_N}(x) = \frac{N}{2\sigma^2}\left[1 - e^{-x/2\sigma^2}\right]^{N-1} \cdot e^{-x/2\sigma^2}. \tag{A1.3}$$

Note that $x$ is always positive or zero because it represents the received power $P_r$. From this, the mean of the maximum can be determined by:

$$\left\langle \lceil \chi_2^2 \rceil_N \right\rangle = \int_0^\infty x \cdot N\left[1 - e^{-x/2\sigma^2}\right]^{N-1} \cdot \frac{1}{2\sigma^2} e^{-x/2\sigma^2}\, dx. \tag{A1.4}$$

Substituting $u = x/2\sigma^2$ and expanding the term in brackets in a binomial series by using $(a+x)^n = \sum_{k=0}^{n}\binom{n}{k}x^k a^{n-k}$, yields:

$$\left\langle \left\lceil \chi_2^2 \right\rceil_N \right\rangle = N2\sigma^2 \sum_{m=0}^{N-1}(-1)^m \binom{N-1}{m} \cdot \int_0^{\infty} u e^{-(m+1)u} du. \tag{A1.5}$$

The integral can be solved by applying integration by parts:

$$\left\langle \left\lceil \chi_2^2 \right\rceil_N \right\rangle = N2\sigma^2 \sum_{m=0}^{N-1}(-1)^m \binom{N-1}{m} \cdot \frac{1}{(m+1)^2}. \tag{A1.6}$$

The factor $N\binom{N-1}{m}\left(\frac{1}{m+1}\right)$ can be recombined as $\binom{N}{m+1}$. If subsequently $n$ is defined as $m$+1, we end up with:

$$\left\langle \left\lceil \chi_2^2 \right\rceil_N \right\rangle = 2\sigma^2 \sum_{n=1}^{N}(-1)^{n-1} \binom{N}{n} \frac{1}{n}. \tag{A1.7}$$

From Eq. (0.155-4) in [42], it is known that $\sum_{k=1}^{n}\frac{(-1)^{k-1}}{k}\binom{n}{k} = \sum_{m=1}^{n}\frac{1}{m}$; applying this result in Eq. (A1.7) yields:

$$\left\langle \left\lceil \chi_2^2 \right\rceil_N \right\rangle = 2\sigma^2 \sum_{n=1}^{N}\frac{1}{n}. \tag{A1.8}$$

Finally, the mean of the maximum can be determined by approximating the finite sum (by using Eq. (0.131) in [42]):

$$\begin{aligned} \left\langle \left\lceil \chi_2^2 \right\rceil_N \right\rangle &= 2\sigma^2 \sum_{n=1}^{N}\frac{1}{n} \approx 2\sigma^2\left(\gamma + \ln(N) + \frac{1}{2N}\right), \\ \left\langle \left\lceil \chi_2^2 \right\rceil_N \right\rangle &= \left\langle \chi_2^2 \right\rangle\left(\gamma + \ln(N) + \frac{1}{2N}\right), \end{aligned} \tag{A1.9}$$

where $\gamma \approx 0.57721$ is the Euler-Mascheroni constant and $\left\langle \chi_2^2 \right\rangle = 2\sigma^2$ is the mean of the original received power Eq. (A1.1).

# References


[1] M. J. Alexander, M. H. Lopez, and M. J. Salter, "Getting the best out of biconical antennas for emission measurements and test site evaluation," *Proc. IEEE Int. Symp. on EMC*, Austin, pp. 84-89, Aug. 1997.

[2] M. J. Alexander, *et al.*, *Measurement Good Practice Guide No. 73 – Calibration and use of antennas focusing on EMC applications*, National Physical Laboratory (NPL), Teddington, UK, Dec. 2004.

[3] "Calibration of Antennas Used for Radiated Emission Measurements in Electromagnetic Interference (EMI) Control," ANSI C63.5, Jun. 1988.

[4] L. R. Arnaut and P. D. West, "Electromagnetic reverberation near a perfectly conducting boundary," *IEEE Trans. Electromagn. Compat.*, Vol. 48, No. 2, pp. 359-371, May 2006.

[5] M. Audone, "A statistical approach for the quantitative evaluation of the immunity levels of devices and systems and high intensity susceptibility signal (HISS) test method," *Proc. 16th Int. Zurich Symp. on EMC*, Feb. 2005.

[6] S. Bakshi, R. Derikx, W. de Graaf, and M. Coenen, "Circuit analysis study for the impulse immunity test (IIT)," *Proc. Int. Symp. on EMC*, Eindhoven, Sep. 2004.

[7] G. Bargboer, "Uncertainties of radiated emission measurements in the near-field region," M.S. thesis, Eindhoven University of Technology, Eindhoven, The Netherlands, January 2006.

[8] P. A. Beeckman, "The influence of positioning tables on the results of radiated EMC measurements," *Proc. IEEE Int. Symp. on EMC*, vol. 1, pp. 280–285, Montreal, Aug. 2001.

[9] P. A. Beeckman, N. van Dijk, and L. P. Janssen, "Inter Laboratory Comparison (ILC) of three standardized emission measurements," *Proc. Int. Symp. on EMC*, Eindhoven, Sep. 2004.

[10] M. C. van Beurden, "Integro-differential equations for electromagnetic scattering. Analysis and computation for objects with electric contrast," Ph.D. dissertation, Eindhoven University of Technology, Eindhoven, The Netherlands, Sep. 2003.

[11] C. E. Brench, "Antenna factor anomalies and their effects on EMC measurements," *Proc. IEEE Int. Symp. on EMC*, Atlanta, pp. 342-346, Aug. 1987.

[12] C. E. Brench, "Antenna differences and their influence on radiated emission measurements," *Proc. IEEE Int. Symp. on EMC*, Washington DC, pp. 440-443, Aug. 1990.

[13] C. Bruns, R. Vahldieck, and P. Leuchtmann, "Analysis and simulation of a 1-18-GHz broadband double-ridged horn antenna," *IEEE Trans. Electromagn. Compat.*, Vol. 45, No. 1, pp. 55-60, Feb. 2003.

[14] C. Bruns and R. Vahldieck, "A closer look at reverberation chambers – 3-d simulation and experimental verification," *IEEE Trans. Electromagn. Compat.*, Vol. 47, No. 3, pp. 612-626, Aug. 2005.

[15] M. Candidi, C. L. Holloway, P. Wilson, D. Camell, "Comparison of radiated emission measurements for 500 MHz to 2 GHz in various EMC facilities," *Proc. Int. Symp. on EMC*, Sorrento, Sep. 2002.

[16] "Specification for Radio Disturbance and Immunity Measuring Apparatus and Methods - Part 1-4: Radio Disturbance and Immunity Measuring Apparatus - Ancillary Equipment - Radiated Disturbances," CISPR 16-1-4, 2003.

[17] "Specification for Radio Disturbance and Immunity Measuring Apparatus and Methods - Part 4-2: Uncertainties, Statistics and Limit Modeling - Uncertainty in EMC Measurements," CISPR 16-4-2, 2003.

[18] "Specification for Radio Disturbance and Immunity Measuring Apparatus and Methods - Part 4-5 Ed. 1: Technical Report, Conditions for the Use of Alternative Test Methods," CISPR 16-4-5, 2006.

[19] "Specification for radio disturbance and immunity measuring apparatus and methods. Part 2-3 Ed. 2: Methods of measurement of disturbances and immunity - Radiated disturbance measurements," CISPR 16-2-3, 2006.

[20] P. Corona, J. Ladbury, and G. Latmiral, "Reverberation-chamber research - then and now: a review of early work and comparison with current understanding," *IEEE Trans. Electromagn. Compat.*, Vol. 44, No. 1, pp. 87-94, Feb. 2002.

[21] L. W. Couch, *Digital and Analog Communication Systems*, sixth edition, Prentice Hall, 2001.

[22] D. B. Davidson, *Computational Electromagnetics for RF and Microwave Engineering*, Cambridge: Cambridge University Press, 2005.

[23] N. van Dijk, "Development and validation of tools for simulation of radiated emission testing," M.S. thesis, Eindhoven University of Technology, Eindhoven, The Netherlands, January 2001.

[24] N. van Dijk, "Numerical tools for simulation of radiated emission testing and its application in uncertainty studies," *IEEE Trans. Electromagn. Compat.*, Vol. 44, No. 3, pp. 466-470, Aug. 2002.

[25] N. van Dijk, "Uncertainties in 3-m radiated emission measurements due to the use of different types of receive antennas," *Proc. Int. Symp. on EMC*, Eindhoven, Sep. 2004.

[26] N. van Dijk, "Uncertainties in 3-m radiated emission measurements due to the use of different types of receive antennas," *IEEE Trans. Electromagn. Compat.*, Vol. 47, No. 1, pp. 77-85, Feb. 2005.

[27] N. van Dijk, P. F. Stenumgaard, P. A. Beeckman, K. C. Wiklundh, and M. Stecher, "Challenging research domains in future EMC basic standards for different applications," *Proc. Int. Symp. on EMC*, Rome, Sep. 2005.

[28] N. van Dijk, "E-field reference comparisons of 3-m radiated-emission results by the use of different types of receive antennas," CISPR/A WG 1 and 2 document, Aug. 2005.

[29] N. van Dijk, "Concepts of unified disturbance sources for immunity -A representative test signal for digitally modulated signals-," Philips AppTech EM&C research report, EMC-05-NVD-001-RRP, Aug. 2005.

[30] N. van Dijk, "Concepts of new unified disturbance sources for immunity testing of multimedia products," *Proc. Int. Symp. on EMC*, Barcelona, Sep. 2006.

[31] N. van Dijk, "Conducted emission measurements on the antenna cable," CISPR/I WG 2 document discussed at Santa Fe meeting, Jan. 2006.

[32] Directive 2004/108/EC of the European parliament and of the council, Dec. 2004. http://ec.europa.eu/enterprise/electr_equipment/emc/directiv/text2004_108.htm

[33] T. J. Dvorak, "Polarization error in fieldstrength measurements," *Proc. IEEE Int. Symp. on EMC*, pp. 134-139, Santa Clara, 1982.

[34] T. J. Dvorak, "Are antenna factors valid in EMC measurements?," *Proc. Int. Symp. on EMC*, Nagoya, pp. 587-590, Sep. 1989.

[35] "Cable Networks for Television Signals, Sound Signals and Interactive Services Part 2: Electromagnetic Compatibility for Equipment," EN 50083-2, June 2006.

[36] "Radio Frequency Devices – Part 15 of FCC rules," 47 CFR Part 15.

[37] M. D. Foegelle, "Coexistence of converged wireless communication devices," *IEEE EMC Society Newsletter*, pp. 77-78, spring 2006.

[38] Peng Gao, "Compliance uncertainty of radiated emission measurement above 1 GHz," M.S. thesis, University of Twente, Enschede, The Netherlands, March 2004.

[39] J. J. Goedbloed, "Uncertainties in EMC compliance testing," in *Proc. IEE Colloq. Implication of Measurement Uncertainties for EMC Testing*, London, U.K., June 11, 1997.

[40] J. J. Goedbloed and A. P. Beeckman, "Uncertainty analysis of the CISPR/A radiated emission Round-Robin Test results," *IEEE Trans. Electromagn. Compat.*, Vol. 46, No. 2, pp. 246-262, May 2004.

[41] K. Gotoh, Y. Yamanaka, and T. Shinozuka, "Numerical study on the disturbance measurements related to the performance of digital wireless communication systems," *Proc. Int. Symp. on EMC*, Sendai, June 2004.

[42] I. Gradshteyn and I. Ryzhik, *Table of Integrals, Series, and Products*, New York: Academic, 1980.

[43] J. E. Hansen, *Spherical near-field antenna measurements*, London: Peregrinus, 1988.

[44] H. Hashemi, "The indoor radio propagation channel," *Proc. IEEE*, Vol. 81, No. 7, pp. 943-968, July 1993.

[45] D. Heirman and M. Stecher, "A history of the evolution of EMC regulatory bodies and standards," *Proc. 16th Int. Zurich Symp. on EMC*, pp. 83-94, Feb. 2005.

[46] D.A. Hill, "Electromagnetic theory of reverberation chambers," NIST Tech. note No. 1506, Dec. 1998.

[47] M. Höijer and M. Bäckström, "How we confused the comparison between high level radiated susceptibility measurements in the reverberation chamber and at the open area test site," *Proc. IEEE Int. Symp. on EMC*, Istanbul, May 2003.

[48] M. Höijer, "Maximum power available to stress onto the critical component in the equipment under test when performing a radiated susceptibility test in the reverberation chamber," *IEEE Trans. Electromagn. Compat.*, Vol. 48, No. 2, pp. 372-384, May 2006.

[49] C. L. Holloway, P. F. Wilson, G. Koepke, and M. Candidi, "Total radiated power limits for emission measurements in a reverberation chamber," *Proc. IEEE Int. Symp. on EMC*, pp. 838-843, Boston, Aug. 2003.

[50] C. L. Holloway and E. F. Kuester, "Modeling semi-anechoic electromagnetic measurement chambers," *IEEE Trans. Electromagn. Compat.*, Vol. 38, No. 1, pp. 300-309, Feb. 1996.

[51] C. L. Holloway, D. A. Hill, J. Ladbury, and G. Koepke, "Requirements for an effective reverberation chamber: unloaded or loaded," *IEEE Trans. Electromagn. Compat.*, Vol. 48, No. 1, pp. 187-194, Feb. 2006.

[52] "Electromagnetic Compatibility - Guide to the Drafting of Electromagnetic Compatibility Publications," IEC Guide 107, second edition, Jan. 1998.

[53] "Electromagnetic Compatibility (EMC) - Part 4-3 Ed. 2.1: Testing and Measurement Techniques – Radiated, Radio-Frequency, Electromagnetic Field Immunity Test," IEC 61000-4-3, 2002.

[54] "Electromagnetic Compatibility (EMC) - Part 4-21 Ed. 1: Testing and Measurement Techniques - Reverberation Chamber Test Methods," IEC 61000-4-21, 2003.

[55] "Wireless LAN Medium Access Control (MAC) and Physical Layer (PHY) – High-Speed Physical Layer in the 5 GHz Band," IEEE 802.11a, 1999.

[56] S. Iskra, W. Thomas, R. McKenzie, and J. Rowley, "Evaluation of potential GPRS 900/1800-MHz and WCDMA 1900-MHz interference to consumer electronics," *IEEE Trans. Electromagn. Compat.*, Vol. 47, No. 4, pp. 951-962, Nov. 2005.

[57] "General Requirements for the Competence of Testing and Calibration Laboratories," ISO/IEC 17025, 1999.

[58] "Acoustics – Determination of Sound Power Levels of Noise Sources Using Sound Pressure – Precision Methods for Reverberation Room," ISO 3741, third edition, 1999.

[59] U. Jakobus and F. M. Landstorfer, "Numerical analysis of errors associated with antenna calibrations and emission testing," in *Proc. 12th Int. Zurich Symp. on EMC*, pp. 441-446, Feb. 1997.

[60] W. Joseph and L. Martens, "The influence of the measurement probe on the evaluation of electromagnetic fields," *IEEE Trans. Electromagn. Compat.*, Vol. 43, No. 2, pp. 339-349, May 2003.

[61] U. Kappel and H. Hirsch, "Statistical conversion factor between measurements of EMI in different test facilities," *Proc. IEEE Int. Symp. on EMC*, pp. 139-144, Seattle, Aug. 1999.

[62] U. Kappel, "Vergleichbarkeit von Verfahren zur Messung der Störfeldstärke," Ph.D. dissertation, D290, University of Dortmund, Dortmund, Germany, Aug. 2003.

[63] P. J. Kerry, "EMC standards – Quo Vadis?," *Proc. IEEE Int. Symp. on EMC*, Istanbul, May 2003.

[64] G. Koepke, D. Hill, and J. Ladbury, "Directivity of the test device in EMC measurements," *Proc. IEEE Int. Symp. on EMC*, pp. 535-539, Washington, Aug. 2000.

[65] J. Ladbury, *et al.*, "Evaluation of the NASA Langley Research Center RC Facility," NIST Tech. note No. 1508, Jan. 1999.

[66] F. Leferink, G. Hilverda, D. Groot Boerle, and W. van Etten, "Radiated electromagnetic fields of actual devices measured in different test environments," *Proc. IEEE Int. Symp. on EMC*, pp. 558-563, Boston, Aug. 2003.

[67] F. Leferink, *et al.*, "The strategic research agenda on EMC in the next (7th) European research framework programme (2007-2013)," *Proc. 2nd Pan-Pacific EMC joint meeting*, Okayama, Japan, May 2006.

[68] T. H. Loh and M. Alexander, "Antenna height scan for minimizing EUT emission measurement uncertainty in Fully Anechoic Chambers above 1 GHz," *Proc. 17th Int. Zurich Symp. on EMC*, pp. 497-500, Singapore, Feb. 2006.

[69] T-H. Loh and M. J. Alexander, "A method to minimize emission measurement uncertainty of electrically large EUTs in GTEM cells and FARs above 1 GHz," *IEEE Trans. Electromagn. Compat.*, Vol. 48, No. 4, pp. 634-640, Nov. 2006.

[70] S. M. Mann and A. C. Marvin, "Characteristics of the skeletal biconical antenna as used for EMC applications," *IEEE Trans. Electromagn. Compat.*, Vol. 36, No. 4, pp. 322-330, Nov. 1994.

[71] G. Manzi, M. Feliziani, P. Beeckman, and N. van Dijk, "Experimental EMC assessment of different ultra wide band technologies," *Workshop Int. Symp. on EMC*, Barcelona, Sep. 2006.

[72] A. Marvin and Y. Cui, "On determining the maximum emissions of enclosures at frequencies above 1 GHz," presented at the *URSI Gen. Assem.*, New Delhi, India, Oct. 23-29, 2005.

[73] J. van der Merwe and M. Coenen, "Experimental wireless system immunity and coexistence testing," *Workshop Int. Symp. on EMC*, Barcelona, Sep. 2006.

[74] T. Morsman, "Common mode broadband immunity test for xDSL ports," CISPR/I WG 4 document discussed at Santa Fe meeting, Feb. 2006.

[75] L. Musso, F. Canavero, B. Demoulin, and V. Berat, "Radiated immunity testing of a device with an external wire: repeatability of reverberation chamber results and correlation with anechoic chamber results," *Proc. IEEE Int. Symp. on EMC*, pp. 828-833, Boston, Aug. 2003.

[76] A. Papoulis, *Probability, Random Variables, and Stochastic Processes*, second edition, New York: McGraw-Hill Book Company, 1984.

[77] S. J. Porter and A. C. Marvin, "A new broadband EMC antenna for emissions and immunity," *Proc. Int. Symp. on EMC*, Vol. 1, pp. 75-79, Rome, Sep. 1994.

[78] S. Ramo, J. R. Whinnery, and Th. Van Duzer, *Fields and Waves in Communication Electronics*, third edition, New York, John Wiley & Sons, 1993.

[79] H. Rohling and D. Galda, "OFDM transmission technique: A strong candidate for next-generation mobile communications," *Radio Science Bulletin*, No. 310, pp. 47-58, Sep. 2004.

[80] A. J. Rowell, D. W. Welsh, and A. D. Papatsoris, "Practical limits for EMC emission testing at frequencies above 1 GHz," University of York, York EMC services, Report AY3601.

[81] A. A. Smith, Jr., "Standard-site method for determining antenna factors," *IEEE Trans. Electromagn. Compat.*, Vol. 24, No. 3, pp. 316-322, Aug. 1982.

[82] M. Stecher, "A weighting detector for the effect of interference on digital radiocommunication services," *Proc. IEEE Int. Symp. on EMC*, Istanbul, May 2003.

[83] M. Stecher, "Improvements in conducted emission measurements," *Proc. IEEE Int. Symp. on EMC*, pp. 191-196, Santa Clara, Aug. 2004.

[84] M. Stecher, "Improved reproducibility of conducted emission measurements," *Proc. 17th Int. Zurich Symp. on EMC*, pp. 509-512, Singapore, Feb. 2006.

[85] P. F. Stenumgaard, "A possible concept of how present radiated emission standards could be amended in order to protect digital communication services," *IEEE Trans. Electromagn. Compat.*, Vol. 46, No. 4, pp. 635-640, Nov. 2004.

[86] P. F. Stenumgaard, "On digital radio receiver performance in electromagnetic disturbance environments," Ph.D. dissertation, Royal Institute of Technology, Radio Communication Systems Laboratory, Sweden, Dec. 2000.

[87] W. L. Stutzman and G. A. Thiele, *Antenna Theory and Design*, second edition, New York, John Wiley & Sons, 1998.

[88] A. G. Tijhuis, Z. Q. Peng, and A. Rubio Bretones, "Transient excitation of a straight thin-wire segment: A new look at an old problem," *IEEE Trans. Antennas Propagat.*, Vol. 40, pp. 1132-1146, Oct. 1992.

[89] D. C. Welsh, D. Bozec, and M. R. Tyndall, "Feasibility study into the application of numerical modelling in EMC standardisation radio emission measurement methods," University of York, York EMC services, Report AY4607, May 2004.

[90] K. C. Wiklundh, "A method to determine the impact from disturbing electrical equipment on digital communication system by using APD," *Proc. Int. Symp. on EMC*, Sorrento, Sep. 2002.

[91] K. C. Wiklundh, "A new approach to derive emission requirements on APD in order to protect digital communication systems," *Proc. IEEE Int. Symp. on EMC*, Istanbul, May 2003.

[92] P. F. Wilson, D. A. Hill, and C. L. Holloway, "On determining the maximum emissions from electrically large sources," *IEEE Trans. Electromagn. Compat.*, Vol. 44, No. 1, pp. 79-86, Feb. 2002.

[93] P. Wilson, C. L. Holloway, and G. Koepke, "A review of dipole models for correlating emission measurements made at various EMC test facilities," *Proc. IEEE Int. Symp. on EMC*, pp. 898-901, Santa Clara, Aug. 2004.

[94] P. Wilson, "Emission and immunity testing: test object electrical size and its implication," *Proc. IEEE Int. Symp. on EMC*, pp. 349-352, Santa Clara, Aug. 2004.

[95] P. F. Wilson, "Advances in radiated EMC measurement techniques," *Radio Science Bulletin*, No. 311, pp. 65-78, Dec. 2004.

[96] A. P. M. Zwamborn and P. M. van den Berg, "The three-dimensional weak form of the conjugate gradient FFT method for solving scattering problems," *IEEE Trans. Microwave Theory Tech.*, Vol. 40, pp. 1757-1766, Sep. 1992.

# Publications of the author

### Journals

- N. van Dijk, "Numerical tools for simulation of radiated emission testing and its application in uncertainty studies," *IEEE Trans. on EMC*, Vol. 44, No. 3, pp. 466-470, Aug. 2002.

- N. van Dijk, "Uncertainties in 3-m radiated emission measurements due to the use of different types of receive antennas," *IEEE Trans. on EMC*, Vol. 47, No. 1, pp. 77-85. Feb. 2005.

- N. van Dijk, P. F. Stenumgaard, P. A. Beeckman, K. C. Wiklundh, and M. Stecher, "Challenging research domains in future EMC basic standards for different applications," *IEEE EMC Society Newsletter*, pp. 80-86 Spring 2006.

### Conferences

- P. A. Beeckman, N. van Dijk, and L. P. Janssen, "Inter Laboratory Comparison (ILC) of three standardized emission measurements," *Proc. Int. Symp. on EMC*, Eindhoven, Sep. 2004.

- N. van Dijk, "Uncertainties in 3-m radiated emission measurements due to the use of different types of receive antennas," *Proc. Int. Symp. on EMC*, Eindhoven, Sep. 2004.

- N. van Dijk, P. F. Stenumgaard, P. A. Beeckman, K. C. Wiklundh, and M. Stecher, "Challenging research domains in future EMC basic standards for different applications," *Proc. Int. Symp. on EMC*, Rome, Sep. 2005.

- N. van Dijk, "Concepts of new unified disturbance sources for immunity testing of multimedia products," *Proc. Int. Symp. on EMC*, Barcelona, Sep. 2006.

- G. Manzi, M. Feliziani, P. Beeckman, and N. van Dijk, "Experimental EMC assessment of different ultra wide band technologies," *Workshop Int. Symp. on EMC*, Barcelona, Sep. 2006.

- S. B. Worm and N. van Dijk, "Susceptibility analysis of oscillators by means of ISF-method," *4th International Workshop on EMC of Integrated Circuits*, EMC Compo 2004, Angers, 2004.

**CISPR Working Group (WG) documents**

- N. van Dijk, "The correlation between a SAR/OATS measurement and a reverberation chamber measurement," CISPR/A WG 2 document, March 2004.

- N. van Dijk, "E-field reference comparisons of 3-m radiated emission results by the use of different types of receive antennas," CISPR/A WG 1 and 2 document, Aug. 2004.

- N. van Dijk, "Use of the correlation method described in CISPR/A/529/CD; reverberation chamber results versus FAR results above 1 GHz," CISPR/A WG 2 document, Jan. 2005.

- N. van Dijk, "Conducted emission measurements on the antenna cable," CISPR/I WG 2 document, Jan. 2006.

- K. Banerjee and N. van Dijk, "Conversion of radiated emission results obtained from a reverberation chamber to 3 m SAR results," CISPR/I WG 2 document, Sep. 2006.

**Reports**

- N. van Dijk, "Development and validation of tools for simulation of radiated emission testing," M.S. thesis, Eindhoven University of Technology, Eindhoven, The Netherlands, January 2001.

- N. van Dijk, "Some initial considerations on the application of mode-stirred chamber for EMC testing," Philips Research Nat.Lab. Tech. note No. 2001/239, June 2001.

- N. van Dijk, "The mode-stirred chamber as EMC test facility," Philips PDSL EM&C research report, EMC-01-NVD-001-RRP, Dec. 2001.

- N. van Dijk, "On the development of future EMC product standards for multimedia and wireless products," Philips PDSL EM&C research report, EMC-04-NVD-002-RRP, Oct. 2004.

- N. van Dijk, "Concepts of unified disturbance sources for immunity – A representative test signal for digitally modulated signals-," Philips AppTech EM&C research report, EMC-05-NVD-001-RRP, Aug. 2005.

# Summary

In the field of Electromagnetic Compatibility (EMC) two phenomena are considered: the emission and the immunity of electronic products. Emission measurements of products are performed to protect radio systems. We are talking about a conducted emission measurement when a current is measured and about a radiated emission measurement when a field quantity is measured. Immunity tests are performed to test the immunity of electronic products against the presence of electromagnetic disturbances.
In the past decade, an evolution in electronic products has been observed. Firstly, electronic products include increasingly functionality. This is explicit for so-called multimedia products. Secondly, an increasing number of electronic products are equipped with radio-communication systems for, e.g., communication with a broadband network or communication with peripheral and associated equipment. New radio-communication systems typically operate at frequencies above 1 GHz and are positioned in the vicinity of other products at home. The receivers of the radio-communication systems, which are typically integrated into multimedia products, are sensitive. The expected proliferation of these 'wireless multimedia products' is enormous. For that reason, these new types of multimedia products include new potential disturbance sources as well as potential new victims. All the more when we realize that currently the EMC standards for multimedia products require radiated emission measurements and radiated immunity tests up to only 1 GHz.
EMC standards are developed by various committees within the International Electrotechnical Commission (IEC). The International Special Committee on Radio Interference (CISPR) develops and maintains basic standards for conducted and radiated emission measurements. These basic standards are developed in CISPR subcommittee A (CISPR/A). Furthermore, CISPR includes subcommittees that develop so-called EMC product standards. For example, CISPR/I is responsible for the development of new EMC product standards for multimedia products, CISPR 32 for emission measurements and CISPR 35 for immunity tests. A few years ago, a new radiated emission measurement method for frequencies above 1 GHz has been developed and published in CISPR 16-2-3. This method is based on a Fully Anechoic Room (FAR). Maintenance of this method is still in progress. Moreover, the understanding of the electromagnetic behavior and uncertainty of measurement methods is an important topic within CISPR/A. For example, the question how receive antenna specifications relate to the uncertainty of the radiated emission measurement.
Another example of a method for performing radiated emission measurements at frequencies above 1 GHz is the Reverberation Chamber (RC). This is a reflective chamber that physically operates as a resonant cavity from which the modes (standing wave patterns) are continuously varied by rotating one or more stirrer(s). A stirrer is an electrically conducting paddle wheel that varies the electromagnetic boundary conditions. The RC method is a statistical method that utilizes the multiple reflections inside a shielded enclosure, while the Semi Anechoic Room (SAR) method and the FAR method are deterministic methods and based on straightforward wave propagation.

The content of this thesis include the results of three studies, which are related to the above-mentioned developments in EMC standards.
The first study addresses the investigation of the deviation in radiated emission results caused by using different types of receive antennas. The receive antenna is used in radiated emission measurements to measure the emission emitted from the EUT. The receive antenna is characterized by a single number only, i.e., its Antenna Factor (AF). Conventionally, the assumption was that if the AF of receive antennas could be determined accurately, then the use of different receive antennas should yield the same radiated emission result. Earlier investigations already indicated that this assumption is questionable.
The deviations due to the use of different receive antennas were investigated by comparing the results obtained by using commonly used receive antennas: tuned dipoles, bow-tie antennas, biconical antennas, log-periodical antennas, and double-ridged waveguide horn antennas. The deviations are investigated for the 3 m SAR facility. The deviations are investigated at frequencies below and above 1 GHz by using simulations. Two antenna-calibration methods were taken into account, i.e., the free space method and the standard-site method. The tuned-dipole result was conventionally used as reference whereas the electric field-strength in absence of the receive antenna was recently introduced as the new reference. The reference obtained by a tuned dipole and the reference obtained by the electric field-strength in absence of the receive antenna were used to determine the deviations. This was performed to investigate the deviation values and their relation to the two references.
In the operating bandwidths of the investigated antennas, a considerable 'receive antenna type' deviation is found of around 2 dB. The level of deviation due to the use of different types of receive antennas (2 to 3 dB) is defined as substantial in relation to the $U_{\mathrm{CISPR}}$ value of 5 dB for 3 m SAR measurements. It was found that multilobing antenna-patterns caused higher deviations. Furthermore, it was found that the level of deviation due to the antenna type is not affected by the way the receive antennas were calibrated. Considering the uncertainties, we could conclude that the E-field reference as proposed in CISPR/A is neither an improvement nor a degradation compared with the tuned-dipole reference. At frequencies above 1 GHz, it was found that the beamwidth of the receive antenna is an important quantity related to the deviation. Approximately, a 60° beamwidth yields -1 dB deviation and a 30° beamwidth yields -4 dB deviation.

The topic of conversion of emission results obtained from the RC method is mentioned in the second study. A standardized conversion method was applied to investigate the so-called conversion factors. These conversion factors are needed when results obtained from the RC method are translated to SAR/FAR results. The interesting feature of the applied conversion method is that the conversion factors are derived based on a reference quantity. The reference quantity is the important quantity for the protection of radio-communication systems. The conversion method is applied to investigate the conversion factors of the RC method towards the SAR method. From the derived conversion factors also the limit based on the SAR method can be translated towards the RC method. This is performed because the limit for the SAR method is successfully used already for many decades. We have numerically investigated the conversion factors of isotropic point sources, tuned dipoles,

and a fixed-length dipole antenna. We have investigated the conversion factors experimentally by considering a CISPR 22 system-EUT configuration based on a TV, PC, and printer. The conversion factor for the RC method to derive a new limit based on the SAR method is approximately 4 dB. This means that the limit for the RC method is approximately 4 dB lower than for the SAR method.
Moreover, the directivity of EUTs was investigated and the influence of the directivity effect on the conversion factors. A statistical model for EUT directivity was reviewed and based on this model a comparison of the directivity effect was performed for a fictitious EUT measured within either a RC or a FAR in the frequency range 1-6 GHz. From the statistical review, we could conclude that the directivity of the EUT plays not an important role in the conversion topic. However, from simulations of a fixed-length dipole of 1.5 m, it became clear that the directivity effect on the conversion factors depends on the polarization of the emissions. Horizontal polarization causes a higher deviation for the RC method while vertical polarization causes a higher deviation for the SAR/FAR method. This means that the polarization behavior of emissions of typical EUT configurations should be investigated in future in order to define proper conversion factors.

In the third study, new concepts of immunity test-signals are investigated. EMC emission measurements or immunity tests are performed in order to cover certain interference scenarios. The conventional interference scenario for immunity tests was based on analog broadcast transmitters relatively far away from in-home electronic products. Mostly, the interference mechanism is nonlinear detection in the product, which accordingly could cause audio or video interference. Based on this interference scenario, the current 1 kHz 80% Amplitude Modulated (AM) signal is applied.
We have defined a new interference scenario, i.e., the coexistence interference scenario. This interference scenario covers the existing situation of multimedia products with integrated radio-communication systems. Here, the disturbances sources are the radio-communication signals that are typically digitally modulated signals. In addition, the disturbance sources are typically in the vicinity of victim products. The victims in the coexistence interference scenario are the sensitive receivers of the radio-communication systems. The receiver function of multimedia products with integrated radio-communication systems is an important function that should be tested on immunity.

Based on these two interference scenarios, the properties of Time Division Multiplexing (TDM) and Frequency Division Multiplexing (FDM) radio-communication signals were investigated. The following radio-communication signals were investigated: GSM signals, DCS signals, Bluetooth signals, wireless LAN (OFDM) signals, and UWB signals.
The time behavior was investigated statistically by applying the Amplitude Probability Distribution (APD). The frequency domain properties were investigated by considering the spectrum. These investigations were supported by MatLab calculations. The time behavior of OFDM radio-communication signals was investigated. The properties of the radio-communication signals were used to propose specifications for so-called Unified Disturbance Source (UDS) signals.
A UDS is defined as an immunity test signal representative for a number of radio-communication signals that has a interference potential equivalent to the actual radio-

communication signals. The study is completed by reviewing experimental evaluations of the UDS signal concepts for the use of coexistence immunity tests. It is an advantage that the UDS signals can be generated by using commonly available test equipment. In this way, representative coexistence immunity tests can be performed cost and time efficiently.

Keywords: electromagnetic compatibility / electromagnetic interference / interference scenario / antenna factor / receive antenna / emission measurement / immunity test / coexistence immunity test / immunity test-signal / reverberation chamber / conversion of emission results / anechoic chamber / wireless communication / measurement uncertainty / EMC standards / multimedia.

# Samenvatting

In het vakgebied van Elektromagnetische Compatibiliteit (EMC) kunnen globaal twee fenomenen beschouwd worden: de emissie en de immuniteit van elektronische producten. Emissiemetingen van elektronische producten worden uitgevoerd voor de bescherming van radio systemen. We spreken van een emissiemeting via geleiding als er een stroom wordt gemeten en van een meting van emissie via straling als een elektromagnetische veldgrootheid gemeten wordt. Immuniteitstesten worden uitgevoerd om elektronische producten te testen op de bestendigheid tegen elektromagnetische stoorsignalen.
De laatste tien jaar konden een aantal ontwikkelingen in elektronische producten waargenomen worden. Ten eerste dat elektronische producten steeds meer functionaliteit bevatten. Dit is per definitie het geval voor zogenaamde multimedia producten. Ten tweede zien we dat steeds meer producten uitgerust zijn met radiocommunicatie systemen. Deze worden gebruikt voor bijvoorbeeld draadloze breedband internet verbindingen of voor communicatie met randapparatuur. Nieuwe radiocommunicatie systemen opereren vooral bij frequencies boven 1 GHz en zijn veelal gepositioneerd dichtbij andere producten. De receivers van de radiocommunicatie systemen zoals ze meestal voorkomen in multimedia producten zijn gevoelig. De te verwachten toepassing en verspreiding van deze zogenoemde 'wireless multimedia producten' is enorm. Om die reden bevatten deze multimedia producten nieuwe potentiële elektromagnetische stoorbronnen en kunnen tevens gevoelig zijn voor storing. Te meer als we ons realiseren dat de huidige EMC normen voor dit soort producten emissie en immuniteitseisen opleggen tot slechts 1 GHz.
EMC normen worden ontwikkeld door verscheidene comités binnen de International Electrotechnical Commission (IEC). Het zogenoemde CISPR (International Special Committee on Radio Interference) comité ontwikkelt en onderhoudt basisnormen voor conducted en radiated emissiemetingen. Deze basisnormen worden ontwikkeld in CISPR subcomité A (CISPR/A). Tevens bevat CISPR subcomités die zogenaamde EMC product normen ontwikkelen. CISPR/I is bijvoorbeeld verantwoordelijk voor de ontwikkeling van nieuwe EMC product normen voor multimedia producten, CISPR 32 voor emissiemetingen en CISPR 35 voor immuniteitstesten. Een paar jaar geleden is er een nieuwe meetmethode voor emissie via straling ontwikkeld en gepubliseerd in CISPR 16-2-3. Deze methode is gebaseerd op een Fully Anechoic Room (FAR) (volledig echovrije meetkamer). Deze methode is overigens nog volop in onderhoud. De gebieden waar CISPR/A actief is kan worden samengevat met: meetapparatuur, meetmethodes en statistiek. Bijvoorbeeld de vraag hoe specificaties voor ontvangstantennes relateren aan de uiteindelijke onzekerheid van de meting.
Een ander voorbeeld van de ontwikkeling van een meetmethode boven 1 GHz is de Reverberation Chamber (RC). Dit is een reflecterende meetkamer die fysisch werkt als een resonante kamer waarvan de modes (staandegolf patronen) continu gevarieerd worden door één of meerdere stirrers. Een stirrer (Nederlands: mixer) is een metalen constructie die rondgedraaid wordt rondom zijn as waardoor de elektromagnetische randvoorwaarden gevarieerd worden. De RC meetmethode is een statistische methode en maakt gebruik van de reflecties van een afgeschermde ruimte terwijl de Semi Anechoic Room (SAR) methode en de FAR methode deterministische methodes zijn en gebaseerd op rechtlijnige

propagatie van de golven. De inhoud van het proefschrift bevat de resultaten van drie studies die verband houden met de bovengenoemde ontwikkelingen in EMC normen.

De eerste studie gaat over het onderzoek naar de afwijkingen van metingen voor de emissie via straling die veroorzaakt worden door het gebruik van verschillende ontvangstantennes. De ontvangstantenne wordt in metingen voor de emissie via straling gebruikt om de emissie van producten te meten. De ontvangstantenne wordt gekarakteriseerd door één enkele parameter, namelijk de antennefactor (AF). Traditioneel werd aangenomen dat als de AF's van ontvangstantennes nauwkeurig bekend zijn dat dan het gebruik van verschillende ontvangstantennes hetzelfde emissie resultaat van de meting zou moeten opleveren. Eerdere onderzoeken hebben reeds aangetoond dat deze aanname twijfelachtig is.
De afwijkingen die te wijten zijn aan het gebruik van verschillende ontvangstantennes zijn onderzocht door de resultaten te vergelijken van verschillende veel gebruikte ontvangstantennes: afgestemde dipolen, biconische antennes, log-periodische antennes en double-ridged waveguide hoorn antennes. De afwijkingen zijn onderzocht voor een 3 m SAR faciliteit. De afwijkingen zijn boven en onder 1 GHz onderzocht door gebruik te maken van simulaties. Twee antenne calibratiemethoden zijn in het onderzoek meegenomen, namelijk de free-space (Nederlands: vrije ruimte) en de standard-site methode. De afgestemde dipool was traditioneel de referentie voor metingen voor de emissie via straling terwijl er recentelijk een nieuwe E-field referentie is geïntroduceerd namelijk de elektrische veldsterkte in afwezigheid van de antenne. Voor het onderzoek naar de afwijkingen zijn de referentie van een afgestemde dipool en de referentie van de elektrische veldsterkte in afwezigheid van de antenne gebruikt. Dit is gedaan om de afhankelijkheid van de afwijkingen te onderzoeken op de referentie die wordt gebruikt.

In de bandbreedte waar de antennes gespecificeerd zijn is een substantiële afwijking in emissieresultaten gevonden van ongeveer 2 dB. Het niveau van afwijking die te wijten is aan het gebruik van verschillende ontvangstantennes (2 tot 3 dB) kan substantiëel genoemd worden vergeleken met de 5 dB waarde voor de 3 m SAR methode die binnen CISPR als acceptabel wordt beschouwd. Het ontstaan van multilobing van de antennes is aangemerkt als een negatieve invloedsfactor in de uiteindelijke afwijking oftewel meer multilobing zorgt voor grotere afwijkingen. De resultaten hebben aangetoond dat de manier van antenne calibratie geen effect heeft op de afwijkingen. Tevens is aangetoond dat het gebruik van de E-field referentie noch een verbetering is noch een verslechtering vergeleken met de afgestemde dipool referentie wat betreft de afwijkingen in emissieresultaten. Voor de frequenties boven 1 GHz kon een duidelijke relatie tussen de bundelbreedte van de antenne en de afwijkingen gevonden worden. Een bundelbreedte van 60° levert een afwijking van ongeveer -1 dB op, terwijl een bundelbreedte van 30° een afwijking oplevert van ongeveer -4 dB.

Het onderwerp van conversie van emissieresultaten verkregen met behulp van de RC methode wordt behandeld in de tweede studie. Een genormaliseerde conversiemethode is toegepast om de zogenoemde conversiefactoren te onderzoeken. Deze conversiefactoren zijn nodig als we resultaten verkregen vanuit de RC methode willen vertalen naar

SAR/FAR resultaten. Het interessante van de gebruikte conversiemethode is dat de conversiefactoren afgeleid worden op basis van een referentie grootheid. Deze referentie grootheid is de belangrijke grootheid ten aanzien van de radiobescherming. Deze conversiemethode is toegepast om daarmee de conversiefactoren te bepalen voor de vertaling van de RC methode naar de SAR methode. Vanuit de afgeleide conversiefactoren kan ook de limiet behorende bij de SAR methode vertaalt worden naar de RC methode. Deze vertaalslag van limieten is van belang om uit te voeren omdat de limieten van de SAR methode al decennia lang een goede radiobescherming bieden. We hebben de conversiefactoren numeriek onderzocht voor isotrope puntbronnen, afgestemde dipolen en voor een dipool met een vaste lengte. Tevens hebben we de conversiefactoren experimenteel onderzocht door een systeem-EUT configuratie bestaande uit een TV, PC en printer te beschouwen. The conversiefactor voor de RC methode om een nieuwe limiet af te leiden die gebaseerd is op de SAR methode is ongeveer 4 dB. Dit betekent dat de limiet voor de RC methode ongeveer 4 dB lager zal moeten liggen als die van de SAR methode.
Bovendien is de richtwerking van het emissiediagram van de EUT's onderzocht en de invloed van deze richtwerking op de conversiefactoren. Een statistisch EUT model voor de richtwerking is besproken. Op basis van dit model is een vergelijking uitgevoerd voor een fictief EUT gemeten in de RC of de FAR in het frequentie gebied van 1-6 GHz. Vanuit deze statistische beschouwing konden we concluderen dat de richtwerking van EUT's niet een belangrijke rol speelt voor het bepalen van de conversiefactoren. Een vergelijkbare afwijking t.o.v. de referentie grootheid is immers gevonden voor zowel de RC methode als de FAR methode. Echter, uit simulaties met een dipoolantenne met een vaste lengte van 1.5 m is gebleken dat het effect van de richtwerking op de conversiefactoren afhangt van de polarisatie van de emissie. Horizontale polarisatie laat een grotere afwijking voor de RC methode zien terwijl verticale polarisatie juist een grotere afwijking voor de SAR/FAR methode laat zien. Dit betekent dat het polarisatie gedrag van de emissie van typische EUT configuraties onderzocht dient te worden in de toekomst om daarmee geschikte conversiefactoren te definiëren.

In de derde studie zijn nieuwe concepten van immuniteitstestsignalen onderzocht. EMC emissiemetingen of immuniteitstesten worden uitgevoerd ten einde bepaalde interferentiescenario's getest te hebben. Het conventionele interferentiescenario voor immuniteitstesten is gebaseerd op analoge vaste radiozenders die zich relatief op grote afstand van de elektronische producten thuis bevinden. Meestal kan het interferentie mechanisme gevonden worden in niet-lineare detectie in het product dat vervolgens audio of video interferentie kan veroorzaken. Gebaseerd op dit interferentiescenario wordt het huidige 1 kHz 80% amplitude gemoduleerde (AM) testsignaal gebruikt. Een tweede en nieuw interferentiescenario is geïntroduceerd, namelijk het coëxistentie interferentiescenario. Dit interferentiescenario dekt de bestaande situatie af van multimedia producten met geïntegreerde radiocommunicatie systemen. Hierbij worden de stoorsignalen gevormd door de radiocommunicatie signalen die typisch digitaal gemoduleerd zijn. Tevens bevinden de stoorsignalen zich dichtbij de producten die potentiëel gestoord kunnen worden. Met name de gevoelige ontvangers van de radiocommunicatie systemen zijn functies die potentiëel gestoord kunnen worden in het coëxistentie interferentiescenario. De ontvanger functie van multimedia producten met

geïntegreerde radiocommunicatie systemen is een belangrijke functie die getest zou moeten worden op immuniteit.
De eigenschappen van Time Division Multiplexing (TDM) signalen en Frequency Division Multiplexing (FDM) signalen zijn onderzocht gebaseerd op deze twee interferentiescenario's. De volgende radiocommunicatie signalen zijn onderzocht: GSM signalen, DCS signalen, Bluetooth signalen, wireless LAN (OFDM) signalen en UWB signalen. Het tijdsgedrag is statistisch onderzocht met behulp van de Amplitude Probability Distribution (APD). De eigenschappen in het frequentie domein zijn geanalyseerd door het frequentie spectrum te beschouwen. De berekeningen zijn uitgevoerd met behulp van MatLab. Het tijdsgedrag van OFDM signalen is onderzocht. De eigenschappen van de radiocommunicatie signalen zijn geanalyseerd om daarmee specificaties op te stellen voor zogenoemde Unified Disturbance Source (UDS) signalen. Een UDS is gedefiniëerd als een immuniteitstestsignaal representatief voor een aantal radiocommunicatie signalen die een stoorpotentiëel hebben dat gelijk is aan de werkelijke radiocommunicatie signalen. De studie is afgerond door het beschouwen van eerste experimentele evaluaties van de UDS signaal concepten voor het gebruik in coëxistentie immuniteitstesten. Het is een voordeel dat de UDS signalen gegenereerd kunnen worden doormiddel van algemeen beschikbare testinstrumenten. Hierdoor kunnen representatieve coëxistentie immuniteitstesten uitgevoerd worden op een kosten en tijdsefficiënte manier.

Trefwoorden: elektromagnetische compatibiliteit / elektromagnetische verstooring / interferentiescenario / coëxistentie interferentiescenario / antennefactor / ontvangstantenne / emissiemeeting / immuniteitstest / immuniteitstestsignaal / conversie van meetresultaten / echovrije meetkamer / reflecterende meetkamer / draadloze communicatie / meetonzekerheid / EMC normen / multimedia.

# Acknowledgement

I experienced the period of writing the Ph.D. thesis as inspiring. It gave inspiration to get the opportunity to write a thesis of studies, which have been performed within Philips. It really was a motivating experience to present and exploit my work in this way.
It motivated me to have many contacts during the review period and the support and encouragement that so many people gave me. Therefore, I would like to thank my Philips colleagues and all my friends. My colleague Konika has supported the work by performing experiments and as living archive, therefore, many thanks!
I would like to thank the members of my committee for a pleasant and fruitful cooperation: Holger Hirsch, Andy Marvin, Peter Zwamborn, and Arthur van Roermund.
Special thanks I would like to give to my tutors Anton, Frank, and Pierre. I am very grateful for the time and effort they have spent by supporting me with personal encouragement and reviewing the thesis. Especially, the critical but constructive view of Pierre has improved this thesis substantially.
I would like to thank Ton Almering for supporting my introduction in the CISPR/I standardization working groups, for a positive cooperation, and for reviewing the thesis. Thanks also to my colleagues Jaco and Stef for reviewing the thesis. I look back on a fruitful scientific cooperation and correspondence with Peter Stenumgaard, Kia Wiklundh, Manfred Stecher, Lutz Dunker, John Ladbury, and Udo Kappel.
Last but not least, I am grateful for the lifelong support and encouragement of my parents and brother (Erik). Above all, I thank God through Jesus Christ our Lord!

# Biography

**Nico van Dijk** was born in Hengelo, The Netherlands, in 1975. He grew up in Borne. In 1998 he received the polytechnics degree (cum laude) in electrical engineering from the Hogeschool Enschede. Nico did confession of his faith in the reformed church (Geref. Kerk) of Borne in 1998.

In September 1998, Nico started his study electrical engineering at the University of Technology in Eindhoven. Nico was secretary of the evangelical student movement Ichthus Eindhoven in 2001/2002. Ichthus is a member movement of the International Fellowship of Evangelical Students (IFES). In 2001, he received the M.S. degree in electrical engineering from the Eindhoven University of Technology. His graduation subjects were electromagnetic waves and antennas.

Since 2001, he is working in the EMC Center of Philips Electronics, The Netherlands. His main research interests are: test methods (especially above 1 GHz) and future standardization, measurement uncertainties, reverberation chamber technology, and power and signal integrity modeling of ICs and System in Package (SiP) devices. In the past years, Nico supervised various graduation students. He has participated in various standardization committees, e.g., the project team for alternative measurement methods, the CISPR/I working groups, and the Joint Task Force (JTF) for reverberation chambers.